

**NASA Technical Memorandum 104566, Vol. 31**

## **SeaWiFS Technical Report Series**

**Stanford B. Hooker, Elaine R. Firestone, and James G. Acker, Editors**

### **Volume 31, Stray Light in the SeaWiFS Radiometer**

**Robert A. Barnes, Alan W. Holmes, and Wayne E. Esaias**



**July 1995**



# NASA Technical Memorandum 104566, Vol. 31

## SeaWiFS Technical Report Series

**Stanford B. Hooker, Editor**  
*NASA Goddard Space Flight Center*  
*Greenbelt, Maryland*

**Elaine R. Firestone, Technical Editor**  
*General Sciences Corporation*  
*Laurel, Maryland*

**James G. Acker, Technical Editor**  
*Hughes STX*  
*Lanham, Maryland*

## Volume 31, Stray Light in the SeaWiFS Radiometer

**Robert A. Barnes**  
*ManTech, Inc.*  
*Wallops Island, Virginia*

**Alan W. Holmes**  
*Santa Barbara Research Center*  
*Goleta, California*

**Wayne E. Esaias**  
*NASA Goddard Space Flight Center*  
*Greenbelt, Maryland*



National Aeronautics and  
Space Administration

**Goddard Space Flight Center**  
Greenbelt, Maryland 20771

1995

This publication is available from the NASA Center for Aerospace Information,  
800 Elkrige Landing Road, Linthicum Heights, MD 21090-2934, (301) 621-0390.

## ABSTRACT

Some of the measurements from the Sea-viewing Wide Field-of-view Sensor (SeaWiFS) will not be useful as ocean measurements. For the ocean data set, there are procedures in place to mask the SeaWiFS measurements of clouds and ice. Land measurements will also be masked using a geographic technique based on each measurement's latitude and longitude. Each of these masks involves a source of light much brighter than the ocean. Because of stray light in the SeaWiFS radiometer, light from these bright sources can contaminate ocean measurements located a variable number of pixels away from a bright source. In this document, the sources of stray light in the sensor are examined, and a method is developed for masking measurements near bright targets for stray light effects. In addition, a procedure is proposed for reducing the effects of stray light in the flight data from SeaWiFS. This correction can also reduce the number of pixels masked for stray light. Without these corrections, local area scenes must be masked 10 pixels before and after bright targets in the along-scan direction. The addition of these corrections reduces the along-scan masks to four pixels before and after bright sources. In the along-track direction, the flight data are not corrected, and are masked two pixels before and after. Laboratory measurements have shown that stray light within the instrument changes in a direct ratio to the intensity of the bright source. The measurements have also shown that none of the bands show peculiarities in their stray light response. In other words, the instrument's response is uniform from band to band. The along-scan correction is based on each band's response to a 1 pixel wide bright source. Since these results are based solely on preflight laboratory measurements, their successful implementation requires compliance with two additional criteria. First, since SeaWiFS has a large data volume, the correction and masking procedures must be such that they can be converted into computationally fast algorithms. Second, they must be shown to operate properly on flight data. The laboratory results, and the corrections and masking procedures that derive from them, should be considered as zeroth order estimates of the effects that will be found on orbit.

---

## 1. INTRODUCTION

The Sea-viewing Wide Field-of-view Sensor (SeaWiFS) is the successor instrument to the NIMBUS-7 Coastal Zone Color Scanner (CZCS). The design requirements for SeaWiFS have been based on the National Aeronautics and Space Administration's (NASA) experience with the operation of CZCS. Among other characteristics, CZCS often contained obvious anomalies in ocean measurements that immediately followed measurements of clouds. For CZCS measurements, and also for those from SeaWiFS, clouds are several times brighter than the ocean surface. In the CZCS measurements, the output from each of the six CZCS bands would overshoot the ocean surface levels on their return from the brighter cloud levels. This would give ocean measurements, on the down-scan side of clouds, that were too low. The recovery from this overshoot would take up to 100 pixels, that is, up to 100 measurements in the CZCS scan line (Mueller 1988). This problem resulted from a faulty design of the CZCS electronics. When CZCS viewed clouds, the analog amplifiers for the CZCS bands saturated. It is believed that these saturating amplifiers pulled down the output from their power supplies. After the instrument had scanned past the bright clouds, it would require up to 100 pixels or more for the amplifiers and their power supplies to stabilize again. The bright target recovery (BTR) performance specification for SeaWiFS was prepared with this CZCS problem in mind.

For CZCS, the problems from cloud interference with ocean measurements occurred only down scan of the cloud. These problems are considered to have been electronic in origin. CZCS experienced no problems from cloud interference up scan of the clouds, and for CZCS, there were no apparent problems with light from clouds contaminating measurements of adjacent ocean pixels; hence, there were no apparent problems with stray light.

CZCS was designed with an 8-bit digital resolution. The minimum value for its measurements was 1/256 of full scale. SeaWiFS has been designed with 10-bit digital resolution. Since it has comparable full scale readings, SeaWiFS is four times more sensitive than CZCS. It can detect effects, both in the water-leaving radiances and in the instrument itself, that could not have been noticed in previous measurements.

In March 1993, during testing of the assembled SeaWiFS instrument, light from bright sources was found to contaminate SeaWiFS measurements, both up scan and down scan from these bright sources. The down-scan response of SeaWiFS approached, but was not within, the BTR specification for instrument performance. The effects of stray light up scan of bright sources were of the same magnitude of those down scan. At the SeaWiFS Preship Review (SPR), an instrument performance appraisal held at the Santa Barbara Research Center (SBRC) in April 1993, it was found that the radiometer did not meet the BTR performance specification. At the same meeting, it

was decided to investigate instrument changes that would reduce the effects of stray light in the instrument.

In May 1993, SBRC, the SeaWiFS manufacturer, presented a set of recommendations for changes to ameliorate stray light in the instrument—the SeaWiFS Stray Light Signal Paths (SSLSP). In August 1993, the Ocean Color Contract was changed to allow modification of the sensor. After completion of the instrument modifications and subsequent testing, a second appraisal of the radiometer's performance—the SeaWiFS Post-Modification Preship Review (SPMPR)—found the instrument to meet all specifications (Barnes et al. 1994a).

## 1.1 Local and Global Area Coverage

SeaWiFS scans across the Earth's surface from west to east. Within the instrument, the scanner rotates in a circle. Each scan of the Earth from the instrument contains 1,285 contiguous pixels over a  $116.6^\circ$  scan centered at nadir, and each pixel is nominally square with a side length of 1.6 mrad (Barnes et al. 1994a). For nadir measurements at the nominal spacecraft altitude of 705 km, the length of the sides of the pixels on the Earth's surface is 1.13 km. The scan lines are nominally perpendicular to the motion of the spacecraft, which moves from north to south. The spacecraft orbit and the spacecraft rotation rate have been designed so that the pixels from adjacent scan lines lie next to each other at nadir. Thus, at nadir the SeaWiFS instrument produces measurements of the Earth's surface in a two-dimensional mosaic of square pixels.

When SeaWiFS samples away from nadir, the path-length between the instrument and the Earth increases. The pixel size at the Earth's surface increases as the instrument's measurement angle increases from nadir. Along each scan line, the pixels remain contiguous, but they are larger at the scan edges than at nadir. As a result, the areal coverage of the Earth from each scan line resembles a bow tie. As explained above, the orbit for SeaWiFS has been designed so that, at nadir, pixels from adjacent scans lie next to each other. Away from nadir, the increasing size of the pixels causes them to overlap in the direction of spacecraft motion. Earth scenes in this format are provided from the SeaStar satellite as local area coverage (LAC). These LAC scenes are provided in two ways. First, as they are obtained, the scenes are transmitted directly to the ground as the instrument passes over local receiving stations. LAC scenes from some of the ground stations will be forwarded to the NASA Goddard Space Flight Center (GSFC) and placed into the SeaWiFS archive. The forwarding process is relatively slow, and the data will become available over a period of weeks to months after transmission from the satellite. Second, specific scenes will be recorded on board the spacecraft for transmission to the ground along with the global SeaWiFS data. These recorded LAC scenes will be sent directly from the satellite to GSFC twice daily. A summary of these two types of LAC data were provided in the overview of the SeaWiFS mission (Hooker et al. 1992).

In order to limit the required onboard data storage and data transmission rate, the mission was designed by NASA to give global area coverage (GAC) by recording every fourth pixel from every fourth scan line for transmission to the ground. These data are transmitted twice daily with the recorded LAC. As a result, each GAC measurement is four pixels removed from its nearest neighbor in both the along-scan and along-track directions.

For stray light in SeaWiFS, LAC and GAC data are distinctly different. SeaWiFS will measure dark ocean radiances adjacent to very bright clouds. The brightness and proximity of those clouds will affect the amount of stray light within the radiometer. The two-dimensional mosaic of LAC measurements will provide that information. For GAC measurements, the 3 pixel gap between measurements severely limits knowledge of the size and brightness of adjacent clouds. This lack of information will reduce the quality of any GAC stray light correction, relative to LAC. Proposed procedures for on-orbit stray light corrections are presented in Sections 11 and 12. These procedures must be tested using actual flight measurements, particularly for the GAC corrections. LAC scenes will be used to test the GAC correction. These LAC scenes will contain complete sets of information on the location and brightness of clouds and other bright sources. They will be subsampled to provide a GAC product. Downlinked GAC data will also be available for any LAC scene. Fixed pixel subsampling has been shown to produce the best statistical agreement between synthesized GAC products and the LAC measurements from which they are obtained (Justice et al. 1989 and McClain et al. 1992). Such equivalence is a prerequisite for testing GAC stray light corrections with LAC scenes.

## 1.2 Stray Light Modifications

The effects of stray light in SeaWiFS were discovered after the construction of the instrument. The radiometer was developed with an engineering design unit that did not completely duplicate the flight instrument's optical characteristics. The SeaWiFS engineering unit was constructed to verify the instrument's basic mechanical and electrical design, particularly the telescope and half-angle mirror combination, and detector combinations (discussed in Section 2), in addition to providing a complete electrical interface for testing the SeaStar spacecraft. The fast-track, 22 month construction schedule for SeaWiFS precluded the fabrication of a complete, flight-like engineering unit; full-scale testing; and then the production and testing of the flight instrument. For SeaWiFS, the engineering and flight units were developed nearly in parallel with each other. As a result, the effects of stray light in SeaWiFS were discovered after the completion of the instrument. This development effort resulted in a radiometer that met all of the prelaunch requirements (Barnes et al. 1994a) except for BTR, which was slightly outside of the

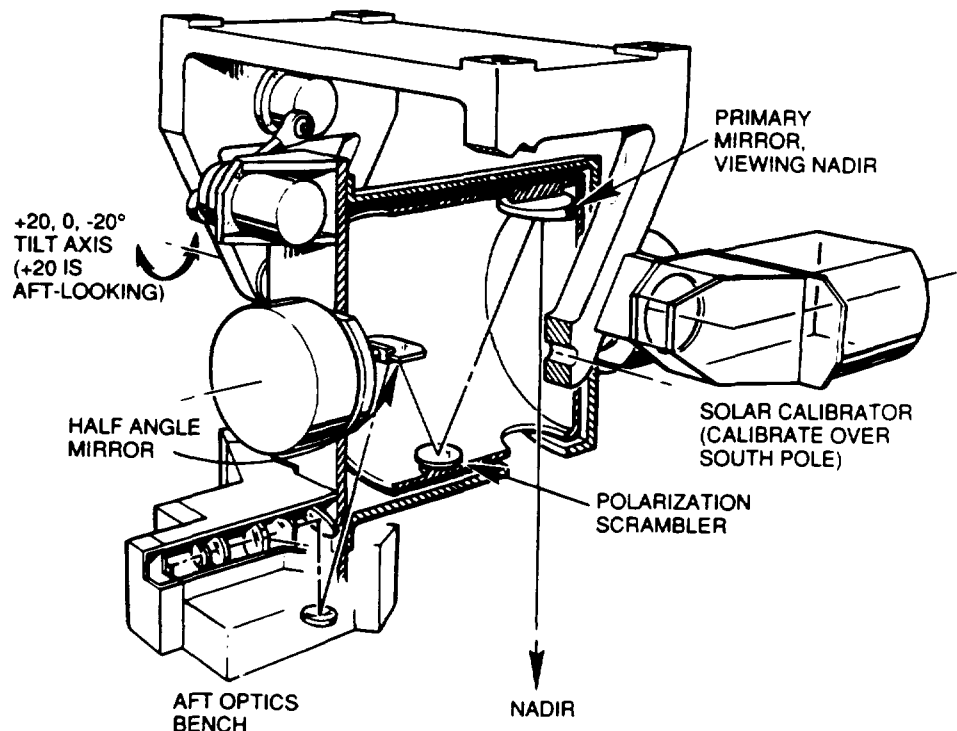


**Fig. 1.** The SeaWiFS scanner assembly. The scanner mounts to the payload shelf using the four mounting points at the top of the figure.

specifications. Stray light effects were found both before and after bright sources and are a part of BTR. As discussed in Section 5, there were electronic recovery tails in the instrument's bright target responses. The corrections for the electronic tails were simple, and with those repairs, the instrument met the BTR specification.

The instrument manufacturer provided to the SeaWiFS Project, a description of the radiometer's stray light paths and their associated corrections (in the SSLSP). These paths are described in Section 6. Risk to the completed flight instrument was the primary consideration in the decision of whether or not to adopt instrument modifications. In particular, modifications to the focal plane assemblies, with their interference filters and detectors, were deemed to be at high risk. The focal planes were difficult to access, and the filters, once fixed in place with epoxy, were too fragile to be removed and replaced. In addition, corrections requiring major modifications to the instrument were rejected because of cost and schedule restrictions.

### 1.3 Document Overview

This document illustrates the magnitude of residual stray light (bright target response) in the completed SeaWiFS flight instrument. It provides procedures for reducing the effects of that stray light in the flight data, thereby

reducing the size of the stray light masks, and increasing the amount of usable data from the instrument. In Sections 2 and 3, a description of the instrument and a summary of the specification for BTR are presented. In Sections 4 and 5, two electronic modifications to the instrument to improve BTR response are discussed: the addition of bilinear gains to allow the detection of clouds, and the very large reduction in the electronic portion of the BTR tail. In Section 6, several stray light sources within the radiometer, and the modifications to the instrument that reduced their effects, are described. Section 7 provides a description of the post-modification stray light measurements. Section 8 uses the along-scan and along-track responses from Section 7 to create an informal stray light budget. Section 9 describes the procedure for the along-scan stray light correction based on laboratory measurements. Section 10 applies this procedure to laboratory scans of bright targets. And finally, in Sections 11 and 12, proposed schemes are given for applying the corrections to LAC and GAC scenes from SeaWiFS.

## 2. INSTRUMENT DESCRIPTION

The SeaWiFS instrument (Fig. 1) is designed to measure Earth-exiting radiances. The sensor's instantaneous field-of-view (IFOV) is  $1.6 \times 1.6$  mrad per pixel, with one

**Table 1.** Constants used in the calculation of the BTR limit in counts. The  $L_{\text{cloud}}$  and  $L_{\text{typical}}$  values come from the performance specifications (see Barnes et al. 1994a, Section 16). The slopes (or sensitivities for each band) come from the radiometric calibration of the instrument (Barnes et al. 1994b).

Band Number	$L_{\text{cloud}}\dagger$	$L_{\text{typical}}\dagger$	$L_{\text{cloud}}/L_{\text{typical}}$	Slope‡	0.5% $L_{\text{typical}}$ [counts]
1	60.0	9.10	6.59	0.0137	3.3
2	66.2	8.41	7.87	0.0134	3.1
3	68.2	6.56	10.4	0.0105	3.1
4	65.6	5.64	11.6	0.00920	3.1
5	65.2	4.57	14.3	0.00746	3.1
6	53.8	2.46	21.9	0.00425	2.9
7	43.0	1.61	26.7	0.00301	2.7
8	34.0	1.09	31.2	0.00215	2.5

†  $\text{mW cm}^{-2} \text{sr}^{-1} \mu\text{m}^{-1}$

‡  $\text{mW cm}^{-2} \text{sr}^{-1} \mu\text{m}^{-1} \text{count}^{-1}$

cross-track scan covering  $\pm 58.3^\circ$  about nadir. The scanner can be tilted to  $+20^\circ$ ,  $0^\circ$ , or  $-20^\circ$  relative to nadir to minimize the number of glint-contaminated measurements in the data. Each pixel value is digitized to 10-bit resolution.

In the instrument, light first strikes the primary mirror, an off-axis parabola, and is then reflected from a second surface polarization scrambler and the half-angle mirror before reaching the field stop. The half-angle mirror removes the rotation of the image due to the rotation of the telescope. This mirror rotates at exactly half the rate of the telescope and polarization scrambler, and uses alternating mirror sides on successive telescope scans. The field stop, located at the entrance to the aft optics, is 50% larger than the detectors and restricts stray light through the system. After the field stop, the light is collimated by another off-axis paraboloid and directed through the aft optics. Dichroic beam splitters divert the light into four focal plane assemblies, each containing two spectral bands delineated by narrow band filters in close proximity to the detector. The optical paths in the aft optics assembly are shown in Fig. 2.

Attention was given in the SeaWiFS design to minimizing the sensitivity of the instrument to polarized light. This is the main reason for the rotating telescope, rather than a rotating entrance mirror. There are other possible instrument designs with less mechanical complexity, but they require large incidence angles on one or more mirrors, producing unacceptable polarization variations along-scan, particularly for the SeaWiFS wavelengths in the blue (412 nm and 443 nm) spectrum. The SeaWiFS design minimizes the angle of light incident on its mirrors. In addition, SeaWiFS uses a polarization scrambler (see Figs. 1 and 2) to further reduce these variations. The scrambler eliminates the need for individual compensators to remove residual polarization at each focal plane assembly. The scrambler consists of two optical wedges that act as a variable wave plate to convert incident polarized light into several cycles of circular, horizontal, and vertical polarized

light across the scrambler's aperture. The sensitivity of the output of SeaWiFS to polarized light was measured in the laboratory, using a source producing plane-polarized light. The rotation of the polarized light through  $360^\circ$  produced changes of 0.25% or less in the eight SeaWiFS bands (Barnes et al. 1994a).

Two instrument bands, each with four detectors aligned in the scan direction, form a focal plane. The four detectors in each group are added using a time delay and integration (TDI) technique to improve signal-to-noise ratios (SNRs). The signal from each detector is amplified, processed through a selectable gain stage, and digitized with a 12-bit analog-to-digital (A/D) converter. The four digital words from a band are then appropriately delayed, summed to obtain the signal-to-noise advantage, truncated to 10 bits, and transmitted to SeaStar through the electronics module. A solar calibrator is mounted on the instrument, allowing the optical system to view a solar illuminated diffuser when passing over the South Pole. The entire spacecraft can be rotated to allow the instrument to view the nearly full moon, which is considered to be a stable calibration source to monitor the long-term repeatability of the SeaWiFS measurements (Woodward et al. 1993).

### 3. BRIGHT TARGET RECOVERY

The BTR specification has been described in the SeaWiFS Prelaunch Acceptance Report (Barnes et al. 1994a). Radiometric data should be relatively free of the effects of overshoot and ringing when the IFOV scans across a steep gradient in radiance, from a maximum of  $L_{\text{cloud}}$  to a minimum of  $L_{\text{typical}}$ . For this radiance step change, the output signal should settle to within 0.5% of its final value ( $L_{\text{typical}}$ ) within 10 pixels. This radiance limit, using values from the specifications, is given in counts in Table 1. It is given to one-tenth of a count since the values are small, relative to the quantization of the data.

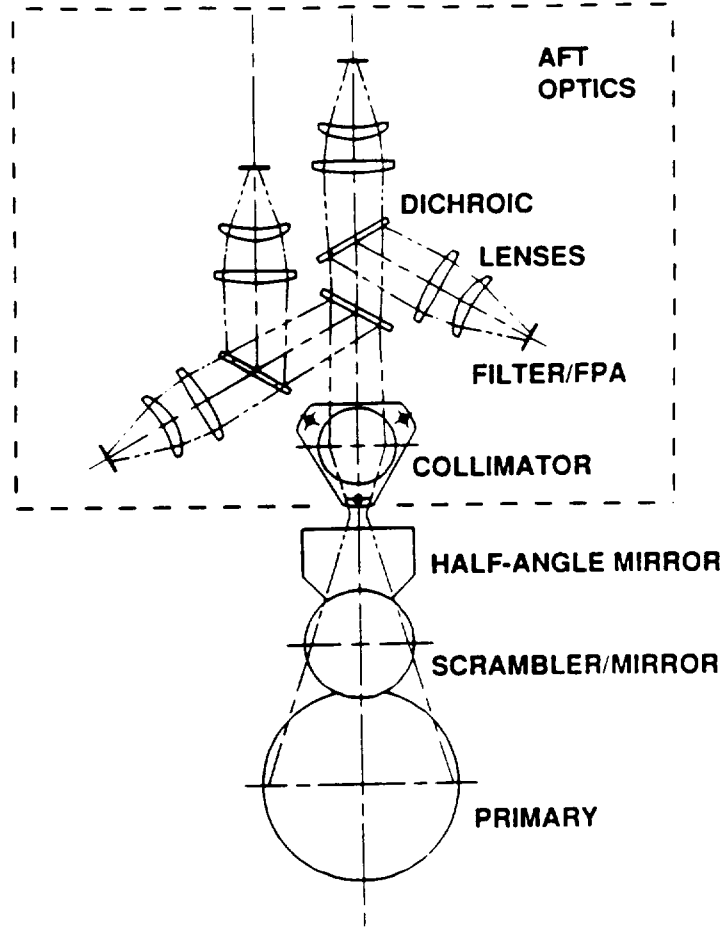


Fig. 2. Schematic diagram of the SeaWiFS aft optics assembly.

During the April 1993 SeaWiFS Preship Review, it was determined that the instrument did not meet the BTR specification. At that time, it was decided that the instrument manufacturer would rework SeaWiFS to improve its stray light characteristics. The results in Table 2 come from laboratory measurements, after the instrument modification, using the output of the SBRC integrating sphere (Barnes et al. 1994a). The measurements were made in four sets, one for each focal plane, using a 3 pixel wide slit. Color glass filters were placed over the output from the sphere to give a spectral shape approximating that of the sun over the wavelength range of the bands on each of the four focal planes.

The results in Table 2 give the distance in pixels required for the instrument to settle to less than 0.5% of  $L_{\text{typical}}$  using the counts given in Table 1. For bands 1–5, the results give the number of pixels required to settle to 3 counts above background. For bands 6–8, the results give the number of pixels required to settle to 2 counts. Table 2 also gives the number of pixels required for the instrument to settle to zero counts after illumination by the slit. All

eight bands settle to within the specification limit within 10 pixels.

**Table 2.** SeaWiFS BTR characteristics. The table gives the number of pixels after the slit ( $P_{\text{slit}}$ ) for the instrument to return to the residual counts allowed in the specification. In addition, the table gives the number of pixels required for the instrument to settle to a level of zero residual counts ( $P_{\text{zero}}$ ). This material is taken from Barnes et al. (1994a).

Band No.	0.5% $L_{\text{typical}}$ [counts]	$P_{\text{slit}}$ [pixels]	Zero Resid. [counts]	$P_{\text{zero}}$ [pixels]
1	3.3	6	0	10
2	3.1	5	0	9
3	3.1	7	0	10
4	3.1	5	0	15
5	3.1	9	0	15
6	2.9	7	0	9
7	2.7	9	0	11
8	2.5	7	0	10

## 4. BILINEAR GAINS

Tests of the instrument have revealed that SeaWiFS measurements will be contaminated by stray light from clouds in adjacent pixels. These tests also showed the stray light contamination to be essentially proportional to the brightness of the adjacent cloud. In order to perform post-launch corrections, the brightness of the clouds must be measured; therefore, SBRC changed the sensor's electronics to allow on-orbit measurements of cloud radiances. These changes maintain the sensitivity of the SeaWiFS ocean measurements, as specified in the requirements for the instrument.

The new electronic configuration uses the four detector circuits in each SeaWiFS band to create bands with bilinear gains. The response for SeaWiFS band 1 (442 nm) is shown in Fig. 3. The channel's high sensitivity, i.e., a few  $\text{mW cm}^{-2} \text{sr}^{-1} \mu\text{m}^{-1} \text{count}^{-1}$ , extends over three-quarters of the band's dynamic range. Above this point, the channel's sensitivity is reduced, allowing the measurement of cloud radiances up to  $60 \text{ mW cm}^{-2} \text{sr}^{-1} \mu\text{m}^{-1}$  (see Fig. 3a). For ocean measurements, the band will have the same response as the original linear gains over a reduced number of counts, i.e., over a reduced dynamic range (see Fig. 3b).

The operation of the four channels in a SeaWiFS band can be illustrated using the radiance levels for band 1. The values for this band are given in Table 3. In Tables 3–6, the process of calculating the knee and endpoint locations for the bilinear gains of SeaWiFS band 1 is shown. The values are given for science gain 1—the standard gain for SeaWiFS ocean measurements—and are given using the output from the band's four channels. This is the standard detector configuration for the instrument. The input radiances, counts, and zero offsets (see Table 3) come from radiometric tests of the instrument found in the SeaWiFS Calibration and Acceptance Data Package (SCADP). The SCADP was generated by SBRC in the course of the characterization and calibration of the SeaWiFS instrument. With the zero offsets removed, the net counts, along with the sphere radiance, are used to calculate the sensitivity, or slope, for each channel (Table 3). Channel 1, with low sensitivity, allows measurement of the high radiances from clouds. Channels 2, 3, and 4, with high sensitivities, allow measurements of the low radiances from oceans. These sensitivities (in mW of radiance per count) are fundamental to the calibration of SeaWiFS. They convert the counts from the instrument into radiances at the instrument's optical input.

The SeaWiFS channels are digitized at 10 bits, and each channel's output ranges from 0–1,023 counts. When the zero offsets are removed, the saturation counts for the four channels in SeaWiFS band 1 range from 1,000–1,005 counts (see Table 4). From these saturation counts and the sensitivities for the channels, it is possible to calculate the saturation radiances for each channel (Table 4). For radiances greater than the saturation radiances, the output

from the SeaWiFS channels will remain at their saturation count levels.

The saturation radiances in Table 4 give the three knee radiances and the maximum radiance for band 1 (gain 1). The knee radiance is the point at which the high sensitivity channels saturate, and the saturation radiance is the point at which the low sensitivity channel saturates. The minimum radiance is zero for zero counts, i.e., for zero counts after the removal of the offset. Using the saturation radiance levels and the sensitivities, it is possible to calculate the number of counts from each channel at the three knees and the two endpoints of the bilinear gains (Table 5). The counts from the four channels are summed and divided by four in Table 5; this models the process performed within SeaWiFS. On orbit, the output from the channels (as selected by the instrument's electronics, based on commands from the ground) will be summed; the result will be sent from SeaWiFS to the SeaStar spacecraft. This digital output is sent, minus its two least significant bits; in other words, it will be sent from the instrument to the spacecraft after division by 4.

The radiances and counts at the three knees and the two endpoints are given in Table 6. For these calculations (and as is recommended for on-orbit operations) the zero offsets are removed at the start of the calculations. This initial step opens up a direct relationship between counts and radiances for ocean measurements. Below the first knee (in the radiance region for ocean measurements), Table 5 gives the information for calculating the sensitivity of band 1:  $10.899/793.64$ , or  $0.013773 \text{ mW/count}$ . Above the third knee (in the radiance region for cloud measurements), the sensitivity is  $0.240158 \text{ mW/count}$ , calculated as  $(60.159 - 11.049)/(1002.25 - 797.76)$ . The ocean portion of the bilinear gain is 17.5 times more sensitive than the cloud portion. This difference in sensitivities becomes greater in sequence for bands 2–8.

The effect of slightly different sensitivities in the three high sensitivity channels is shown in Fig. 4. In this case, the knee is not sharp, but it has two internal segments, rather than just one segment before and one segment after. This results in a region of uncertainty in the transition between the ocean and cloud sensitivity regimes. The revised electronic configuration that gives SeaWiFS the ability to detect clouds also defines the method in which the knees for the bilinear gains are calculated (Tables 3–6). If the detector configuration for a band is changed, then the knees for the bilinear gains must be recalculated.

## 5. ELECTRONIC RECOVERY TAIL

Each SeaWiFS band has an electronic offset of approximately 20 counts. This zero offset is necessary to guarantee that the instrument can measure down to zero light. A schematic drawing of the input circuitry for each A/D converter is shown in Fig. 5. In this circuitry, the zero offset (called the bipolar offset) and the input signal enter the A/D converter on different pins. Within the A/D

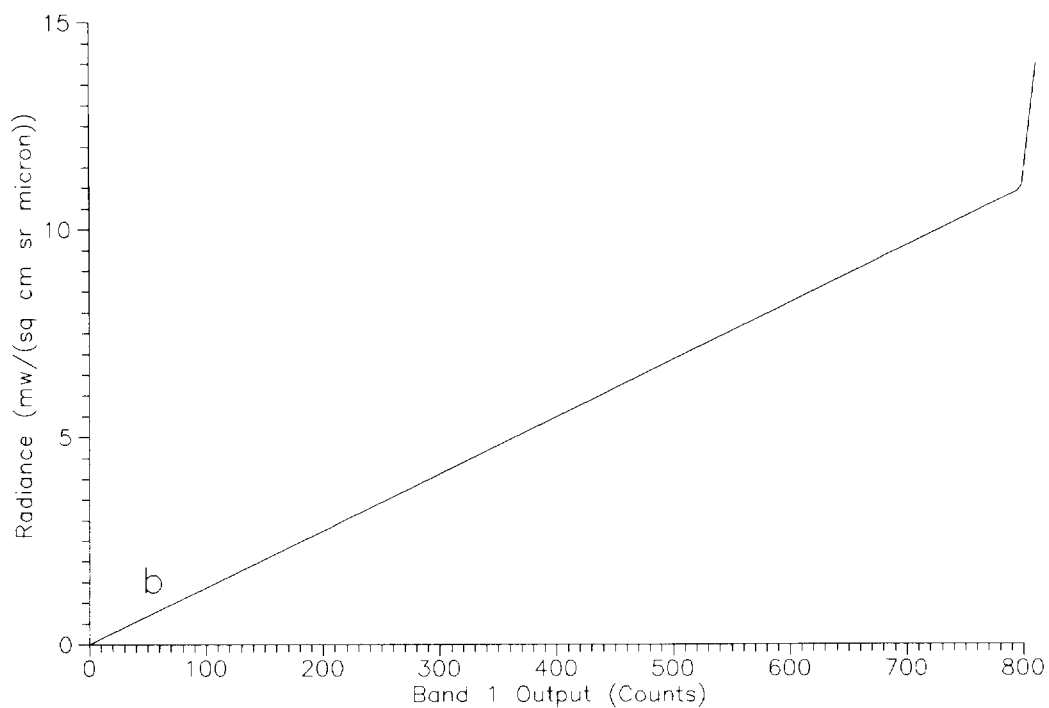
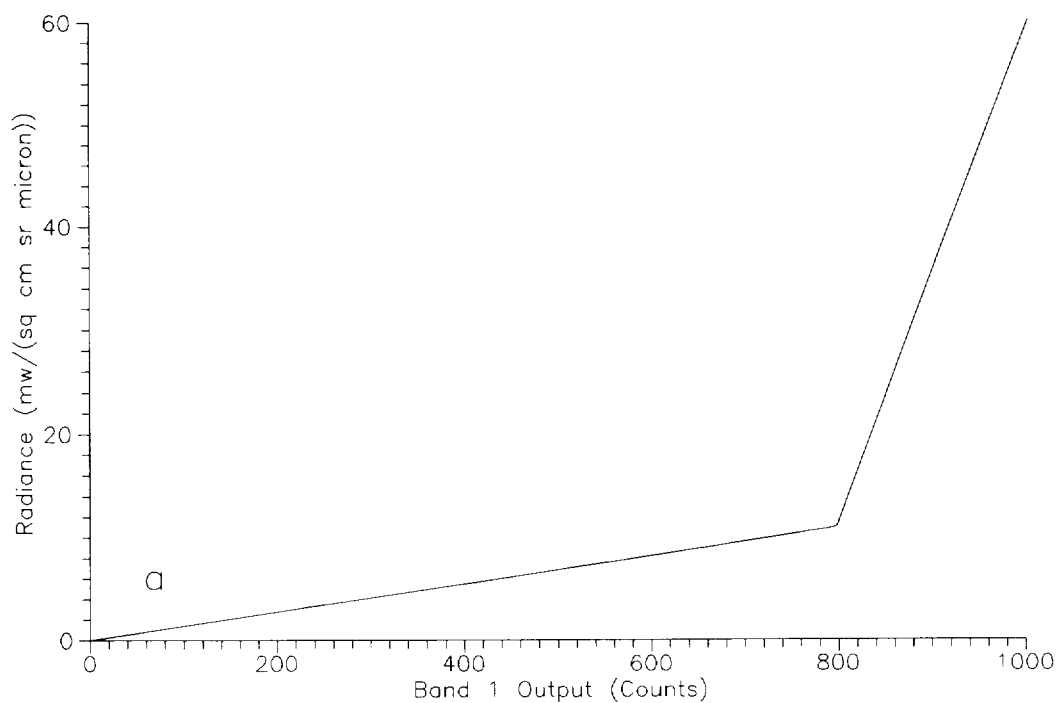


**Fig. 3.** The instrument response for SeaWiFS band 1 with a bilinear gain. a) The response from 0–1,000 counts is displayed. The slope from 0–800 counts shows greater sensitivity, i.e., fewer radiance units per count. b) The response from 0–800 counts is displayed. This is the working range for ocean measurements from band 1.

**Table 3.** The input values and calculated sensitivities for the four channels of band 1. The sensitivities are calculated from the sphere radiances and net counts.

<i>Channel Number</i>	<i>Radiance [mW]</i>	<i>Measurement [counts]</i>	<i>Offset [counts]</i>	<i>Net Counts</i>	<i>Sensitivity [mW/count]</i>
1	9.246	175	21	154	0.060039
2	9.246	871	23	848	0.010903
3	9.246	859	18	841	0.010994
4	9.246	871	21	850	0.010878

**Table 4.** Saturation counts and saturation radiances for the four channels. The saturation radiances are calculated from the saturation counts and the sensitivities. The offset has been removed from both the zero and saturation counts.

<i>Channel Number</i>	<i>Zero</i>	<i>Saturation Counts</i>	<i>Saturation Radiance [mW]</i>
1	0	1,002	60.159
2	0	1,000	10.903
3	0	1,005	11.049
4	0	1,002	10.899

**Table 5.** Calculated instrument output at the saturation radiances for the four channels, in counts. The counts at the knees are calculated from the knee radiances and the sensitivities. The total counts for each channel cannot exceed the saturation counts.

<i>Channel Number</i>	<i>Zero</i>	<i>Knee 1</i>	<i>Knee 2</i>	<i>Knee 3</i>	<i>Saturation</i>
1	0.00	181.54	181.60	184.03	1,002.00
2	0.00	999.64	1,000.00	1,000.00	1,000.00
3	0.00	991.39	991.75	1,005.00	1,005.00
4	0.00	1,002.00	1,002.00	1,002.00	1,002.00
<i>Sum</i>	0.00	3,174.57	3,175.35	3,191.03	4,009.00
<i>Sum/4</i>	0.00	793.64	793.84	797.76	1,002.25
<i>Radiance [mW]</i>	0.00	10.90	10.90	11.05	60.16

**Table 6.** Knees and endpoint locations for the bilinear gains. These are the values in the last two rows of Table 5.

<i>Location</i>	<i>Radiance [mW]</i>	<i>Counts</i>
Zero	0.000	0.00
Knee 1	10.899	793.64
Knee 2	10.903	793.84
Knee 3	11.049	797.76
Saturation	60.159	1,002.25

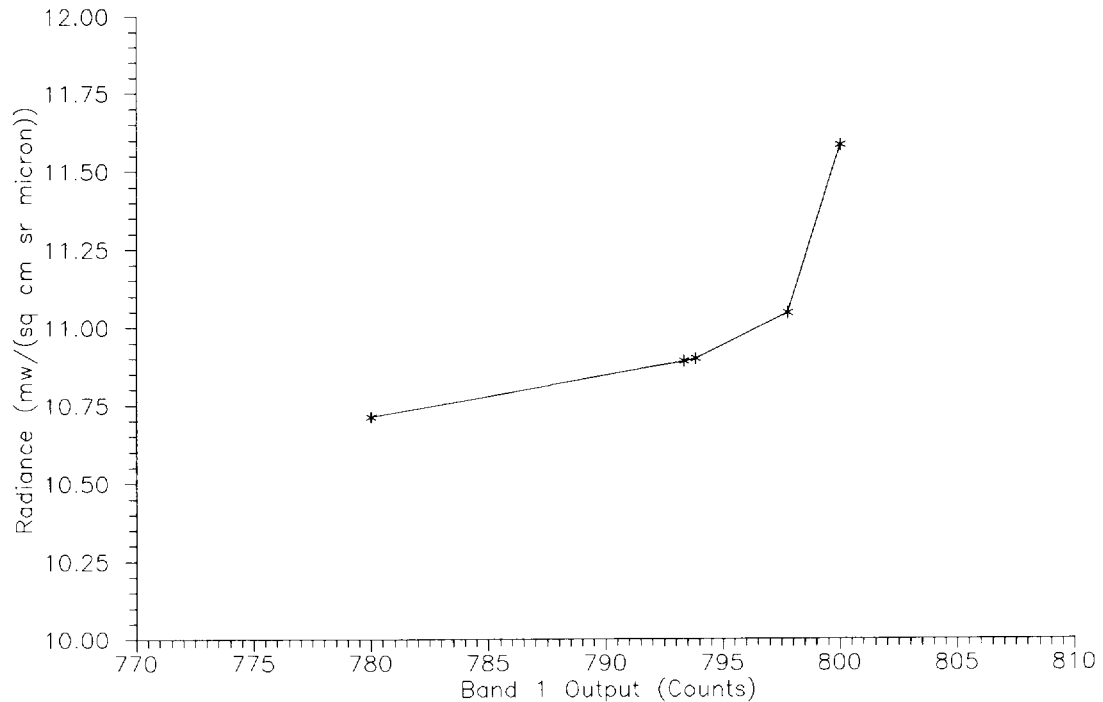


**Fig. 4.** An expanded view of the change in slope of the bilinear gain for band 1. The figure shows the effect of differences in the sensitivities of the three high sensitivity channels. The two segments between 793 and 798 nm are created as the two higher sensitivity channels saturate in turn. For *real world* measurements, the change in slope does not occur at one radiance level only.

converter, however, the two voltages are summed at the input to the converter's sample and hold circuit. This summation point couples the responses of the two circuits with each other. In the original design for the SeaWiFS electronics, the zero offset was 5 counts, instead of the 20 counts in the final design. The size of the offset in the A/D circuitry is determined by the size of resistor R115 (see Fig. 5). The original design also had a capacitor (C40) in parallel with resistor R115. This resistor-capacitor (RC) pair comprises a standard type of electronic filter to reduce high frequency noise. The circuit was designed with a capacitance for C40 of  $1 \mu\text{F}$ . The residual stray capacitances in the circuit are on the order of picofarads, smaller by 4–5 orders of magnitude than C40. For SeaWiFS, this circuit was originally included to remove possible high-frequency noise in the zero offset, even though the zener diode was expected to produce a quiet voltage level.

This RC pair also has a time period for response to sharp voltage changes. This time constant is determined by the product of the resistance and the capacitance in the RC circuit. The constant gives the time period for the voltage in the RC circuit to adjust to  $[1 - e^{-1}]$ , or 63%, of the voltage difference (Diefenderfer 1972). For SeaWiFS, such a voltage change occurs when the instrument scans

from a bright cloud to the dark surface of the ocean. During measurements of the bright cloud, the large voltage of the input signal into the A/D converter is coupled to the RC circuit through the A/D bipolar offset. The capacitor charges to that voltage over several time constants. When the input voltage drops as the instrument scans onto the comparatively *dark* ocean, the capacitor then discharges to the original level over several time constants. For the original design, the resistor was set to give a voltage equivalent to 5 counts. Along with C40, this gave a time constant that is 0.25 of the measurement period for a SeaWiFS pixel. That measurement period is  $42 \times 10^{-6}$  s (Barnes et al. 1994a). After one measurement period, or four time constants, the RC circuit in the original design would have a voltage within 2% of the input voltage from the comparatively dark ocean. After two measurement periods, or eight time constants, the voltage would settle to 0.03% of the ocean value.

When the instrument was modified to give a 20 count offset, the resistance of resistor R115 was increased by a factor of four. During this modification, the capacitor was unchanged; as a result, the RC time constant was multiplied by 4. Thus, during initial testing of the radiometer in the SPR, there were very small, but noticeable, electronic

tails from the RC circuits in the BTR test results. For example, for SeaWiFS band 8 the residual electronic tail at 10 pixels from the bright source was approximately 1 count; in this case, the tail was about 40% of the allowed BTR response. As part of the stray light modifications in the SPMPR, capacitor C40 was clipped from all of the zero offset circuits in the instrument. This change has reduced the electronic portion of the instrument's bright target response to an insignificant level. Although other capacitances remain in the circuit, the electronic recovery tail has been reduced by more than two orders of magnitude. Measurements of the system noise in SeaWiFS have not indicated any problems from the removal of the C40 capacitors; the SNRs for all bands significantly exceed the specification requirements (Barnes et al. 1994a).

There is an additional interesting characteristic of the zero offset circuits. There are 32 detectors in SeaWiFS, but only 16 offset circuits; thus, each band has two offset circuits for four detectors. In each band, the endmost detectors—detectors 1 and 4—share the same offset circuit with the adjacent detectors, detectors 2 and 3, respectively. This causes a coupling of pairs of detectors through the offset circuit—an intraband electronic cross talk. The effect is short range, covering only 1–2 pixels, and is part of the system level response to performance tests, such as the line spread functions used to determine the modulation transfer function (MTF) (Barnes et al. 1994a). Intraband electronic cross talk is a component of the MTF and does not play an independent role in the instrument's BTR.

## 6. STRAY LIGHT SOURCES

In the SSLSP, SBRC presented a description of the stray light paths within the SeaWiFS radiometer and a set of recommended changes to reduce stray light in the instrument. The SBRC analysis showed several stray light paths located in the instrument's along-scan direction. In addition, there was one significant stray light path in the direction perpendicular to the instrument's scan, i.e., in the along-track direction. This source (secondary reflections from the polarization scrambler) is discussed in Section 6.2.

Individual sources of stray light are discussed here in Section 6. The instrument's stray light response, based on the response to a 1 pixel wide bright source, is given in Section 7. Those results are used as the basis for an informal stray light budget (Section 8) that gives the ranges (in pixels) over which the principal stray light sources contribute to the instrument's response.

The response of the instrument, along with the stray light sources in the along-scan direction, is shown in Fig. 6. The figure shows the instrument response before modifications were made to ameliorate the bright target response in the instrument; thus, this figure also shows the effect of the electronic tail that was described in the preceding section. Figure 6 shows the stray light signal paths for the

four even bands in the instrument. As described earlier, SeaWiFS has four focal planes, each focal plane containing two bands. With regard to the scan direction of the instrument, the odd bands on each focal plane are located before the even bands, i.e., light from a ground or ocean target will strike the odd band on a focal plane before it strikes the even band. This creates an asymmetry in the stray light response for the even and odd bands on a focal plane. The odd bands experience more stray light after, i.e., down scan of, a cloud than they do before the cloud. The additional stray light comes from interband (between band) optical cross talk from the even band on the focal plane. Conversely, the even bands experience more stray light before, i.e., up scan of, a cloud than after; again, this is due to optical cross talk. The effects of cross talk are described in more detail in Section 6.5.

Figure 7 gives an example of the stray light paths for one of the even SeaWiFS bands. As discussed above, most of the stray light paths in an even band contribute to the response before a bright source. The use of an even band has an advantage for the example in Fig. 6, since the effect of the premodification electronic tail is isolated after the bright source, so it, and the stray light effects, can be shown separately.

The data in Fig. 6 are the recorded values from the instrument as it viewed a bright slit 6 pixels wide. These data have not been taken from the digital output of the sensor, as the resolution of the standard digital output does not have the sensitivity to distinguish the very small radiances that exist several pixels away from the source. They lie below the quantization limit of the digital data. For the test results in Fig. 6, the output from the band was measured with a lock-in amplifier and a voltmeter. Using several sensitivity ranges for the amplifier, it was possible to obtain the dynamic range required to measure the band's output over five orders of magnitude.

Each of the stray light paths in Fig. 6 is discussed in the sections that follow. In addition, one section includes a discussion of the secondary reflections from the polarization scrambler. The discussion sequence duplicates the path of the radiance transmitted through the instrument, from the primary mirror into the focal plane assemblies.

### 6.1 Primary Mirror Scatter

Primary mirror scatter is a minor contributor to stray light over the range of pixels shown in Fig. 6. To the right (down scan) of the bright source, the premodification electronic tail provides the major portion of the residual signal. With the removal of the electronic tail, the other stray light sources still dominate over primary mirror scatter, as they do to the left (up scan) of the bright source. For this reason, it was decided to retain the original primary mirror in the radiometer, rather than to install a mirror with reduced scatter. Primary mirror scatter, however, remains a contributor to the optical blur near the bright source in

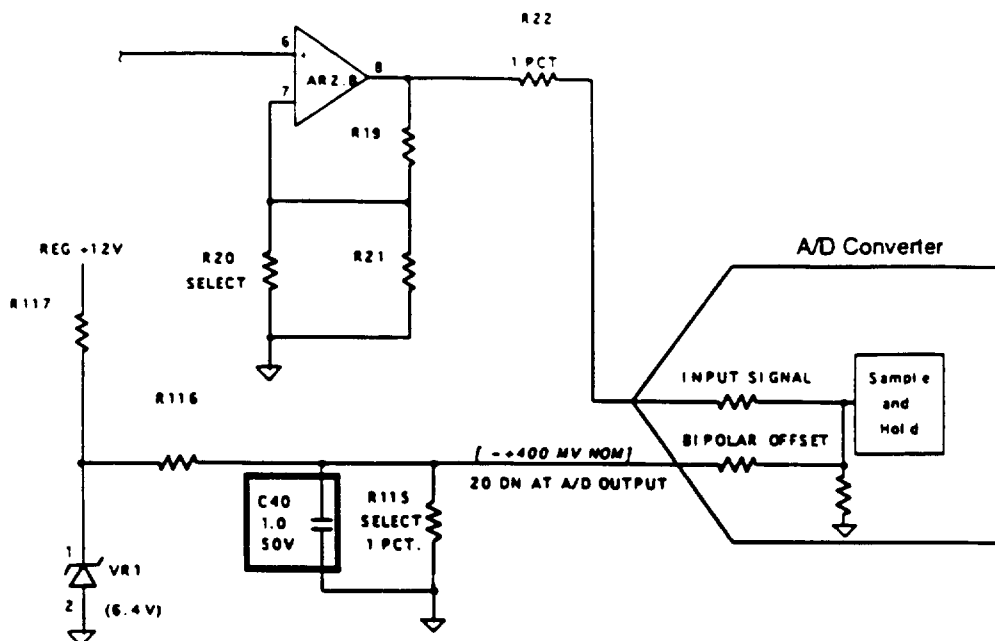


Fig. 5. Zero offset circuitry for each SeaWiFS channel. There are 16 of these circuits in the SeaWiFS electronics. The bipolar offset creates a constant voltage that gives a 20 count offset in the output from the A/D converter. Capacitor C40 in each circuit created an electronic tail in each channel's response to bright targets. As part of instrument modifications to improve the sensor's response to stray light, this capacitor has been removed from all of the SeaWiFS circuits.

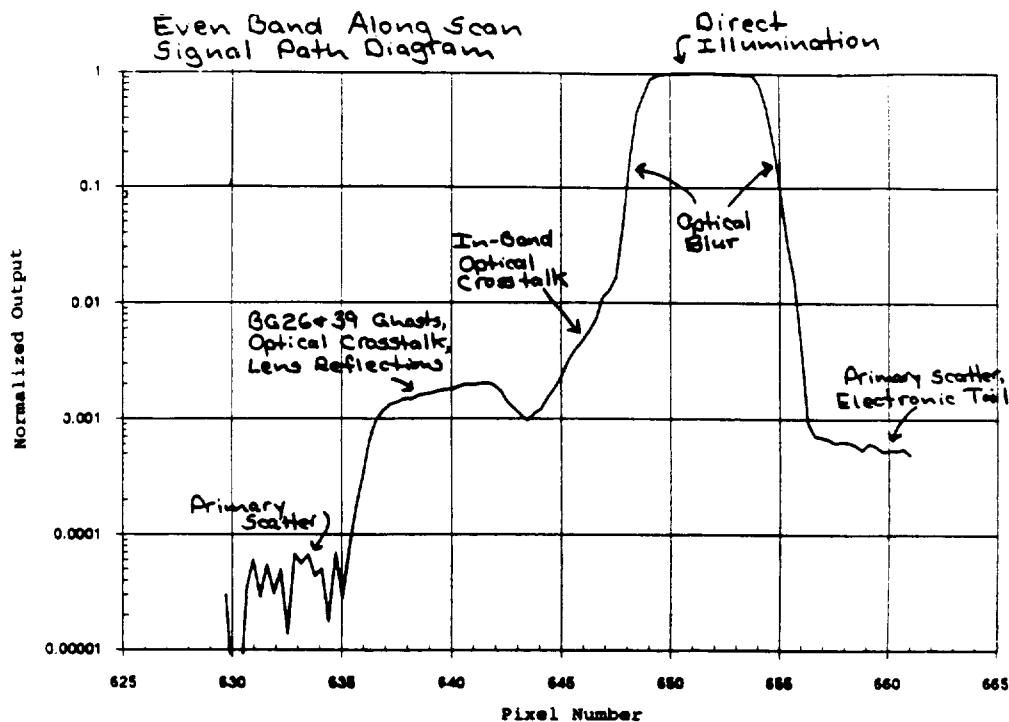


Fig. 6. Stray light paths in the SeaWiFS radiometer. For the even band in this example, the dominant stray light sources occur before the bright source. For odd bands, the dominant sources occur after the bright source.

Fig. 6, and contributes to scatter from other stray light sources farther out.

Additional measurements of stray light, not shown here, were made at distances of up to 35 pixels from the bright source. These so-called *deep scans* in the along-scan and along-track directions show residual scattered light from the primary mirror to be five orders of magnitude below the bright source radiance. From these measurements, it is possible to calculate the bidirectional reflectance distribution function (BRDF) for the primary mirror:

$$R_B = 1.93e^{-61.5\alpha}, \quad (1)$$

where  $R_B$  is the BRDF, and  $\alpha$  is the off-axis angle, in radians, as documented in the SSLSP.

For large area bright targets outside the instrument's field of view (FOV), the scattered light from the mirror sums and can become a substantial stray light source. There is an aperture at the instrument's optical inlet (see Fig. 2). This aperture attenuates radiance at the primary mirror for angles equal to 60 SeaWiFS pixels and greater. The effect of light, well outside the FOV from clouds, should resemble the effect of light within the instrument's FOV that has been scattered from atmospheric aerosols. In flight, these instrumental and atmospheric effects may be very difficult to separate.

## 6.2 Polarization Scrambler Reflections

The polarization scrambler consists of two crystalline magnesium fluoride ( $MgF_2$ ) wedges with a reflective coating on the lower surface. The scrambler acts as a second surface mirror in the SeaWiFS optical train. The  $MgF_2$  wedges in the scrambler create several cycles of varying polarization in the reflected light across its aperture. The incorporation of this scrambler into a design based on a rotating telescope has reduced the residual polarization in SeaWiFS to 0.25% or less for all eight bands (Barnes et al. 1994a).

The original design of the polarization scrambler, as described in the SeaWiFS Critical Design Review (SCDR) held at SBRC, produced two secondary reflections that straddle the image in the along-track direction. The secondary reflections from that design were located about 5 pixels from the center, and had an intensity about 0.5% of that in the central pixel, as documented in the SSLSP. These along-track secondary reflections are shown in Fig. 7. Figure 7 also shows the response of the polarization scrambler plus the response of a mirror that was substituted for the scrambler.

As part of the instrument modifications to remove stray light, the original polarization scrambler was replaced with a modified unit. The front surface of the modified polarization scrambler was given a very slight wedge, relative to the mirrored back surface of the scrambler. The geometry of the new scrambler collapses the secondary reflections

onto the image from the central pixel at the optical stop in the optical inlet for the aft optics (Fig. 8). Although it may not be immediately obvious from the figure, ray traces predicted the effect in the improved geometry. In addition, post-modification testing using a laser light source showed the reflections to converge onto the central beam as a cardboard target was moved away from the scrambler. The post-modification testing also showed no secondary reflections from the scrambler in the along-scan direction.

## 6.3 BG26 and BG39 Filter Reflections

There are two broadband glass color filters in the SeaWiFS aft optics assembly (Fig. 2). These filters (Schott catalog numbers BG26 and BG39) play an important role in the laboratory calibration of the radiometer (Barnes et al. 1994b). Reflections from these filters (referred to as *ghosts* in Fig. 6) combine with both in-band optical cross talk and the reflections from the final focusing lenses in a region located 5–12 pixels from the edge of the bright source. The reflections from the color filters are thought to be far out of focus and very diffuse at the detectors—diffuse to the point that they do not have the characteristics of an image. Although referred to as *ghosts*, they are actually more characteristic of stray light. Lens reflections and optical cross talk are discussed in the following sections. The sum of these three stray light sources gives a signal that is about 0.2% the magnitude of the bright source. In the laboratory testing of stray light in SeaWiFS, there was no effort to separate the stray light from these sources.

The *ghosts* from the broadband filters are reflections from their optical surfaces of the upwelling light from the focal plane assemblies (see Fig. 2). The source of this upwelling light is reflections off the interference filters on the focal planes. These interference filters are all of dichroic design without components that absorb light. They either transmit or reflect the incoming radiation (Barnes et al. 1994b). Thus, the path for these *ghosts* is reflection from the interference filters, reflection from the broadband filters, and transmission back through the interference filters.

As part of the instrument changes to ameliorate stray light in the instrument, modifications were made to the mounting rings for the two broadband absorptive filters. The new mounting rings tilted the filters by about 5° from the optical path, moving the reflections away from the focal planes. Since the responses of the filters are very broad (Barnes et al. 1994b), this modification created no significant effect in the spectral response of the radiometer.

## 6.4 Focusing Lens Reflections

A diagram of one SeaWiFS focal plane assembly is shown in Fig. 9. This figure includes the focusing lenses associated with each assembly. The path for *ghosts* from these lenses is similar to that for the broadband filters, with reflections off the interference filters, to the lenses,

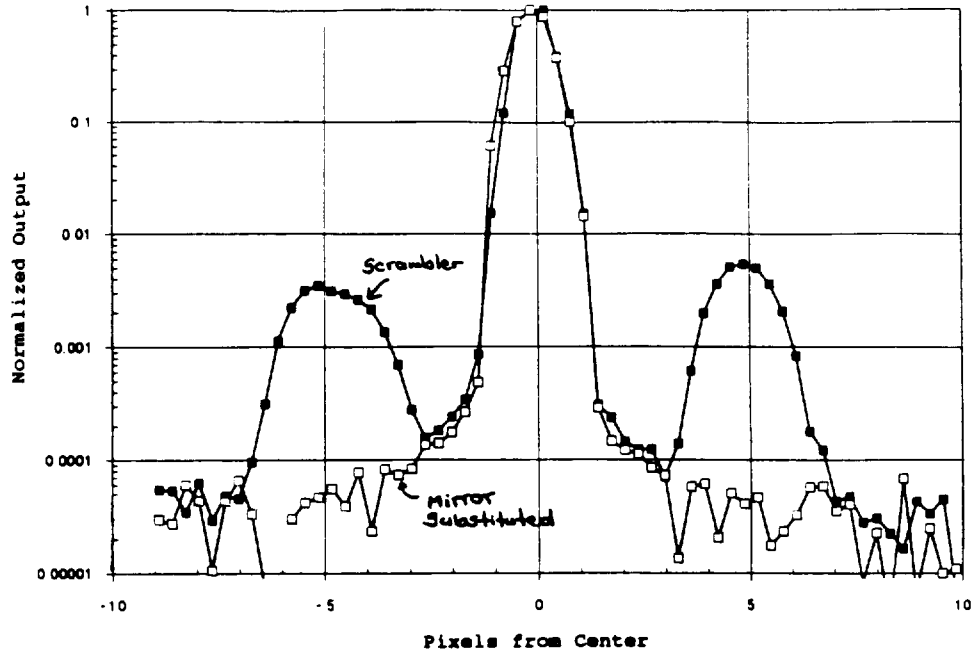


**Fig. 7.** Secondary reflections from the scrambler in the along-track direction. The secondary reflections (dark symbols) are displaced in the along-track direction. These stray light sources have magnitudes about 0.5% of that from the bright source. With the substitution of a mirror (open symbols), the secondary reflections in the along-track direction disappear. There is no sign of secondary reflections from the scrambler in the along-scan direction.

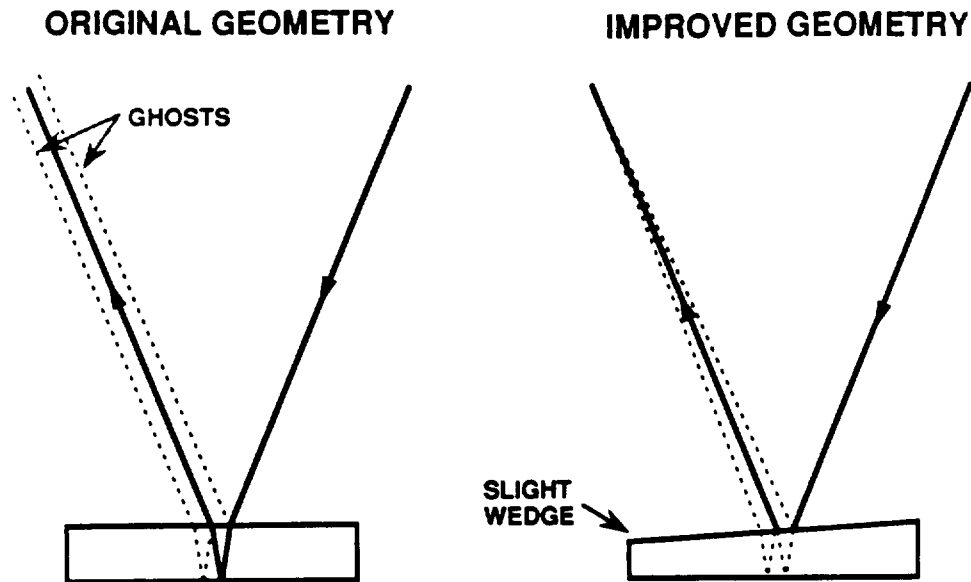


**Fig. 8.** Modification to the polarization scrambler. The original geometry for the scrambler produced two secondary reflections in the along-track direction. The improved geometry incorporates a slight wedge in the along-track direction. This wedge causes the reflections to collapse onto the central image at the optical stop at the entrance to the aft optics. The reflections, called *ghosts* in the figure, are diffuse and unfocused.

and back through the interference filters to the detectors. The effect of reflections from the focusing lenses is potentially much more severe than for the broadband filters; but for SeaWiFS, the lens reflections are severely out of focus at the detectors. Indeed, all of the stray light *ghosts* within SeaWiFS are well out of focus and extremely diffuse.

This possibility was considered in the initial design of the radiometer found in the SCDR from SBRC. For that reason, the focusing lenses were given a general antireflection coating; however, these coatings were not optimized for individual focal planes. As part of the testing of stray light within the instrument, there was a spectral scan of one of the lenses in the same lot as the flight parts. Over the range of wavelengths measured by SeaWiFS, the reflectances of the lenses were less than 2%. It was decided that the minor reduction in stray light, which might result from special tailoring of the antireflection coatings of the lenses, was not worth the risk that would accompany the removal and replacement of the lenses in the focal plane assemblies. Changes to the focusing lenses, therefore, were not part of the modifications to ameliorate stray light within the radiometer.

## 6.5 Optical Cross Talk Between Bands

The SeaWiFS instrument is designed with two bands on each focal plane assembly. The bands are placed end-to-end with a saw cut between the two detector arrays (see Fig. 10). The two interference filters that cover each focal plane are connected over the saw cut with black epoxy. In the SeaWiFS focal plane assemblies, there are open spaces between the black epoxy joints and the saw cuts. These open spaces provide paths for optical cross talk between bands. The SeaWiFS interference filters do not absorb light—they either transmit or reflect it. The wires, bond pads, and the light shield metallization around the detectors in each band, are gold or aluminum and provide shiny surfaces to reflect light. The active surfaces on the detector arrays are either a dull or glossy black. For the most part, light that is reflected from the surface of a SeaWiFS detector array will pass back through the interference filter (Fig. 10). This is particularly true for wavelengths where the transmission of the filter is nearly 100%. There are, however, wavelengths where the transmission of the interference filters are a few percent or less. Any light that is transmitted through the filter at these wavelengths can reflect from the bottom of the filter. This reflected light can bounce between the detector arrays and the filters in an alternating fashion until it is absorbed by the array or transmitted through the filter.

In this manner, a very small amount of light can pass between the bands on a focal plane assembly. Since the two interference filters on a focal plane transmit at different wavelengths, light passing between bands can encounter a near perfect reflecting surface from the filter of the other band. It is estimated that 15 reflections are required for

specular optical cross talk to occur. The light shield metallization around the detectors is somewhat rough, so the primary source of optical cross talk is probably a single, low angle reflection between bands.

Between-band cross talk can be removed by placing a septum below the junction between the filters. Such a septum would have been reasonably simple to fabricate during the initial construction of the radiometer. In this process, the filters would have been joined with an excess of black epoxy hanging below the junction between the filters; whereupon the epoxy would have been trimmed so it would reach from the filter junction to a point just above the sawcut between the detector arrays (Fig. 10). This septum would have blocked the optical path between the two bands on each focal plane. The SeaWiFS interference filters, however, have long since been epoxied into place. Their removal is exceptionally difficult and risky. This fact was demonstrated experimentally during the thermal vacuum testing of SeaWiFS in the spring of 1993. At that time, the focal plane assembly for bands 5 and 6 failed because of an electrical problem (Barnes et al. 1994b). When the band 5 interference filter was removed, i.e., dug out from the focal plane assembly, it was chipped and had to be replaced. Added cost, and the potential for delays in fabrication and instrument delivery, as well as a subsequent launch delay could have resulted from further operations on the filters. Based on this evidence, it was decided to leave the status quo. Septa were not added to the focal plane assemblies.

Optical cross talk between bands on a focal plane assembly is a function of the spectral shape of the measured radiance, in addition to the stray light characteristics of the instrument. The bright sources within the set of ocean measurements are clouds and, in the near-infrared, land and vegetation. For the purposes here, clouds are considered to be white, i.e., their reflective properties are almost spectrally flat over the wavelengths measured by SeaWiFS; thus, cloud radiances measured by SeaWiFS will have a spectral shape that very closely approximates the spectral shape of solar flux. This assumption is central to the post-modification measurements of residual stray light within the instrument. These measurements require the use of a light source that has the spectral shape of the sun. Since the tests are performed individually for the two bands on each focal plane assembly, the spectral shape must be maintained only over the wavelength range for each pair of bands. Additional spectral source shapes, such as those anticipated for land measurements, were not included in the stray light measurements at SBRC.

The selection of the low-sensitivity cloud channel for each SeaWiFS band was made with the effects of stray light in mind. SeaWiFS has been designed such that the outer detectors have reduced gain for cloud sensing. Channel 1 of each odd band is illuminated by a bright source first, and channel 4 of each even band is illuminated last. These are the low sensitivity cloud channels in SeaWiFS.

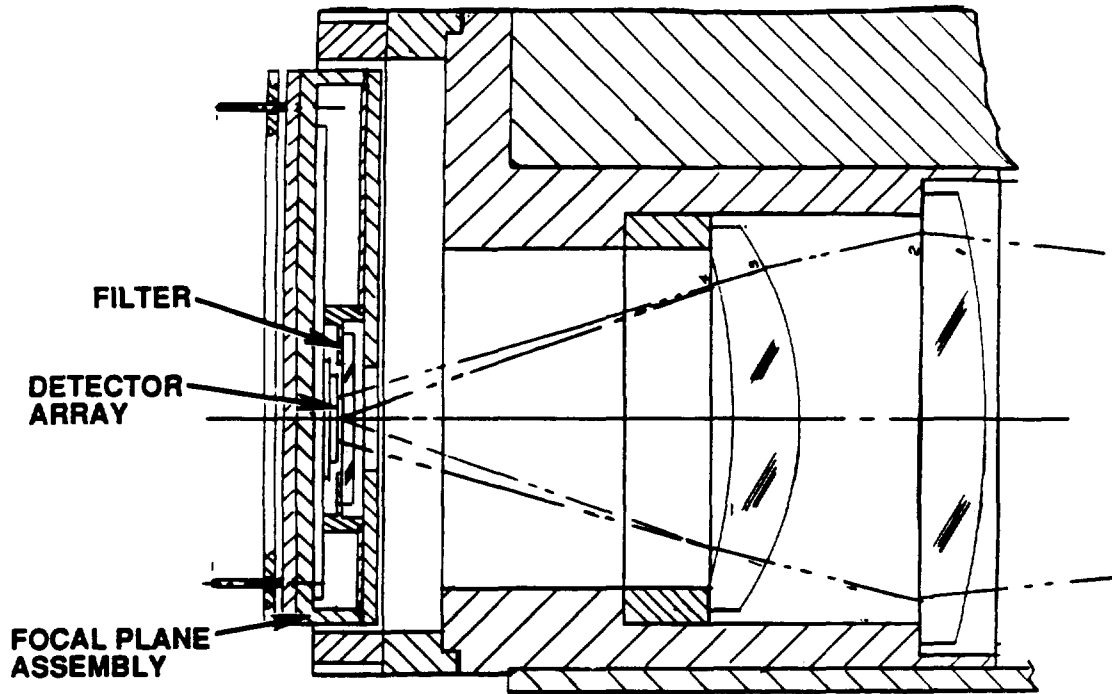


Fig. 9. A focal plane assembly and its focusing lenses. This entire structure can be removed from the instrument in one piece. The focal plane assembly contains two filters and two detector arrays. The focusing lenses are a minor source of stray light in the radiometer.

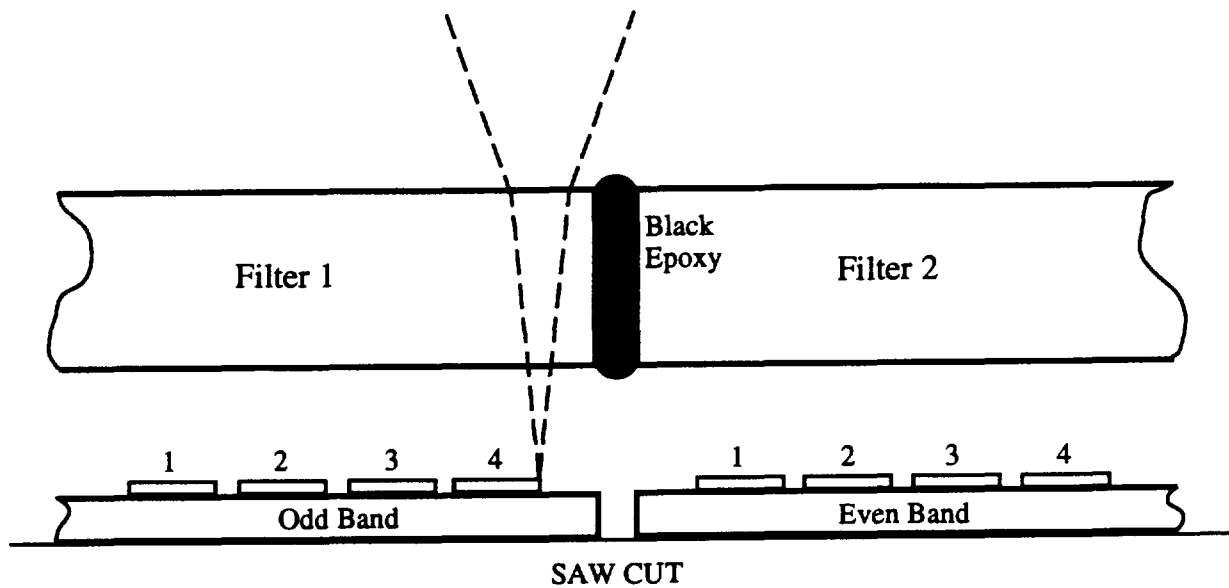


Fig. 10. The interference filters and detector array in a focal plane assembly. There are two bands within each assembly, and each filter covers the four detectors in a band. The odd band is located up scan of the even band. There is a pathway for optical cross talk between bands, with light reflecting in an alternating fashion between the underside of the filters and the surfaces of the detector arrays.

The optical cross talk described in this section dominates the asymmetric response to bright targets by SeaWiFS. Other, smaller sources of asymmetry also exist within the instrument. Successor instruments should be tested for those secondary asymmetric stray light sources.

## 6.6 Summary of Proposed Modifications

In the SSLSP, SBRC proposed a set of eight possible changes to ameliorate stray light in SeaWiFS, along with the risks to the instrument resulting from each. [These were presented at the Stray Light Paths Review at GSFC on 27 May 1993. The decision whether or not to implement these changes was made at the Performance Specification Modification Meeting at Orbital Sciences Corporation (OSC) 3 August 1993.] These possibilities and the decisions on their implementations are listed in Table 7.

**Table 7.** Possible stray light modifications to the SeaWiFS radiometer. Implemented modifications are denoted with a checkmark (✓). Those modifications that were not implemented are denoted with an ×.

Mod. No.	Possible Modification	Implementation
1	Tilt BG26 and BG39 filters.	✓
2	Add septa to focal planes.	×
3	Rotate filters (plus the addition of septa).	×
4	Add custom anti-reflection coatings on the final focusing lenses.	×
5	Add wedge to scrambler face.	✓
6	Replace primary mirror.	×
7	Eliminate electronic tail.	✓
8	Add cloud sensors.	✓

Among the possibilities discussed, is exchanging the positions of some of the filters, since the stray light responses of the even and the odd bands are different (Section 6.5). One of the principal data products from SeaWiFS measurements is the ratio of the response of band 2 (443 nm) to band 5 (555 nm). It would be possible for the filters for bands 5 and 6 to be interchanged, so that bands 2 and 5 would be in the even position on their respective focal planes. Then, both measurements in the band 2 to band 5 ratio would have similar stray light characteristics.

In a similar manner, the same effect could be obtained by interchanging the filters in the focal plane for bands 1 and 2, placing band 2 in the odd position on its focal plane. As discussed above, however, there is difficulty and risk in digging out the interference filters from their epoxy mountings; as with the proposal to add septa between the interference filters, this potential modification was not implemented.

During the period prior to the SeaWiFS Stray Light Paths Review in May 1993, a large number of scenarios were proposed to reduce the effects of stray light in the instrument. Many of these scenarios were summarized in an unpublished internal memorandum to the SeaWiFS Project (included in this document as Appendix A).

## 7. POST-MODIFICATION TESTS

Post-modification stray light measurements were performed as part of the stray light modifications to SeaWiFS (Barnes et al. 1994a). The measurements were made at several slit widths (in the along-scan direction) and at several slit heights (in the along-track direction). They were made with two sets of radiances to examine the linearity of the residual stray light with the intensity of the bright radiant source (see the SCADP). The measurements used the SBRC 100 cm spherical integrating sphere as the light source. Schott optical glass filters, placed in front of the exit port of the sphere, were used to obtain spectral shapes for each of the measurements approximating that for solar flux. The test apparatus is described in the following section.

### 7.1 Measurement Apparatus

The measurement apparatus for residual stray light in SeaWiFS is shown in Fig. 11. The apparatus consists of a target aperture on the exit port of the SBRC integrating sphere and a collimating lens. The 15.24 cm diameter of the lens provides a collimated output from the source that overfills the input aperture for SeaWiFS. The target aperture on the integrating sphere has been designed to hold both a 5.08×5.08 cm piece of optical colored glass and a target mask. The sphere is positioned a distance from the instrument such that a 2.92 mm wide slit in the target mask subtends an angle of 1.6 mrad, the angular width of a SeaWiFS pixel.

The vertical dimension of the opening in the target panel is equivalent to 10 SeaWiFS pixels. Target masks 1, 2, and 3 have widths equivalent to 1, 3, and 10 SeaWiFS pixels. Combined with the vertical dimension of the opening in the target panel, these masks produce images of 1×10, 3×10, and 10×10 pixels. Since SeaWiFS was positioned to scan in the horizontal during these measurements, the slit widths in the target masks determined the along-scan sizes of the test images, and the slit heights determined the along-track size.

Mask 4 was used for measurements of the along-track response of SeaWiFS. This mask produced an image of 1×3 pixels, with the along-track portion of the image 3 pixels in size. For the along-track measurements, a series of SeaWiFS scans were taken, with adjustments of the vertical position of the integrating sphere made using a screw crank. In the test procedure, the vertical position of the sphere was continuously adjusted by a distance equal to

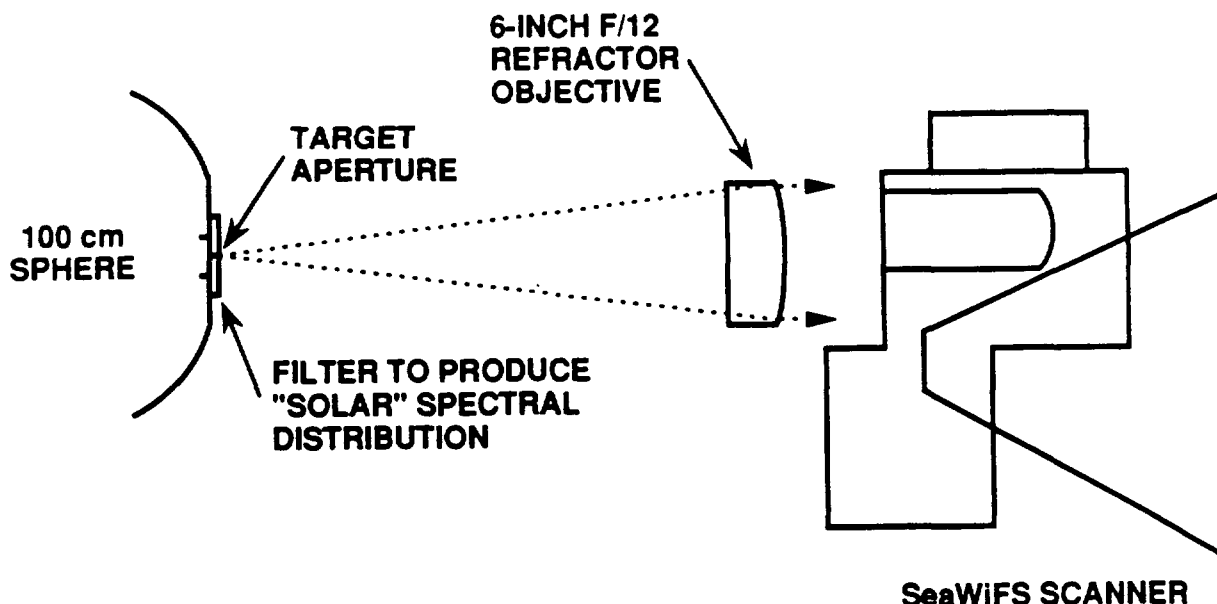


**Fig. 11.** The test apparatus for the measurement of residual stray light in SeaWiFS. The 15.24 cm, F/12 lens collimates the flux from the integrating sphere.

one-sixth of a SeaWiFS pixel between sets of scans by the sensor; thus, the along-track residual stray light measurements were oversampled by a factor of six.

## 7.2 Intensities of the Bright Sources

The SeaWiFS performance specifications require each SeaWiFS band to settle to a radiance value that is within a specified radiance step above the background ocean radiance. The size of that radiance step is 0.5% of the typical radiance ( $L_{\text{typical}}$ ) for that band (Barnes et al. 1994a). According to the specifications, the output from the sensor should meet that radiance level within 10 pixels of the edge of a bright source. The SeaWiFS BTR specification uses a percentage of the  $L_{\text{typical}}$  values, rather than an absolute set of radiances expressed in units of  $\text{mW cm}^{-2} \text{sr}^{-1} \mu\text{m}^{-1}$ . For that reason, the discussions of stray light in this document will refer to the bright radiances from the sources, and to the residual stray light radiances within the instrument, in terms of their  $L_{\text{typical}}$  values.

The typical ocean radiances ( $L_{\text{typical}}$ ) and the maximum cloud radiances ( $L_{\text{cloud}}$ ) expected for SeaWiFS measurements on orbit are listed in Table 22 of Barnes et al. (1994a). Those radiances are shown in Fig. 12a. As can be seen in the figure, the maximum cloud radiances have a peak value of about  $68 \text{ mW cm}^{-2} \text{sr}^{-1} \mu\text{m}^{-1}$  for SeaWiFS band 3, and the  $L_{\text{typical}}$  radiances have a peak of about  $9 \text{ mW cm}^{-2} \text{sr}^{-1} \mu\text{m}^{-1}$  for band 1. The nature of the two

sets of radiances is such that the ratio  $L_{\text{cloud}}/L_{\text{typical}}$  increases with SeaWiFS band number (Fig. 12b); thus, the SeaWiFS cloud radiances vary from about 6.5 times the value of  $L_{\text{typical}}$  for band 1, to about 31 times the value of  $L_{\text{typical}}$  for band 8 (see Table 22 of Barnes et al. 1994a).

The fluxes from the SBRC test apparatus were set, as closely as possible, to provide the radiances equivalent to  $L_{\text{cloud}}$  and  $0.5L_{\text{cloud}}$ ; however, the limited output from the SBRC sphere in the shorter wavelengths severely limited the quality of this equivalence (Fig. 13). The cloud radiances from Fig. 12b are repeated in Fig. 13 for reference. The radiances that are 3 and 10 pixels wide come from SeaWiFS measurements of the test images from the sphere. For band 1 in Fig. 13b, the image from the SBRC test apparatus has a radiance of about  $0.5 L_{\text{typical}}$ . For bands 7 and 8, in Fig. 13a, the radiances are 25 and 30 times the value of  $L_{\text{typical}}$ , respectively.

## 7.3 Theoretical Band-to-Band Response

To allow for an analysis of the SeaWiFS bands over a wide range of optical overdrives, the assumption was made that the stray light responses of the eight bands are similar, at least to a very good approximation. This assumption allows the conclusion that the shorter wavelength bands, tested at small optical overdrives, will behave in the same manner as the longer wavelength bands when optical overdrives are large. Conversely, it allows the conclusion that

### Stray Light in the SeaWiFS Radiometer

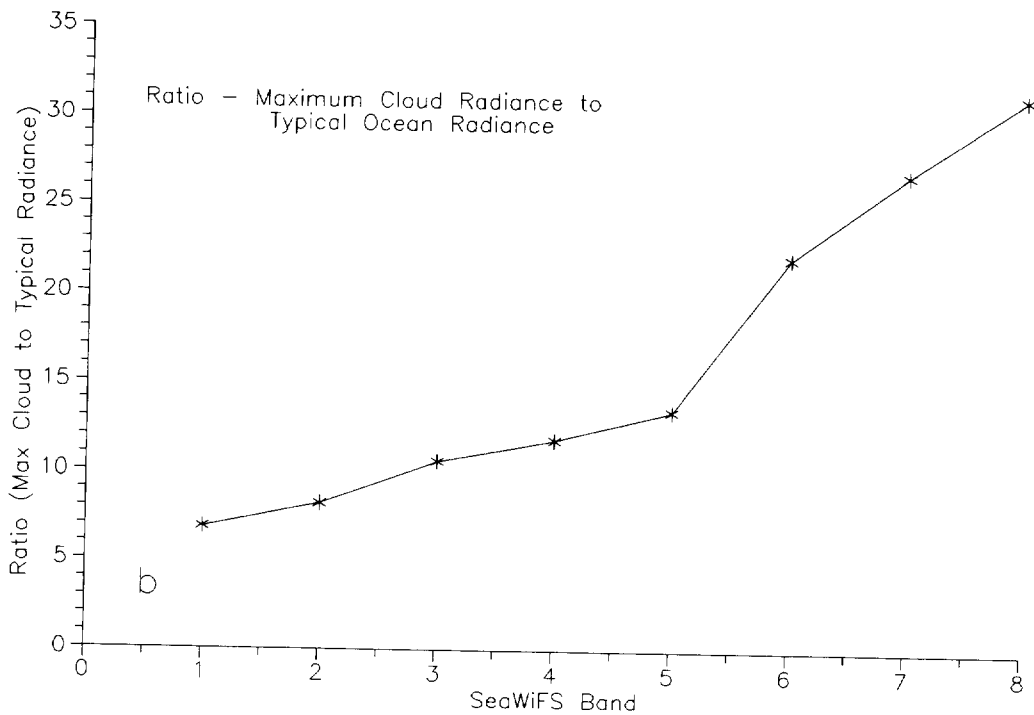
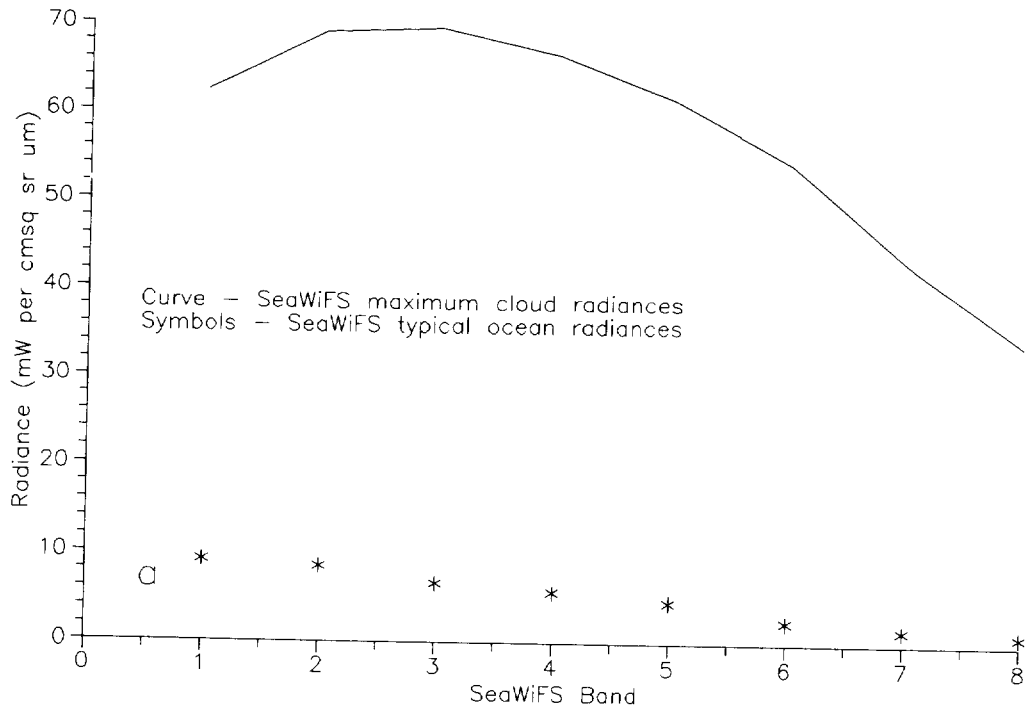


**Fig. 12.** SeaWiFS cloud and typical ocean radiances. Shown here are the: a) radiances for the eight SeaWiFS bands; and b) cloud radiances given in reduced units. Here they are given as their ratios to the typical ocean radiances.

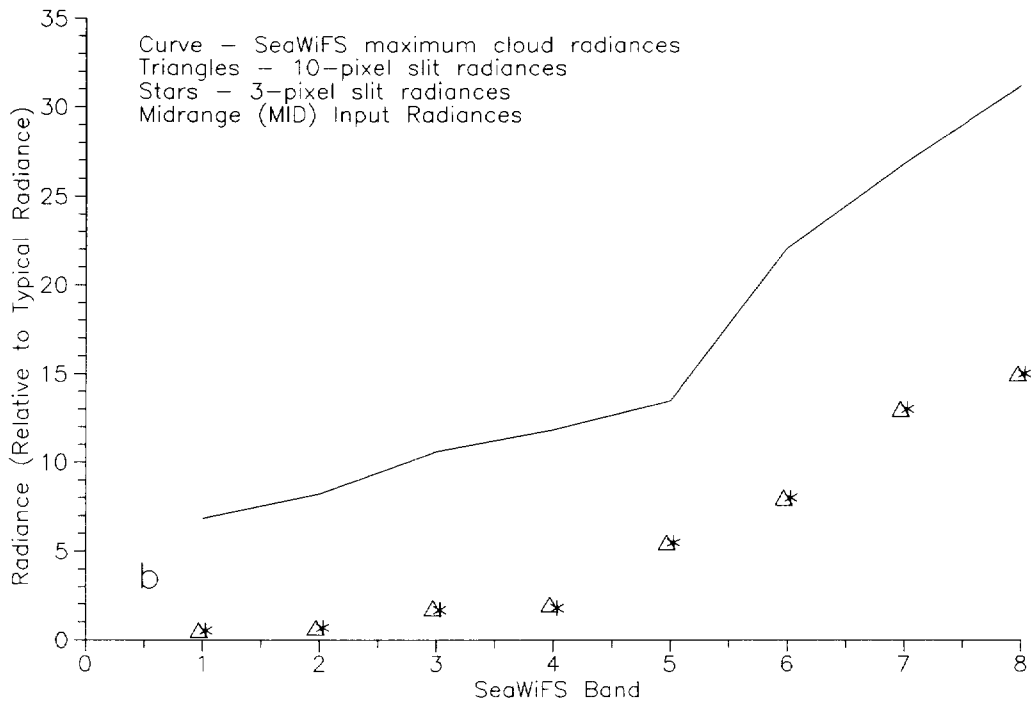
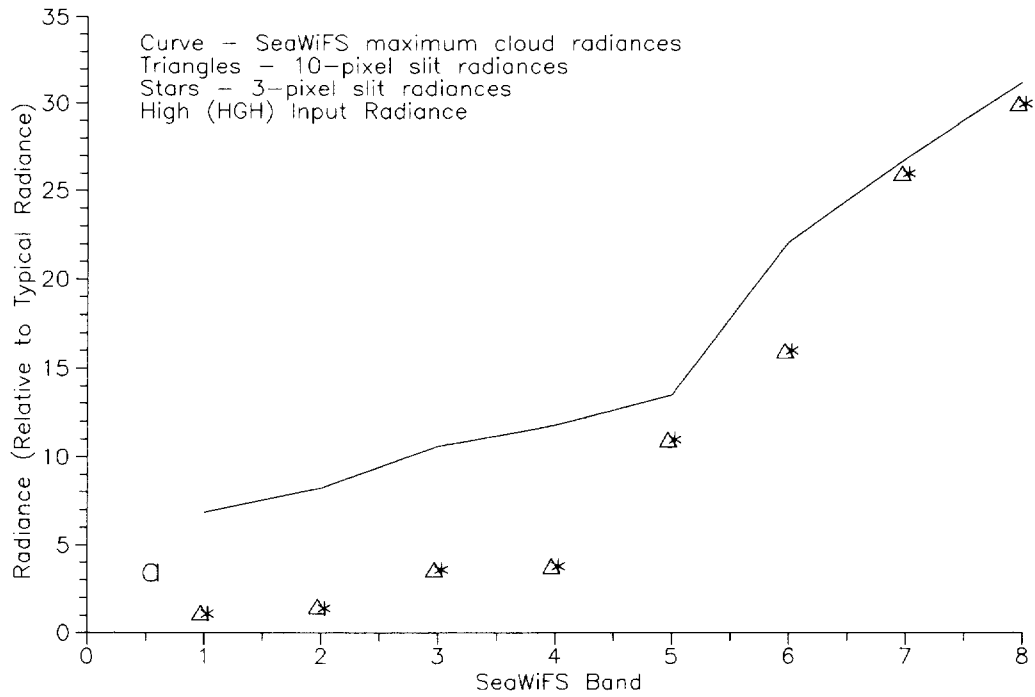


**Fig. 13.** Radiances from the SBRC test apparatus. These radiances are given in the same reduced units as the maximum cloud radiances for each band. The radiances are given for images that are 3 and 10 pixels wide. Shown here are the: a) radiances from the high output settings of the SBRC integrating sphere; and b) radiances from the midrange output settings of the SBRC integrating sphere.

the longer wavelength bands, tested at large optical overdrives, will behave like the shorter wavelength bands when overdrives are small. It assumes that none of the bands have peculiarities in their bright target responses.

The assumption of band-to-band uniformity works better for the sets of four odd and four even SeaWiFS bands, since there is evidence in the test results of odd-even band differences due to optical cross talk. These odd-even differences are relatively slight, and their characteristics show up in all of the pairs of odd-even bands. As discussed above, this odd-even band difference in stray light response was predicted before the post-modification tests. Indeed, the character of the predicted odd-even differences was one of the principal guides for the design of the post-modification measurements.

Consistent and explainable effects, such as these, must be demonstrated in the test results, if the assumption of band-to-band uniformity in stray light response is to be believed. The analysis presented below will refer to this assumption; however, the proposed stray light corrections are tailored individually to the eight SeaWiFS bands. For these corrections, very small differences in the responses of the bands become significant. The stray light corrections can be a few tenths of a percent or less of the radiance from the bright source. At levels above this, it will remain important to check the assumption that the stray light response is consistent from band to band.

## 7.4 Source Brightness Response

With the effective removal of the electronic recovery tail (Section 5.0), there has been no sign of any significant electronic component to the instrument's bright target response at a distance of more than one or two pixels from the edge of the bright source. There is a small electronic overshoot in each band's electronic response 1 pixel after a bright source (see Fig. 1 of Barnes et al. 1994a). The effect derives from the design of the Goldberg noise reduction circuit in each band's intermediate electronics. That response, in the along-scan direction, is present in the test results, and it will be present in the measurements on orbit. That response will be located within 1-2 pixels from the edge of bright sources. This overshoot will be discussed in the analysis of the test results presented below.

Without an electronic effect, the remaining response to a bright source is caused by scattered or reflected light from the bright source. As the brightness of the source varies, so does the amount of scattered or reflected light within the radiometer and the amount of stray light in the radiometer's measurements. This is the assumption of a stray light response linear with source brightness; again, it will be important to check this assumption in the results.

## 7.5 Along-Scan Responses

The characterization of residual stray light in the instrument was performed using a 1 pixel wide image positioned at the nadir pixel for SeaWiFS, pixel 643. The

SeaWiFS response was measured with the standard detector configuration for the radiometer and with science gain 1. Each band's response to that bright impulse was measured over a range of 20 pixels on either side of the nadir pixel. Over these 41 pixels, the output for each band was summed, and each summation was normalized to unity. The calculations presented here assume that all energy from the impulse is contained within the 41 pixels of the instrument output.

The along-scan impulses and responses are listed in Table 8. The results are given for the range from 13 pixels before the impulse (pixel offset -13) to 15 pixels after the impulse (pixel offset 15). The responses are given for the standard detector configuration for SeaWiFS, i.e., for measurements using all four detectors in each band. Stray light measurements, using the same impulses, have also been made individually for each detector in each band. They are part of the SeaWiFS bio-optical archive and storage system (Westphal et al. 1994). If changes to the detector configurations are required on orbit, these test data can be used to construct additional responses.

Table 8 gives the averages and standard deviations for the odd and even band responses. Each of the eight responses summarized in Table 8 was normalized to unity before the calculation of the table's results. The standard deviations in Table 8 range from about one-third to about one-half of the corresponding mean values. These small standard deviations are a measure of the band-to-band similarity in the instrument response; however, there is still the need for individually tailored responses for each band in the stray light correction procedure presented below.

The impulse from the 1 pixel wide bright image is shown in Fig. 14. The abscissa has been changed so that the impulse is at pixel zero, rather than pixel 643. The spread of this input into the odd band response is shown in Fig. 15. This figure gives the average response for the four odd SeaWiFS bands (bands 1, 3, 5, and 7). Figure 15a shows that almost 99% of the response of the odd bands can be found within two pixels of the source. Figure 15b shows the remaining 1% of the odd band response, i.e., the response that is three or more pixels from the source. In these figures, the instrument scans left to right. Figure 15b shows the effect of optical cross talk on the response of the odd bands on the SeaWiFS focal planes. There is a significantly longer and larger response after the bright source. For each odd band, this increased response results from additional stray light from the even band (Section 6.5). It is felt that the addition of a septum between the focal planes would greatly reduce this additional stray light and make the down-scan response in Fig. 15b nearly identical to the up-scan response.

The spread of the impulse into the even SeaWiFS bands is shown in Fig. 16. In the same manner as before, this figure gives the average response for the four even bands, and

**Table 8.** Along-scan impulse and response. The impulse represents the illumination from a 1 pixel wide slit. The responses come from the SCADP measurements performed at SBRC. The response values give the means and standard deviations for the four odd and four even bands. All functions have been normalized to give integrated values of unity.

Pixel Offset	Along-Scan Impulse	Odd Band Response		Even Band Response	
		Mean	$\sigma$	Mean	$\sigma$
-13	0.0	0.000000	0.000000	0.000000	0.000000
-12	0.0	0.000000	0.000000	0.000047	0.000011
-11	0.0	0.000000	0.000000	0.000150	0.000036
-10	0.0	0.000000	0.000000	0.000263	0.000066
-9	0.0	0.000000	0.000000	0.000435	0.000104
-8	0.0	0.000025	0.000016	0.000638	0.000147
-7	0.0	0.000069	0.000030	0.000773	0.000185
-6	0.0	0.000198	0.000079	0.000969	0.000238
-5	0.0	0.000573	0.000202	0.001136	0.000202
-4	0.0	0.001661	0.000553	0.001458	0.000187
-3	0.0	0.004368	0.001589	0.003672	0.001050
-2	0.0	0.012424	0.004133	0.009061	0.002671
-1	0.0	0.149717	0.057032	0.124966	0.067547
0	1.0	0.703367	0.029070	0.765813	0.082545
1	0.0	0.097853	0.086333	0.061887	0.081895
2	0.0	0.016655	0.005364	0.014468	0.012949
3	0.0	0.005788	0.002888	0.008829	0.002597
4	0.0	0.002021	0.000866	0.003241	0.000861
5	0.0	0.001459	0.000944	0.001259	0.000442
6	0.0	0.001127	0.000708	0.000493	0.000252
7	0.0	0.000931	0.000636	0.000214	0.000157
8	0.0	0.000675	0.000438	0.000106	0.000106
9	0.0	0.000541	0.000332	0.000049	0.000064
10	0.0	0.000310	0.000117	0.000025	0.000043
11	0.0	0.000154	0.000025	0.000025	0.000043
12	0.0	0.000059	0.000036	0.000015	0.000026
13	0.0	0.000017	0.000030	0.000007	0.000013
14	0.0	0.000007	0.000013	0.000000	0.000000
15	0.0	0.000000	0.000000	0.000000	0.000000
<i>Sum</i>	1.0	1.0		1.0	

as with the odd bands, almost 99% of the even band response can be found within two pixels of the source. A comparison of Figs. 15a and 16a shows a marked similarity in the pattern of the response. For the even bands, the response in the central pixel is about 6% greater than for the odd bands. As a result, the even band responses for pixels  $-1$  and  $+1$  are smaller. The overall assessment is that the relationships illustrated in Figs. 15a and 16a between these two pixels are similar.

A comparison of the lower level responses in the outer pixels (Figs. 15b and 16b) shows more of a mirror image with respect to the central pixel. The extended down-scan tail in the response of the odd bands is mirrored by the extended up-scan tail in the even bands. In both cases, the extended tails for the bands are caused by cross talk from the bands that share the focal planes with them. For both

the odd and even bands, the tails with cross talk extend about 11–12 pixels. For the responses without cross talk, the tails extend about 7–8 pixels.

## 7.6 Along-Track Responses

The impulse in the along-track direction comes from a 3 pixel wide bright source. The measured along-track response is shown in Fig. 17. The vertical scales for Figs. 17a and 17b duplicate those for the respective parts of Figs. 15 and 16, but the horizontal scales of Figs. 17a and 17b have been expanded by a factor of three. The spacing of the data points in Fig. 17 reflects the oversampling in the measurements discussed in Section 7.1. Figure 17 shows six along-track measurements per pixel. Again, for both the along-scan and along-track stray light results presented

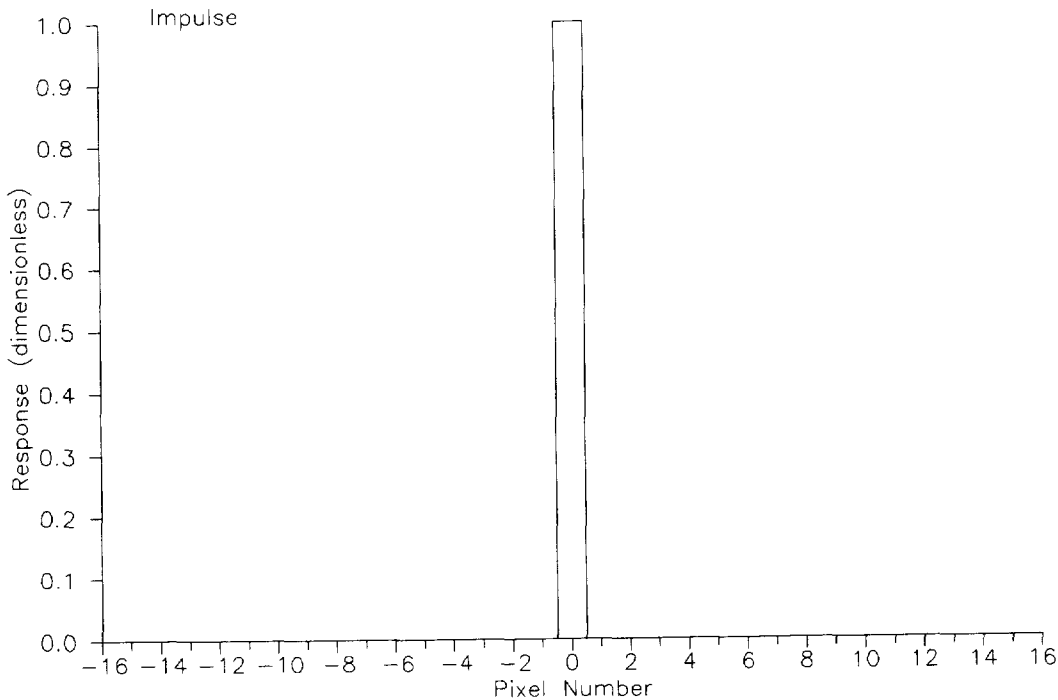


**Fig. 14.** Impulse for the stray light responses. The impulse has been set to unity, since it represents all of the input light to the instrument.

here, a pixel is defined as a square with a side length of 1.6 mrad, which will be 1.13 km for nadir measurements made from an altitude of 705 km (Barnes et al. 1994a). The 2 pixel plateau at the top center of the response derives directly from the width of the illuminated slit. The half-power points for the response are 3 pixels apart.

Figure 18 shows the along-track response in a format identical to the along-scan figures. This was obtained by removing just over 1.5 pixels from the central plateau in Fig. 17a to create a narrower response. The responses in Figs. 18a and 18b have been prepared for qualitative purposes only. They do show, however, that the side lobes of the secondary reflections from the scrambler have been moved from 5 pixels from the central image (see Fig. 7), to 1 pixel from the center. In addition, the along-track stray light response exists for only 1 to 2 pixels from the central image. This width is significantly less than that for either the odd or even along-scan stray light results. The along-track results are also presented in Table 9. This table does not separate the results into odd and even bands, since there are no significant odd-even band differences. The standard deviations in Table 9 are also reasonably small when compared with the mean values. The narrower stray light response in the along-track direction in SeaWiFS results from the basic design of the focal plane assemblies.

As shown in Fig. 10, each SeaWiFS band is 4 pixels long (in the along-scan direction), but only 1 pixel wide.

**Table 9.** Along-track impulse and response. The impulse represents the illumination from a 1 pixel wide slit. The responses come from measurements in the SCADP. The response values give the means and standard deviations for the SeaWiFS bands. All of the functions have been normalized to give integrated values of unity.

Pixel Offset	Along-Track Impulse	Response	
		Mean	$\sigma$
-6	0.000000	0.000000	0.000000
-5	0.000000	0.000003	0.000009
-4	0.000000	0.000100	0.000120
-3	0.000000	0.000238	0.000217
-2	0.000000	0.002165	0.001704
-1	0.000000	0.176247	0.045494
0	1.000000	0.645052	0.013227
1	0.000000	0.175668	0.041982
2	0.000000	0.000511	0.000183
3	0.000000	0.000016	0.000018
4	0.000000	0.000000	0.000000
Sum	1.0	1.0	

The field stop at the inlet to the aft optics masks the bands in the focal planes, leaving an open area that is approximately 6 pixels long by 2 pixels wide per band. The narrower the mask, the less stray light there is in the measurement. Thus, the reduction of the along-scan mask is one method for reducing stray light in that direction; such a suggestion was raised by W. Esaias (see Appendix A). For SeaWiFS, reducing the along-scan masks over the band areas would eliminate using some of the detectors through vignetting and reduce the signal-to-noise improvement from the use of those detectors. This suggestion was not implemented. Remodeling the instrument to separate the individual detectors and place them under individual filters was also considered impractical.

## 8. STRAY LIGHT ASSESSMENT

There are three primary contributors to the BTR in SeaWiFS—MTF/optical blur, optical cross talk under the interference filters, and mirror BRDF. Mirror BRDF, or primary mirror scatter, was discussed in Section 6.1, and included a calculation of the angular dependence of the BRDF. Primary mirror scatter remains a stray light source after all other sources have been removed. The ranges over which primary mirror scatter dominates SeaWiFS BTR are given in Table 10. These ranges can be compared with results from the laboratory measurements in Fig. 15 (along-scan odd band response), Fig. 16 (along-scan even band response), and Fig. 18 (along-track response).

Optical cross talk has been described in Section 6.5. It is the primary source of asymmetry in the along-track BTR from SeaWiFS. For the stray light budget presented here, optical cross talk covers all sources of reflections under the interference filters. For the odd bands, intraband optical cross talk, i.e., reflections under the interference filter within a band, dominates from 3–5 pixels before a bright source. The so-called *excess* stray light from interband cross talk extends to 9 pixels after the bright source. The same along-scan cross talk occurs in the even bands, except that the *excess* interband cross talk comes before the bright source.

The MTF has been discussed in terms of the line spread function in Barnes et al. (1994a). The MTF is called optical blur in Fig. 6. In optical terms, this effect creates a *blur circle* that extends 1 or 2 pixels around each pixel. Other effects, such as intraband electronic cross talk and reflections from the focusing lenses, are present in BTR; however, they are considered to be secondary contributors to stray light in SeaWiFS.

## 9. ALONG-SCAN CORRECTION

The individual responses for the eight SeaWiFS bands are listed in Table 11. These values have been taken from the SCADP, which also gives a brief description of their derivation. The application of responses to remove residual stray light from an individual pixel uses the response of

that pixel plus the responses of pixels near it. Each pixel is treated, in turn, as the central pixel in the response. The correction is applied in two parts. First, the so-called *missing signal* from the central pixel is restored. For the odd bands, approximately 30% of the original impulse is removed from the central pixel in the response (Table 8). For the even bands, about 24% of the central pixel is removed and must be replaced. Second, the light added to the central pixel must be removed from its neighbors.

The stray light correction illustrated in Table 12 includes only five pixels; the pixel to be corrected and the two pixels on either side of it. This was done to produce a simplified explanation. In practice, the SeaWiFS along-scan stray light correction will involve many more pixels, and the correction is applied after the counts have been converted into radiances. Using the notation from Table 12, the stray light correction ( $F_{SL}$ ) for an individual pixel proceeds in the following sequence.

*Step 1:* Set the correction term to zero:

$$F_{SL} = 0. \quad (2)$$

*Step 2:* Replace the *missing signal* from pixel  $P_0$ , as in

$$F_{SL} = F_{SL} + R_0 \left[ \frac{1 - K_0}{K_0} \right], \quad (3)$$

where  $R_0$  designates the radiance of pixel  $P_0$ , and  $K_0$  is the correction constant for pixel  $P_0$ .

*Step 3:* Remove the contributions from the adjacent pixels. This example includes only two pixels up scan and down scan. In practice, there will be many more.

$$F_{SL} = F_{SL} - R_{-2} \left[ \frac{K_{+2}}{K_0} \right], \quad (4)$$

$$F_{SL} = F_{SL} - R_{-1} \left[ \frac{K_{+1}}{K_0} \right], \quad (5)$$

$$F_{SL} = F_{SL} - R_{+1} \left[ \frac{K_{-1}}{K_0} \right], \quad (6)$$

and

$$F_{SL} = F_{SL} - R_{+2} \left[ \frac{K_{-2}}{K_0} \right]. \quad (7)$$

*Step 4:* Apply the correction to the radiance:

$$R_0 = R_0 + F_{SL}. \quad (8)$$

The correction in Step 2 is straightforward, since the radiance and the correction constant come from the same pixel. For Step 3, the location of the pixel under correction, relative to the source of radiance, determines the appropriate correction constant.

In the tests summarized below, the stray light corrections were accomplished using a commercial spreadsheet

## Stray Light in the SeaWiFS Radiometer

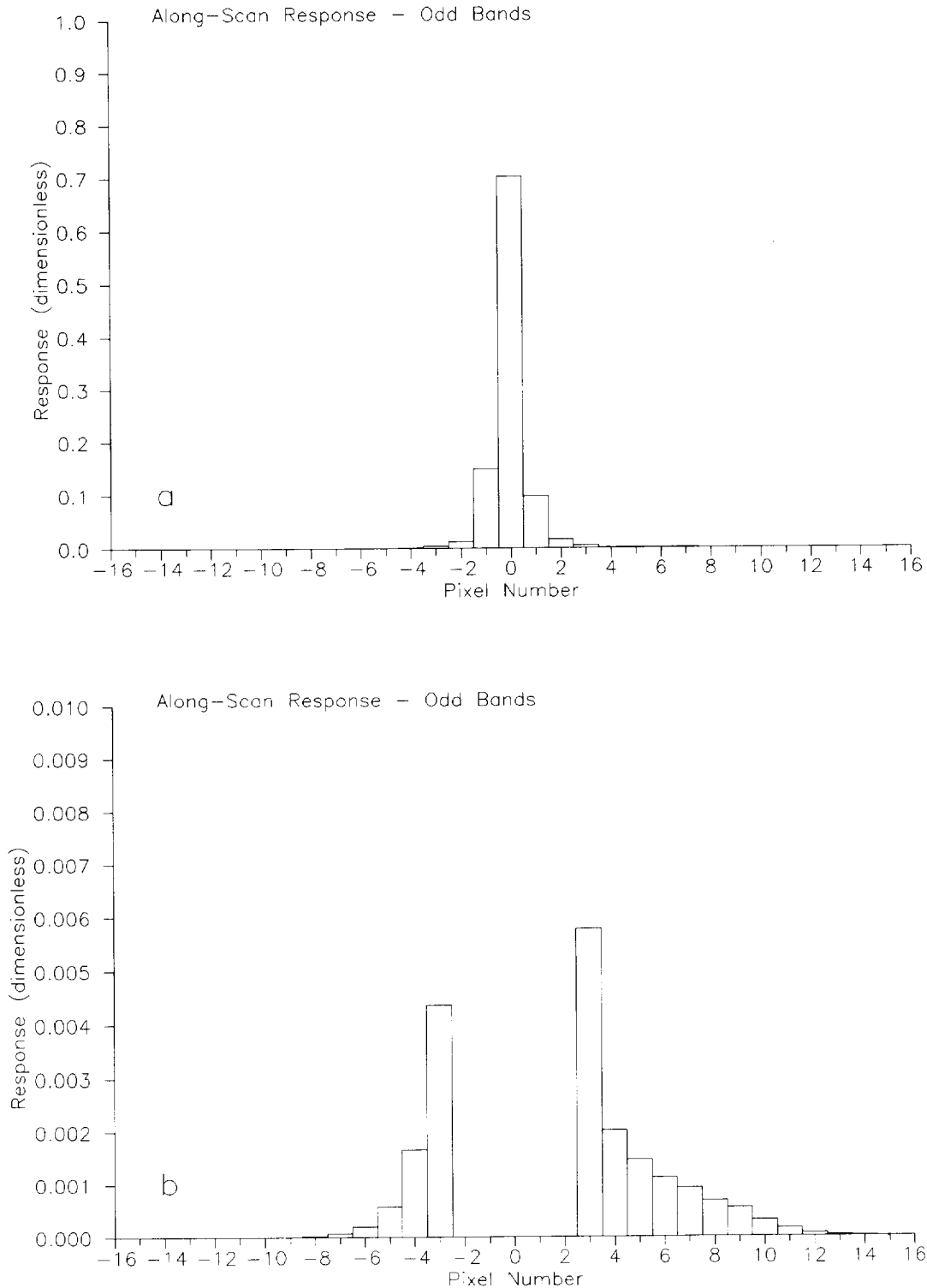


**Fig. 15.** The response for the odd bands on the SeaWiFS focal plane assemblies. This is the instrument response in the along-scan direction. The total response from the two portions of this figure is equal to unity, since it represents all of the response to the impulse in Fig. 14. The figure shows: a) the response of the central pixel and its immediate neighbors when the ordinate is set to unity; and b) the response of the outer pixels when the ordinate is set to 1% of full scale. The excess stray light in the higher number pixels, relative to the pixels on the lower number side, is the result of optical cross talk from the even bands.

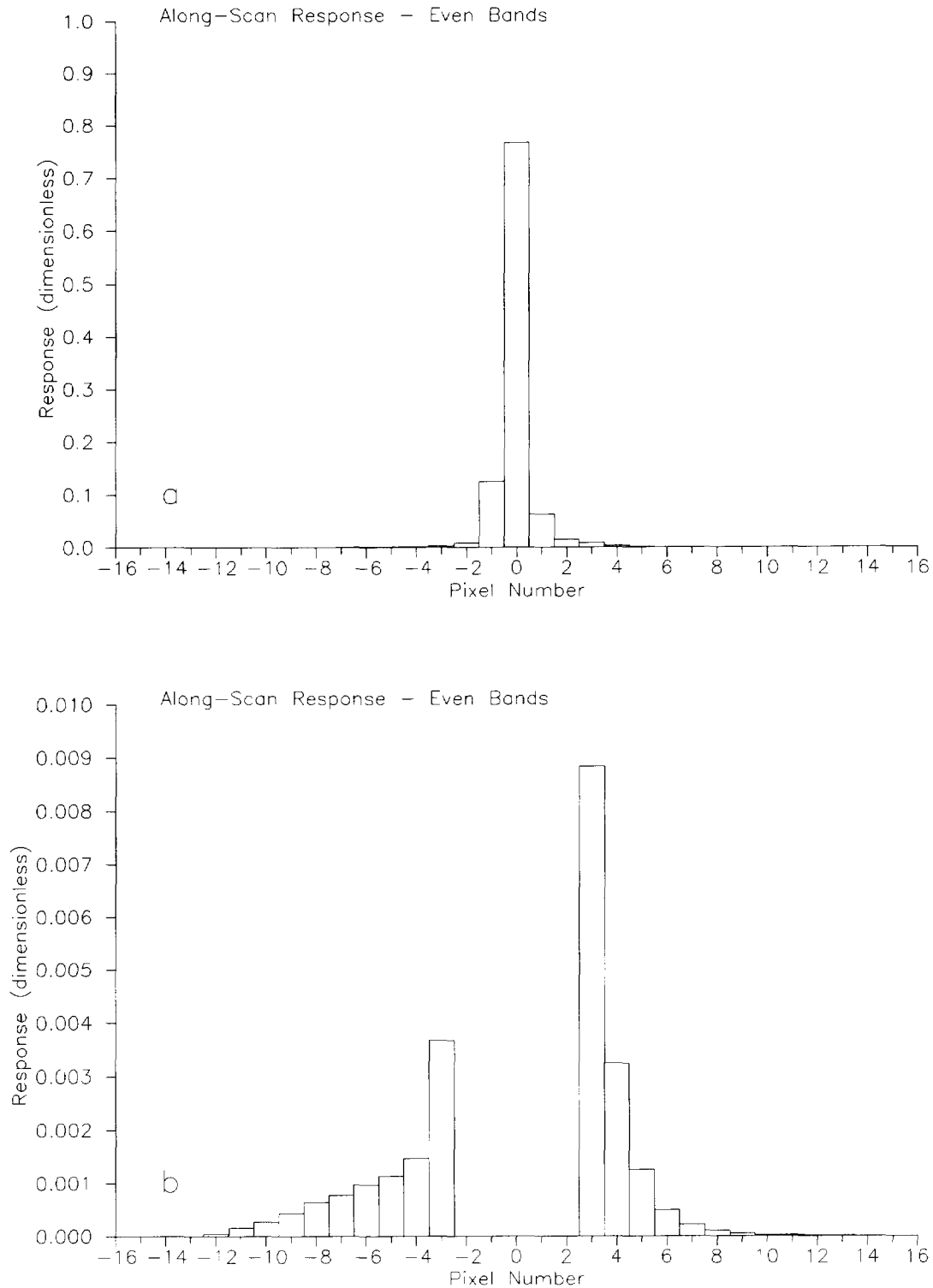


**Fig. 16.** The response for the even bands on the SeaWiFS focal plane assemblies. This is the instrument response in the along-scan direction. The total response from the two portions of this figure is equal to unity, since it represents all of the response to the impulse in Fig. 14. The figure shows: a) the response of the central pixel and its immediate neighbors when the ordinate is set to unity; and b) the response of the outer pixels when the ordinate is set to 1% of full scale. The excess stray light in the higher number pixels, relative to the pixels on the lower number side, is the result of optical cross talk from the even bands.

## Stray Light in the SeaWiFS Radiometer

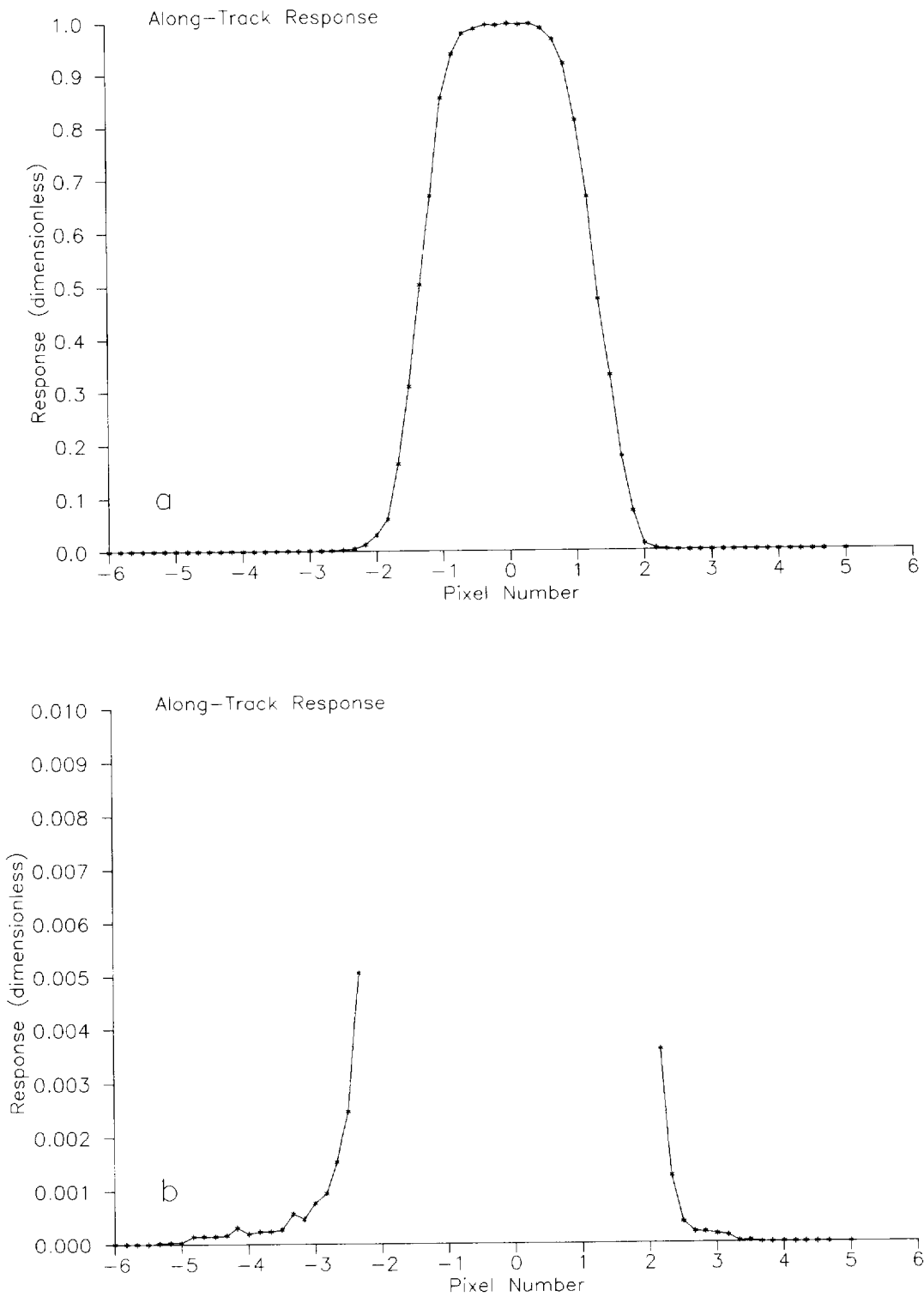


**Fig. 17.** Measurements of the response in the along-track direction. These measurements were made by adjusting the height of the light source (Section 7.1). The measurements of the along-track response are oversampled by a factor of 6.

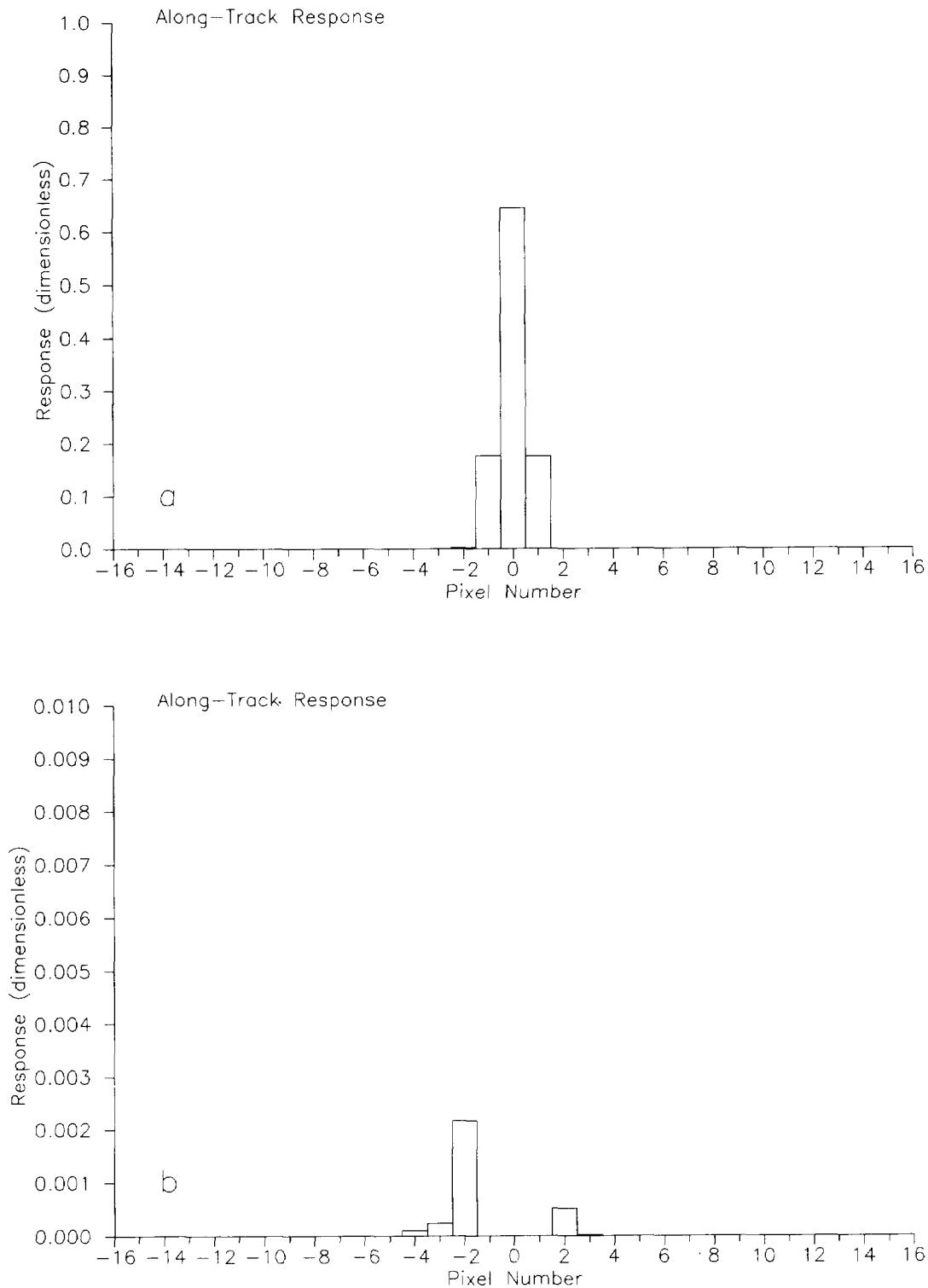


**Fig. 18.** The response in the along-track direction. This response represents all eight SeaWiFS bands. The total response from the two portions of this figure is equal to unity, since it represents all of the response to the impulse in Fig. 14. The figure shows: a) the response of the central pixel and its immediate neighbors when the ordinate is set to unity; and b) the response of the outer pixels when the ordinate is set to 1% of full scale.

**Table 10.** Primary BTR components. This is a qualitative summary of the principal components in the BTR/stray light response of SeaWiFS. The pixel ranges give estimates for the regions over which each component dominates the BTR/stray light response. (The + sign indicates the pixel enumerated and beyond.)

Scan Direction	BTR Component	Pixels Before Source		Pixels After Source	
		Odd Band	Even Band	Odd Band	Even Band
Along-Scan	MTF/Optical Blur	1-2	1-2	1-2	1-2
	Optical Cross Talk	3-5	3-9	3-9	3-5
	Mirror BRDF	6+	10+	10+	6+
Along-Track	MTF/Optical Blur	1-2	1-2	1-2	1-2
	Mirror BRDF	3+	3+	3+	3+

**Table 11.** Along-scan responses for SeaWiFS bands 1-8. These are the constants used in the correction procedure.

Pixel Offset	Band 1 (412 nm)	Band 2 (443 nm)	Band 3 (490 nm)	Band 4 (510 nm)	Band 5 (555 nm)	Band 6 (670 nm)	Band 7 (765 nm)	Band 8 (865 nm)
-13	0.00000	0.00000	0.00000	0.00000	0.00000	0.00000	0.00000	0.00000
-12	0.00000	0.00005	0.00000	0.00006	0.00000	0.00005	0.00000	0.00003
-11	0.00000	0.00015	0.00000	0.00020	0.00000	0.00016	0.00000	0.00010
-10	0.00000	0.00030	0.00000	0.00034	0.00000	0.00027	0.00000	0.00016
-9	0.00000	0.00050	0.00000	0.00052	0.00000	0.00049	0.00000	0.00026
-8	0.00004	0.00074	0.00004	0.00070	0.00002	0.00077	0.00000	0.00039
-7	0.00010	0.00090	0.00010	0.00078	0.00005	0.00099	0.00003	0.00048
-6	0.00030	0.00110	0.00025	0.00090	0.00015	0.00131	0.00010	0.00064
-5	0.00080	0.00130	0.00075	0.00104	0.00045	0.00142	0.00031	0.00087
-4	0.00240	0.00148	0.00199	0.00156	0.00134	0.00170	0.00097	0.00119
-3	0.00639	0.00519	0.00546	0.00442	0.00342	0.00296	0.00235	0.00241
-2	0.01758	0.01335	0.01565	0.01040	0.00921	0.00607	0.00769	0.00716
-1	0.13183	0.10236	0.21913	0.10948	0.06523	0.05654	0.19012	0.23871
0	0.73314	0.87317	0.74859	0.85724	0.66876	0.71775	0.68751	0.66864
1	0.06392	-0.00445	-0.00273	-0.00104	0.23318	0.20043	0.09758	0.05559
2	0.02000	0.03400	0.02000	-0.00416	0.00743	0.01400	0.02000	0.01600
3	0.01039	0.01335	0.00621	0.00910	0.00297	0.00558	0.00377	0.00803
4	0.00350	0.00440	0.00180	0.00300	0.00149	0.00197	0.00135	0.00385
5	0.00300	0.00148	0.00149	0.00090	0.00059	0.00082	0.00080	0.00193
6	0.00230	0.00055	0.00110	0.00026	0.00052	0.00030	0.00062	0.00090
7	0.00200	0.00020	0.00085	0.00008	0.00045	0.00011	0.00045	0.00048
8	0.00140	0.00007	0.00066	0.00003	0.00035	0.00004	0.00031	0.00029
9	0.00110	0.00002	0.00050	0.00000	0.00030	0.00002	0.00028	0.00016
10	0.00050	0.00000	0.00032	0.00000	0.00022	0.00000	0.00021	0.00010
11	0.00013	0.00000	0.00020	0.00000	0.00015	0.00000	0.00014	0.00010
12	0.00000	0.00000	0.00007	0.00000	0.00007	0.00000	0.00010	0.00006
13	0.00000	0.00000	0.00000	0.00000	0.00000	0.00000	0.00007	0.00003
14	0.00000	0.00000	0.00000	0.00000	0.00000	0.00000	0.00003	0.00000
15	0.00000	0.00000	0.00000	0.00000	0.00000	0.00000	0.00000	0.00000

**Table 12.** Application of the along-scan stray light correction. The correction in this table is demonstrated for a reduced set of five pixels. The correction is shown for the central pixel,  $P$ , only.

Correction Variable	Pixel				
	$P_{-2}$	$P_{-1}$	$P_0$	$P_{+1}$	$P_{+2}$
Radiance	$R_{-2}$	$R_{-1}$	$R_0$	$R_{+1}$	$R_{+2}$
Correction Constant	$K_{-2}$	$K_{-1}$	$K_0$	$K_{+1}$	$K_{+2}$
Complete Correction	$R_0(1 - K_0) - R_{-2}K_{+2} - R_{-1}K_{+1} - R_{+1}K_{-1} - R_{+2}K_{-2}$				

program. In that program, all calculations were made with radiances that were not corrected for stray light. This spreadsheet technique gives results that are different from calculations which correct pixels in series down a scan line. In that type of calculation, called a *moving window* calculation, some of the radiances used in the stray light correction have been adjusted for stray light, and some have not. The actual correction routine for flight data will not duplicate the spreadsheet process that derived these corrections; however, there are other algorithms that can provide essentially identical results.

## 10. ALONG-SCAN TEST RESULTS

The 32 stray light tests presented here correspond to the combination of radiances and slit widths in Figs. 13a and 13b. There are two sets of radiances, called high and midrange, and there are two slit widths—3 pixels and 10 pixels. A sample calculation from the test results is presented in Table 13.

### 10.1 Sample Calculations

The results in Table 13 are for SeaWiFS band 7, with high radiance, and a 10 pixel slit. For the calculations, a subset of pixels ranging from pixels 601–680, is taken from the 1,285 pixel scan line. The laboratory measurements were made in a darkened room with an illuminated slit (Section 7.1). From those measurements, the instrument output (in counts) for pixels 601–620 was averaged to provide the zero (or dark) count; this zero count was subtracted from all of the pixels in the subset. The dark-corrected counts have been converted into radiances using the prelaunch calibration constants in Barnes et al. (1994b) for bilinear gains (Section 4).

These measured radiances form the input for the stray light correction. For band 7, with high radiance and a 10 pixel slit (Table 13), the input radiance shows a peak value of about  $41.8 \text{ mW cm}^{-2} \text{ sr}^{-1} \mu\text{m}^{-1}$  at pixel 640. The output radiance from the stray light correction for that pixel is nearly the same. The radiance at pixel 640, in normalized units, is very close to  $L_{\text{cloud}}$  and is about 26 times greater than  $L_{\text{typical}}$ .

The 10 pixel bright source extends from pixel 634 to pixel 643. In all of the test set measurements, the right-most edge of the bright source has been placed at pixel 643. The zero values in this case (pixels 615–620 and 657–660)

range from  $0.001\text{--}0.004 \text{ mW cm}^{-2} \text{ sr}^{-1} \mu\text{m}^{-1}$ ; i.e., from approximately 0.33–1.33 counts above the zero offset calculated from pixels 601–620. In other terms, the zero values range from 0.06–0.25% of  $L_{\text{typical}}$ . On the surface, this is a small offset, but the SeaWiFS performance specifications call for the output of the band to fall within 0.5% of  $L_{\text{typical}}$  within 10 pixels of the bright source. In these results, where 2 or 3 counts are equivalent to 0.5% of  $L_{\text{typical}}$ , these zero values can be significant.

The decision was made not to fine tune the zero values in these calculations. In addition, the decision was made not to fine tune the responses in these calculations. A hypothetically *improved* set of response constants could remove more of the residual stray light tails in Table 13. Individual tailoring of these parts of the calculations could produce improved results. Those improvements would be of laboratory measurements of bright slits, and will not be made on orbit. There can, and will be, multiple bright sources in each scan of the Earth. Most of those bright sources, clouds in particular, will not have the sharp edges characteristic of laboratory slits.

Extrapolation of these controlled laboratory measurements of stray light to the conditions to be found on orbit is not completely straightforward. As a result, it was decided to define the procedure for stray light reduction before analysis of the actual measurements and to use those results without empirical fitting. The calculation of the zero values and the constants in the along-scan responses were not adjusted. Based on the test results presented here, improving the laboratory results in this manner does not necessarily lead to better results from orbit. In essence, scatter, and possibly some bias, has been retained in these test results.

### 10.2 Results

The laboratory stray light correction results are shown in Figs. 19–50. The data from which these results were calculated have been stored by the SeaWiFS Project (Westphal et al. 1994), and are available to the interested user. Each of these figures has four subpanels, a–d, respectively, and the format for each part is the same from figure to figure. In all of the figures, the abscissa runs from pixel 615 to pixel 665. Figure 19 will be used for illustrative purposes. Subpanels 19a and 19b show the input (uncorrected) radiances for the measurement, with 19a scaled to show the

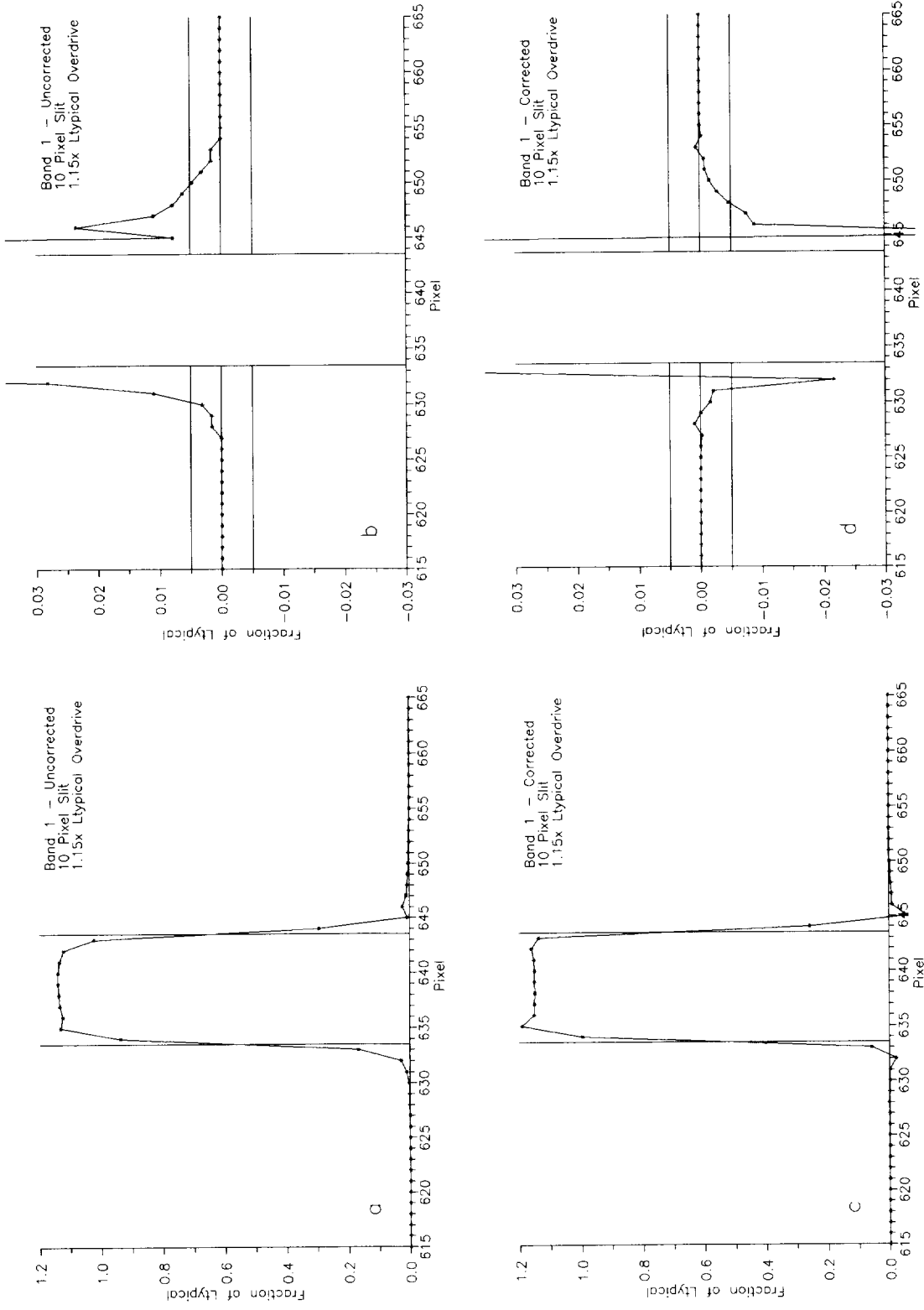


**Fig. 19.** The input and output responses from the stray light correction for band 1 are given, with experimental parameters of high input radiance and a 10 pixel slit. The radiance is  $1.15 L_{\text{typical}}$ . **a)** The input values are scaled to the peak radiances from the source. **b)** The input values are scaled to  $\pm 0.03 L_{\text{typical}}$ . (The one-time overshoot in the band's response past the bright source at pixel 645 is instrumentally based.) **c)** The output values from the stray light correction procedure are scaled to the peak radiances from the source. **d)** The output values are scaled to  $\pm 0.03 L_{\text{typical}}$ . (The correction creates a one-time overshoot before the bright source at pixel 632, and exaggerates the instrumental overshoot after the source at pixel 645.)

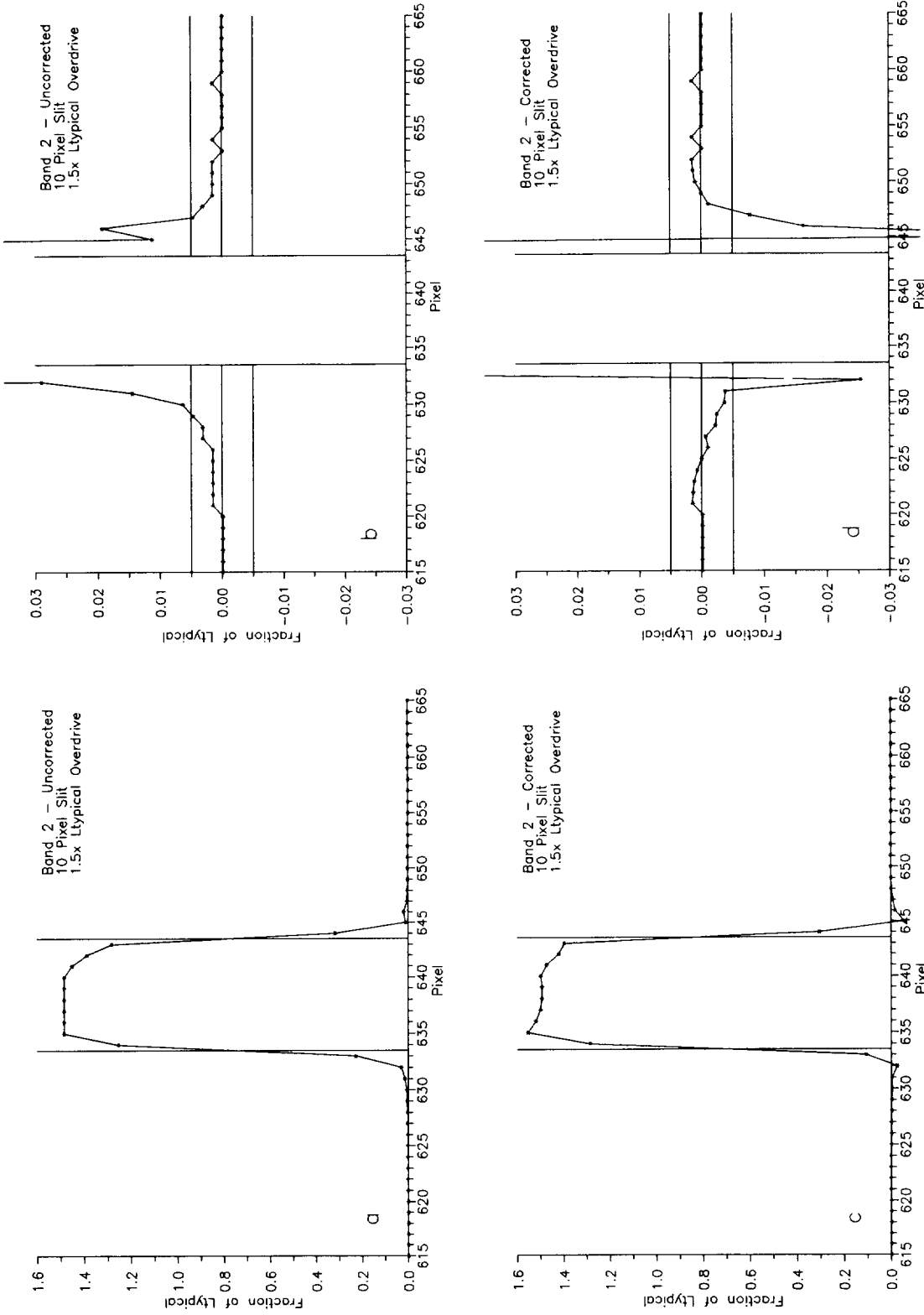


**Fig. 20.** The input and output responses from the stray light correction for band 2 are given, with experimental parameters of high input radiance and a 10 pixel slit. The radiance is  $1.15 L_{\text{typical}}$ . **a)** The input values are scaled to the peak radiances from the source. **b)** The input values are scaled to  $\pm 0.03 L_{\text{typical}}$ . (The one-time overshoot in the band's response past the bright source at pixel 645 is instrumentally based.) **c)** The output values from the stray light correction procedure are scaled to the peak radiances from the source. **d)** The output values are scaled to  $\pm 0.03 L_{\text{typical}}$ . (The correction creates a one-time overshoot before the bright source at pixel 632, and exaggerates the instrumental overshoot after the source at pixel 645.)

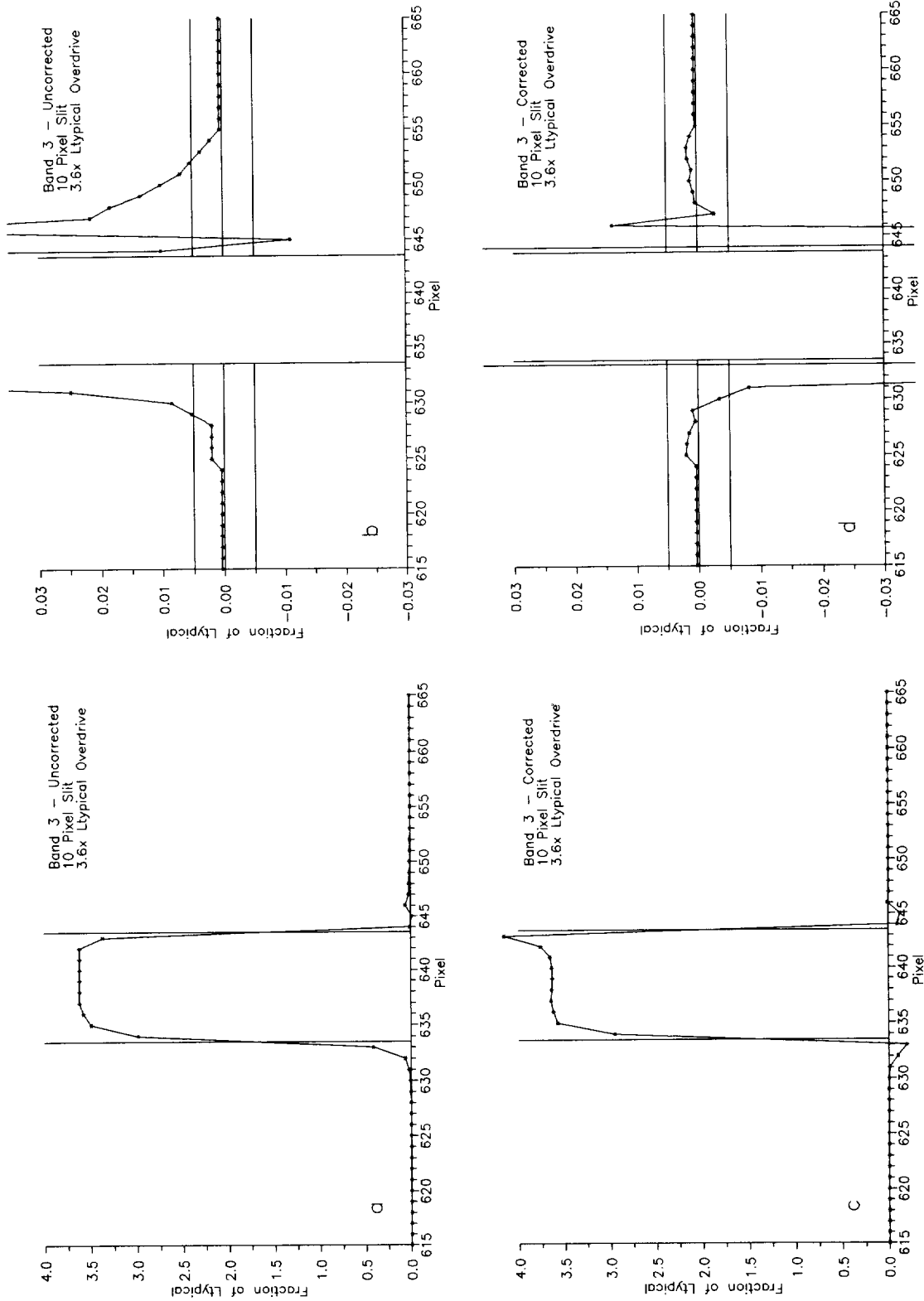


**Fig. 21.** The input and output responses from the stray light correction for band 3 are given, with experimental parameters of high input radiance and a 10 pixel slit. The radiance is  $1.15 L_{\text{typical}}$ . **a)** The input values are scaled to the peak radiances from the source. **b)** The input values are scaled to  $\pm 0.03 L_{\text{typical}}$ . (The one-time overshoot in the band's response past the bright source at pixel 645 is instrumentally based.) **c)** The output values from the stray light correction procedure are scaled to the peak radiances from the source. **d)** The output values are scaled to  $\pm 0.03 L_{\text{typical}}$ . (The correction creates a one-time overshoot before the bright source at pixel 632, and exaggerates the instrumental overshoot after the source at pixel 645.)

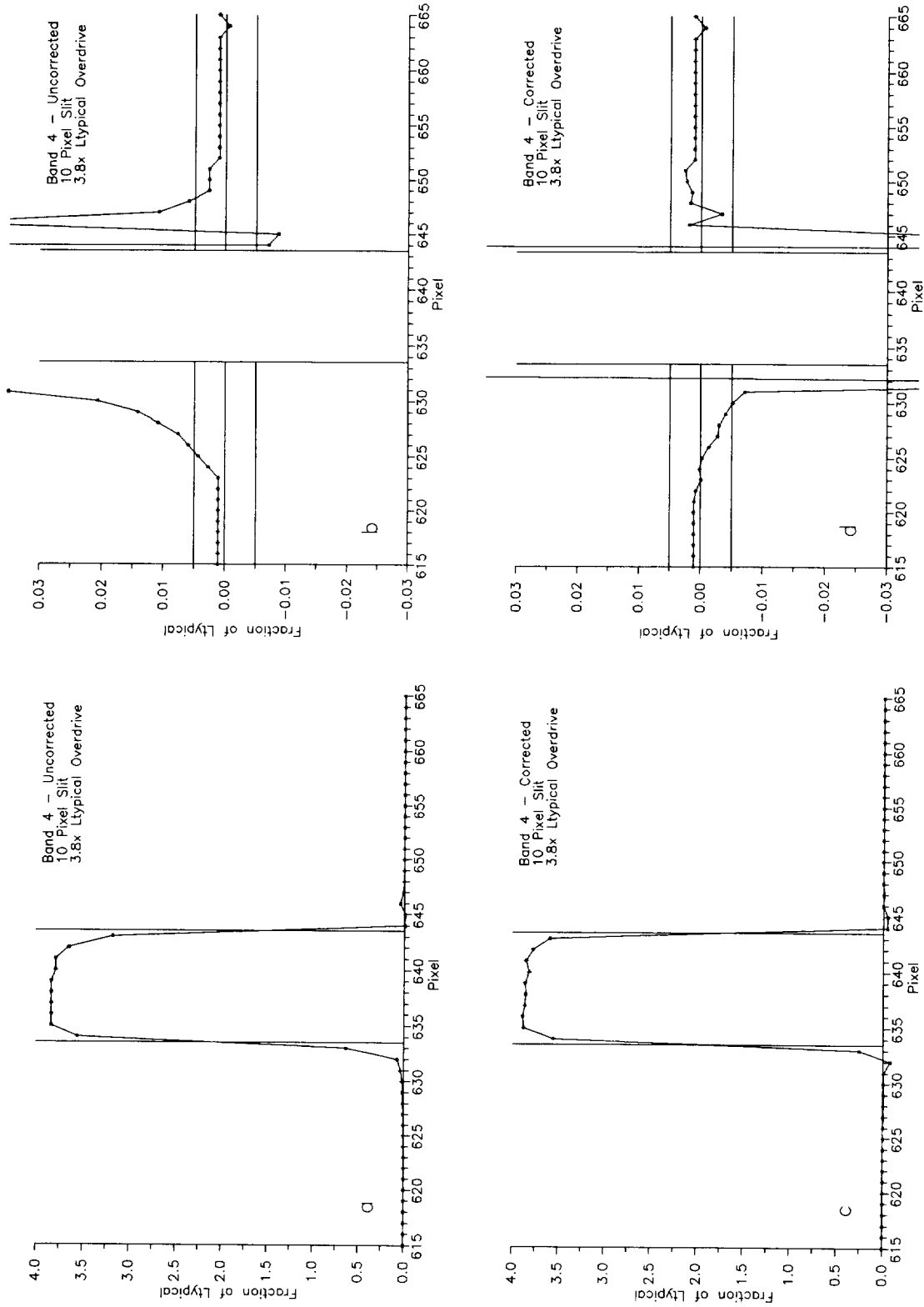


**Fig. 22.** The input and output responses from the stray light correction for band 4 are given, with experimental parameters of high input radiance and a 10 pixel slit. The radiance is  $1.15 L_{\text{typical}}$ . **a)** The input values are scaled to the peak radiances from the source. **b)** The input values are scaled to  $\pm 0.03 L_{\text{typical}}$ . (The one-time overshoot in the band's response past the bright source at pixel 645 is instrumentally based.) **c)** The output values from the stray light correction procedure are scaled to the peak radiances from the source. **d)** The output values are scaled to  $\pm 0.03 L_{\text{typical}}$ . (The correction creates a one-time overshoot before the bright source at pixel 632, and exaggerates the instrumental overshoot after the source at pixel 645.)

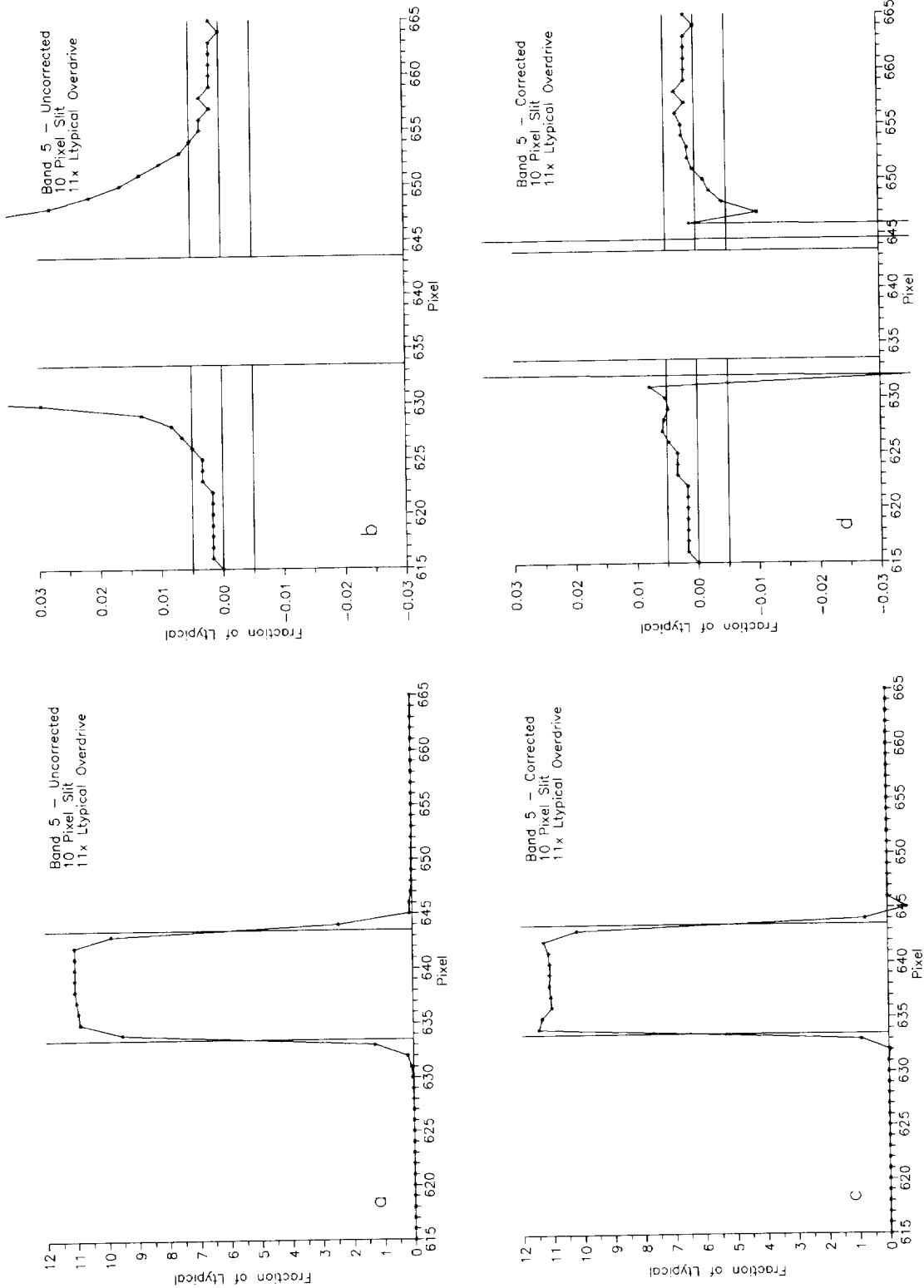


**Fig. 23.** The input and output responses from the stray light correction for band 5 are given, with experimental parameters of high input radiance and a 10 pixel slit. The radiance is  $1.15 L_{\text{typical}}$ . **a)** The input values are scaled to the peak radiances from the source. **b)** The input values are scaled to  $\pm 0.03 L_{\text{typical}}$ . (The one-time overshoot in the band's response past the bright source at pixel 645 is instrumentally based.) **c)** The output values from the stray light correction procedure are scaled to the peak radiances from the source. **d)** The output values are scaled to  $\pm 0.03 L_{\text{typical}}$ . (The correction creates a one-time overshoot before the bright source at pixel 632, and exaggerates the instrumental overshoot after the source at pixel 645.)

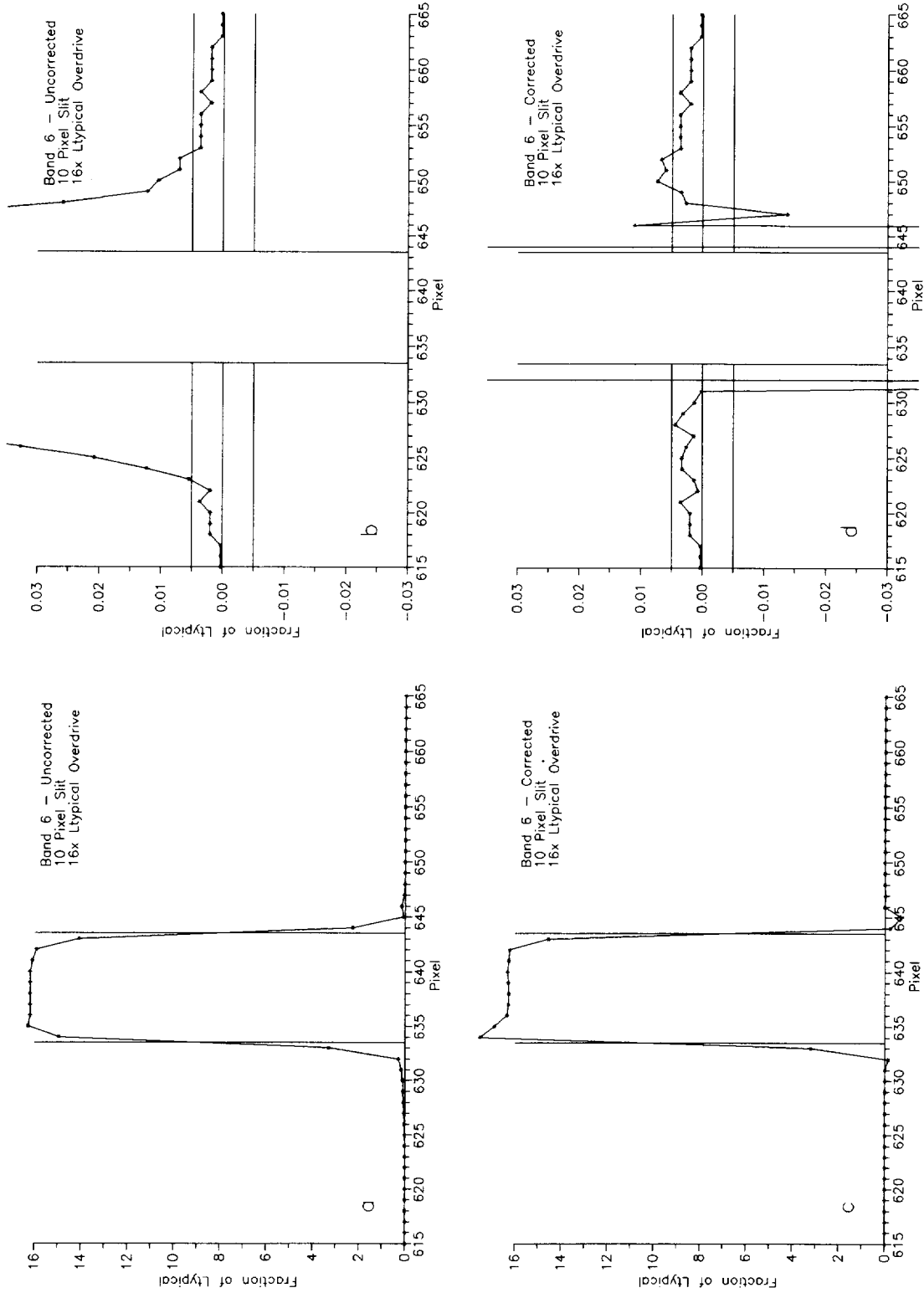


**Fig. 24.** The input and output responses from the stray light correction for band 6, with experimental parameters of high input radiance and a 10 pixel slit. The radiance is  $1.15 L_{\text{typical}}$ . a) The input values are scaled to the peak radiances from the source. b) The input values are scaled to  $\pm 0.03 L_{\text{typical}}$ . (The one-time overshoot in the band's response past the bright source at pixel 645 is instrumentally based.) c) The output values from the stray light correction procedure are scaled to the peak radiances from the source. d) The output values are scaled to  $\pm 0.03 L_{\text{typical}}$ . (The correction creates a one-time overshoot before the bright source at pixel 632, and exaggerates the instrumental overshoot after the source at pixel 645.)

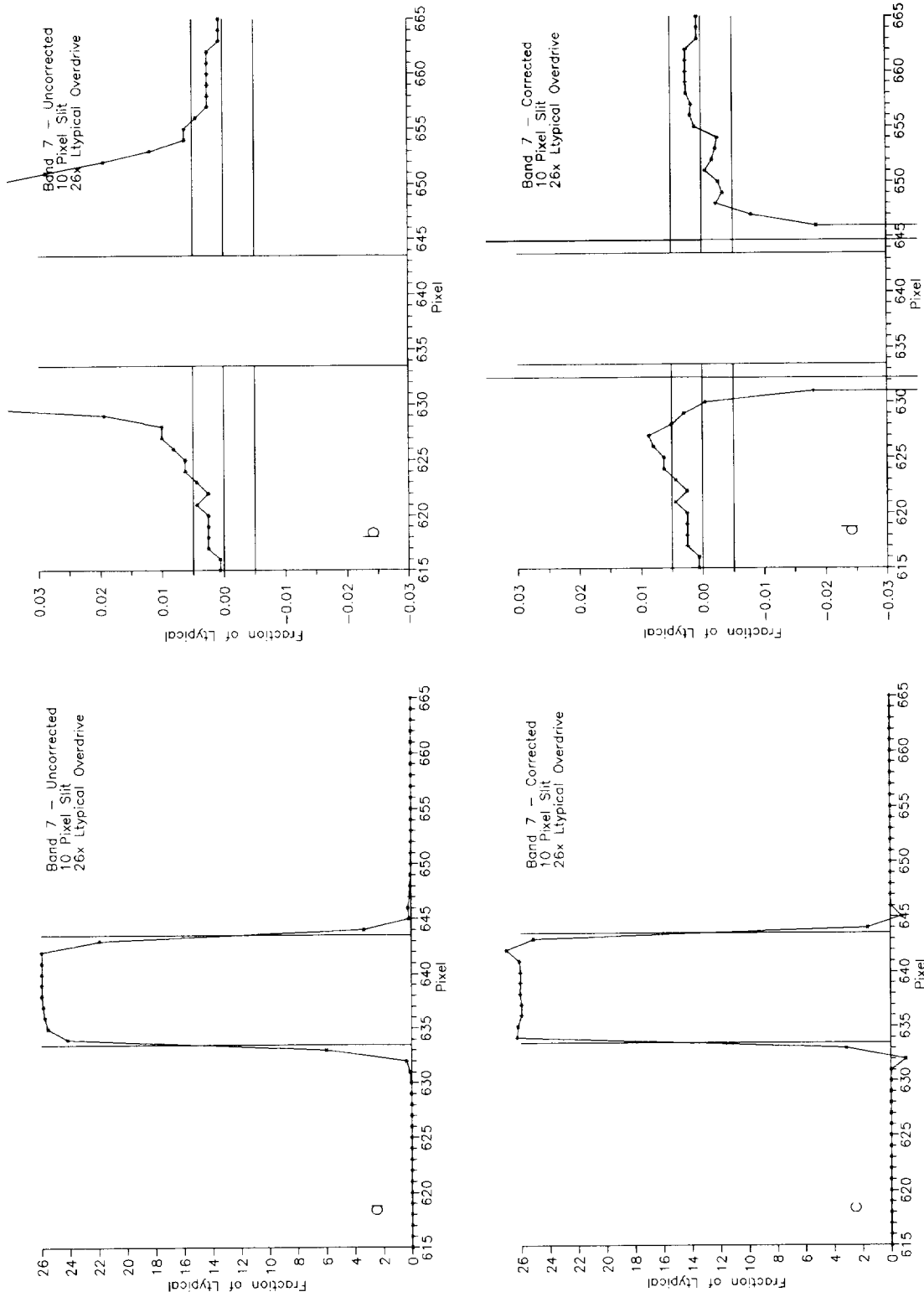


**Fig. 25.** The input and output responses from the stray light correction for band 7 are given, with experimental parameters of high input radiance and a 10 pixel slit. The radiance is  $1.15 L_{\text{typical}}$ . **a)** The input values are scaled to the peak radiances from the source. **b)** The input values are scaled to  $\pm 0.03 L_{\text{typical}}$ . (The one-time overshoot in the band's response past the bright source at pixel 645 is instrumentally based.) **c)** The output values from the stray light correction procedure are scaled to the peak radiances from the source. **d)** The output values are scaled to  $\pm 0.03 L_{\text{typical}}$ . (The correction creates a one-time overshoot before the bright source at pixel 632, and exaggerates the instrumental overshoot after the source at pixel 645.)

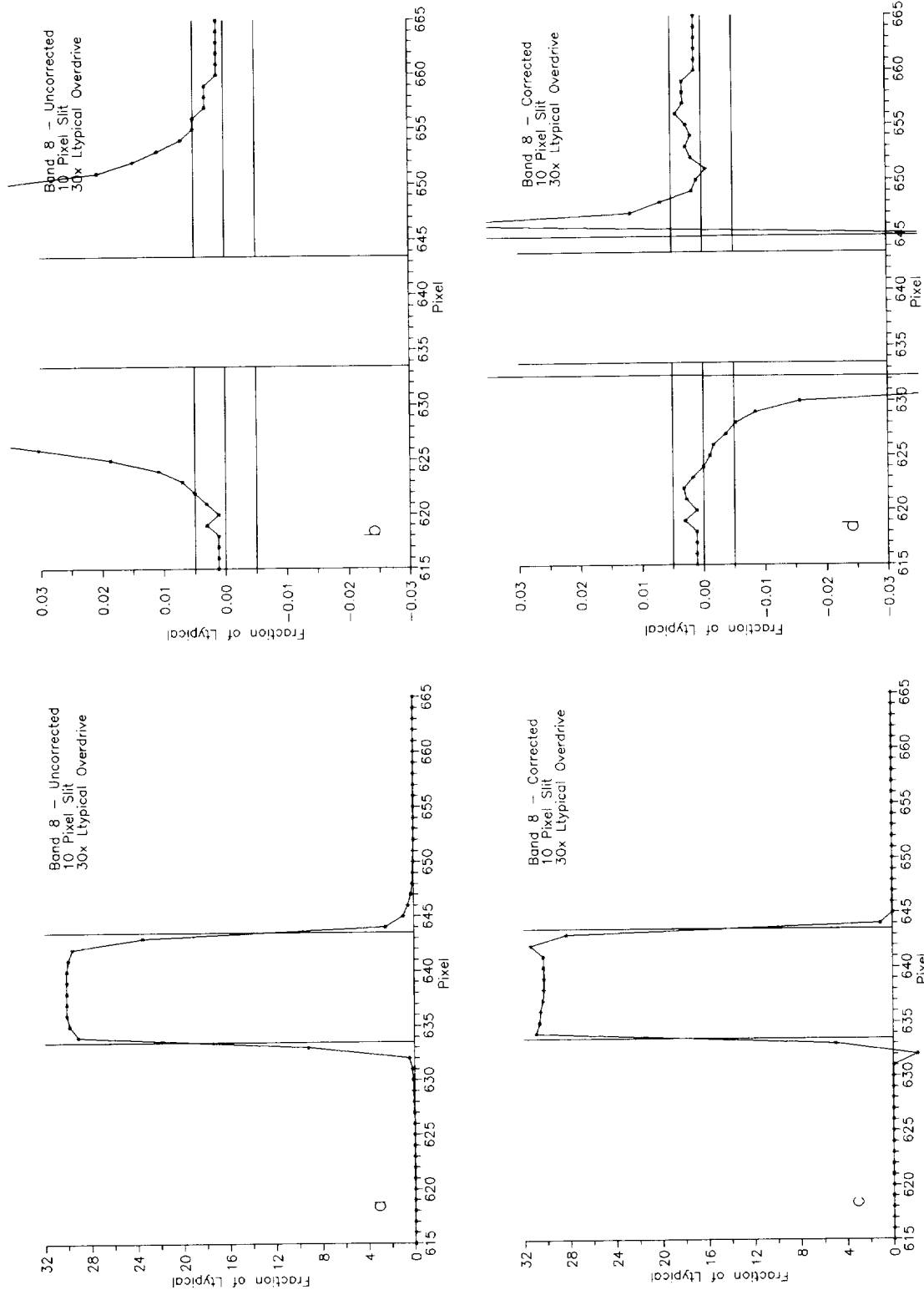


**Fig. 26.** The input and output responses from the stray light correction for band 8 are given, with experimental parameters of high input radiance and a 10 pixel slit. The radiance is  $1.15 L_{\text{typical}}$ . **a)** The input values are scaled to the peak radiances from the source. **b)** The input values are scaled to  $\pm 0.03 L_{\text{typical}}$ . (The one-time overshoot in the band's response past the bright source at pixel 645 is instrumentally based.) **c)** The output values from the stray light correction procedure are scaled to the peak radiances from the source. **d)** The output values are scaled to  $\pm 0.03 L_{\text{typical}}$ . (The correction creates a one-time overshoot before the bright source at pixel 632, and exaggerates the instrumental overshoot after the source at pixel 645.)

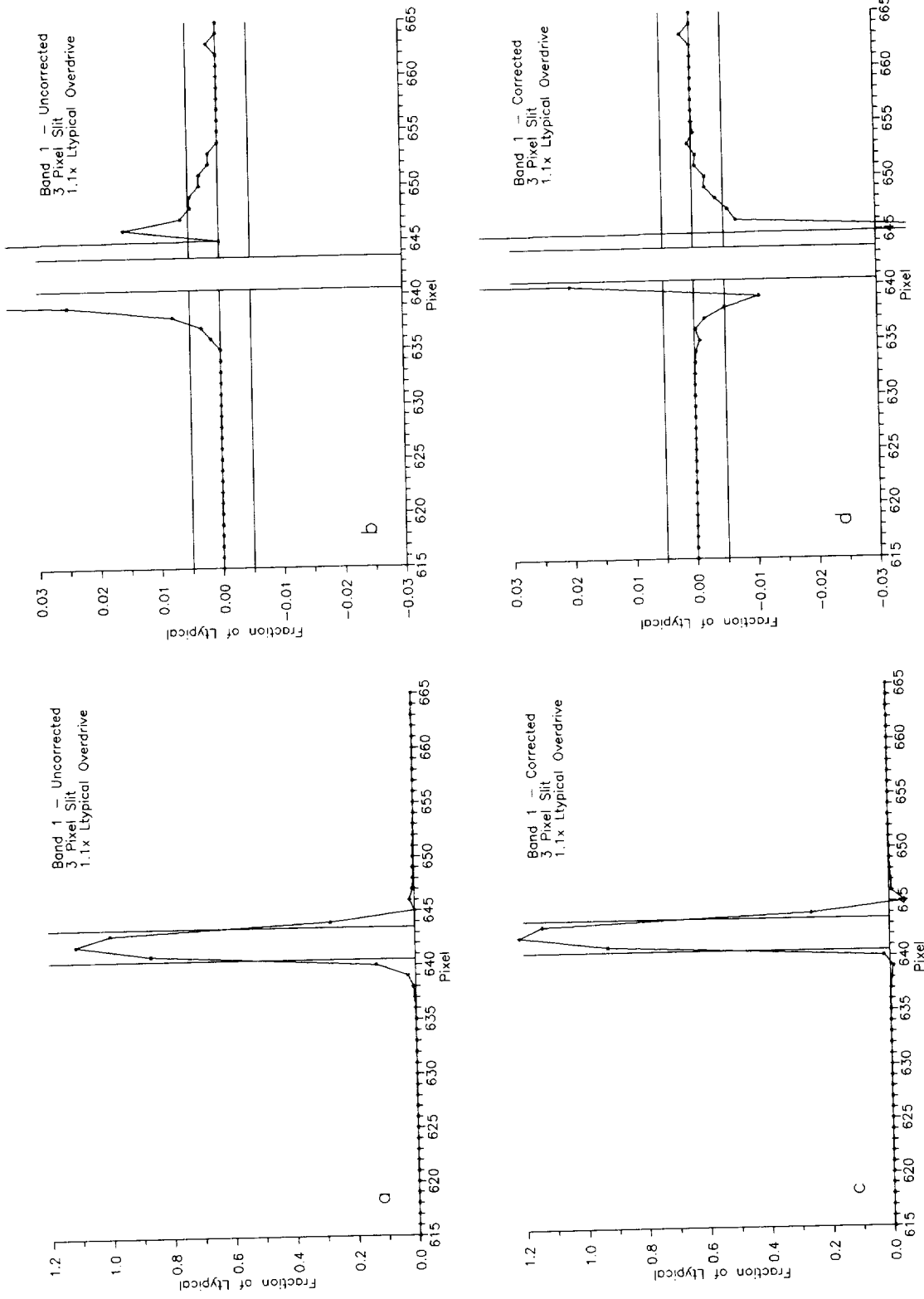


**Fig. 27.** The input and output responses from the stray light correction for band 1 are given, with experimental parameters of high input radiance and a 10 pixel slit. The radiance is  $1.15 L_{\text{typical}}$ . **a)** The input values are scaled to the peak radiances from the source. **b)** The input values are scaled to  $\pm 0.03 L_{\text{typical}}$ . (The one-time overshoot in the band's response past the bright source at pixel 645 is instrumentally based.) **c)** The output values from the stray light correction procedure are scaled to the peak radiances from the source. **d)** The output values are scaled to  $\pm 0.03 L_{\text{typical}}$ . (The correction creates a one-time overshoot before the bright source at pixel 632, and exaggerates the instrumental overshoot after the source at pixel 645.)

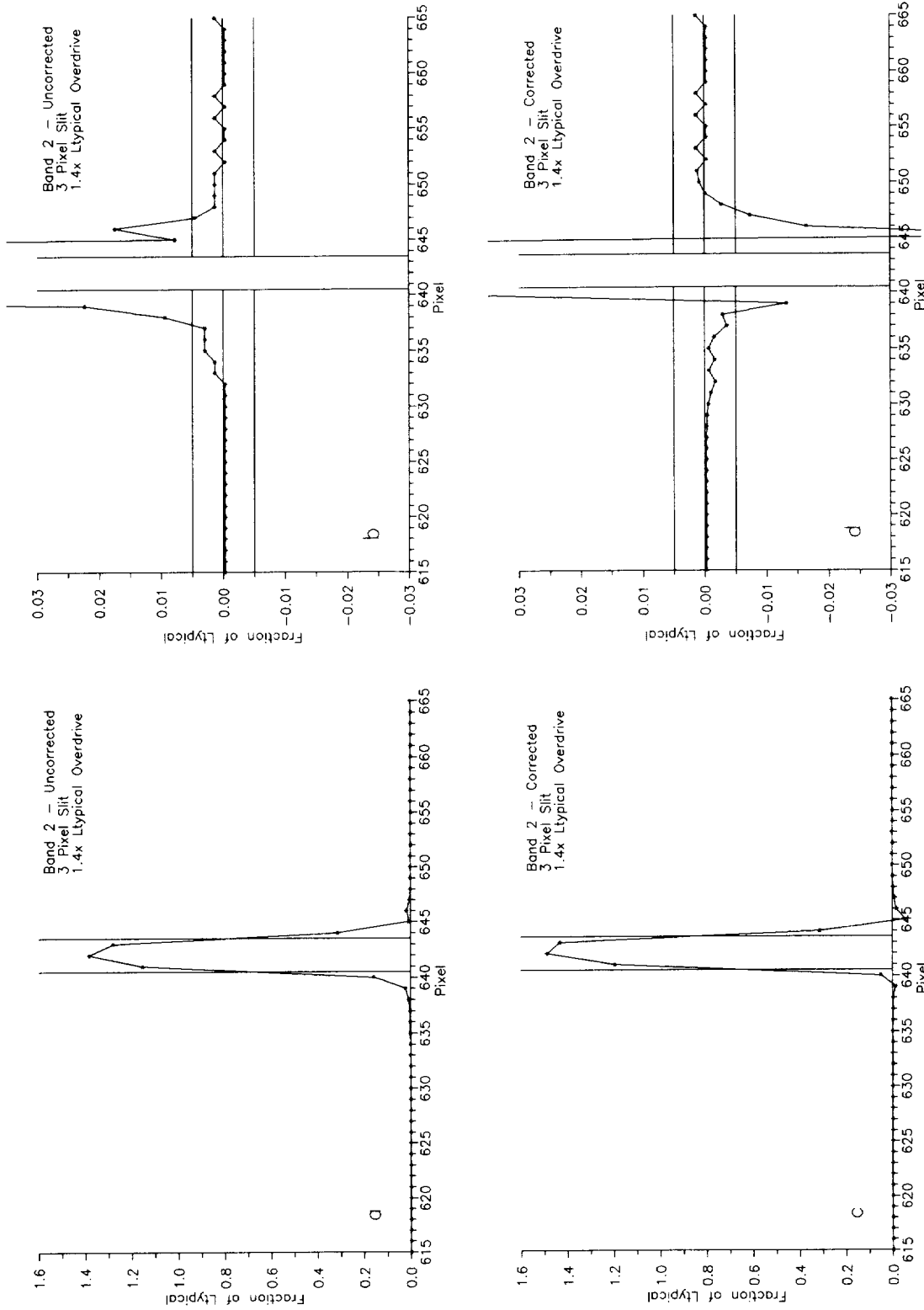


**Fig. 28.** The input and output responses from the stray light correction for band 2 are given, with experimental parameters of high input radiance and a 10 pixel slit. The radiance is  $1.15 L_{\text{typical}}$ . **a)** The input values are scaled to the peak radiances from the source. **b)** The input values are scaled to  $\pm 0.03 L_{\text{typical}}$ . (The one-time overshoot in the band's response past the bright source at pixel 645 is instrumentally based.) **c)** The output values from the stray light correction procedure are scaled to the peak radiances from the source. **d)** The output values are scaled to  $\pm 0.03 L_{\text{typical}}$ . (The correction creates a one-time overshoot before the bright source at pixel 632, and exaggerates the instrumental overshoot after the source at pixel 645.)

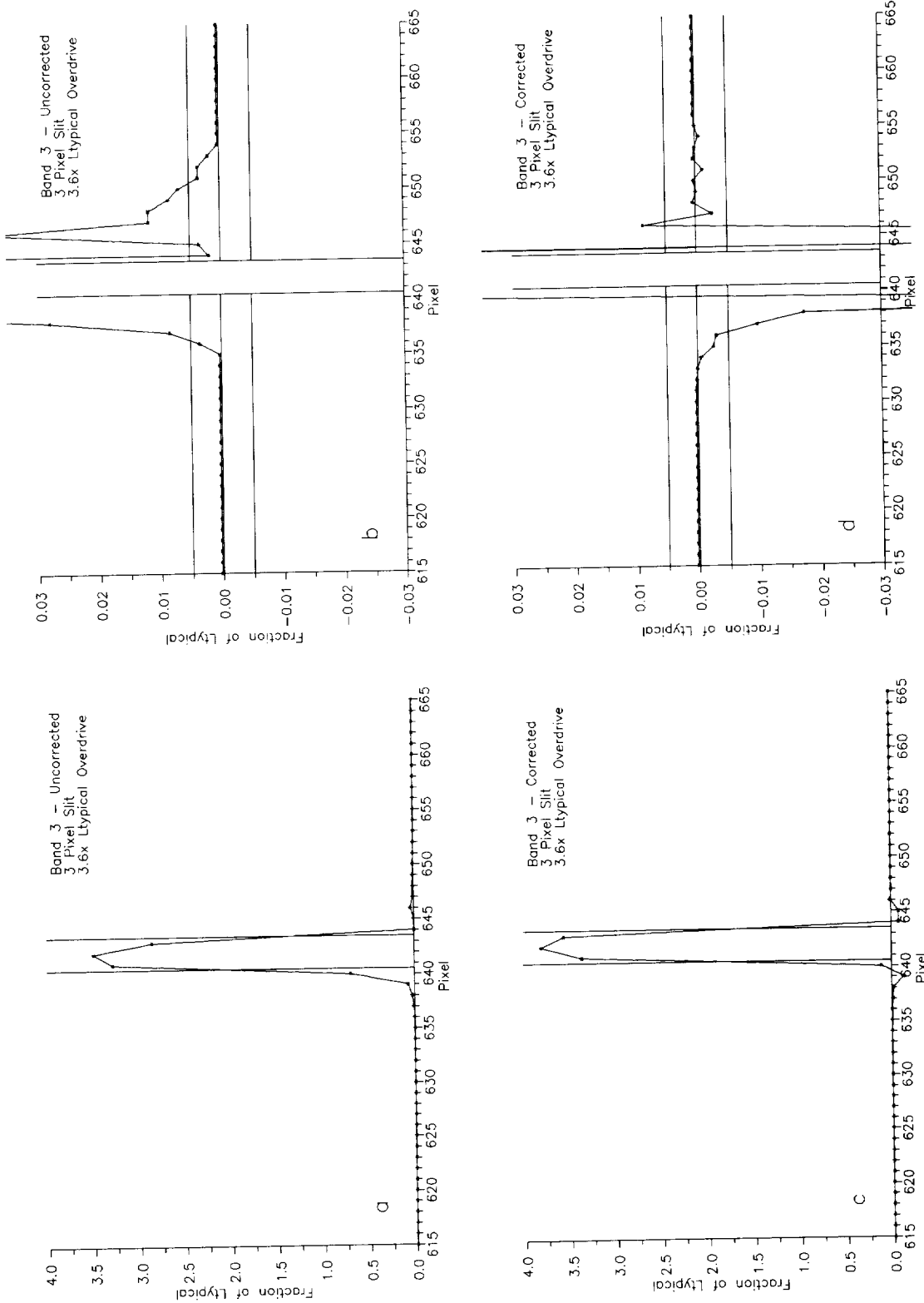


**Fig. 29.** The input and output responses from the stray light correction for band 3 are given, with experimental parameters of high input radiance and a 10 pixel slit. The radiance is  $1.15 L_{\text{typical}}$ . **a)** The input values are scaled to the peak radiances from the source. **b)** The input values are scaled to  $\pm 0.03 L_{\text{typical}}$ . (The one-time overshoot in the band's response past the bright source at pixel 645 is instrumentally based.) **c)** The output values from the stray light correction procedure are scaled to the peak radiances from the source. **d)** The output values are scaled to  $\pm 0.03 L_{\text{typical}}$ . (The correction creates a one-time overshoot before the bright source at pixel 632, and exaggerates the instrumental overshoot after the source at pixel 645.)

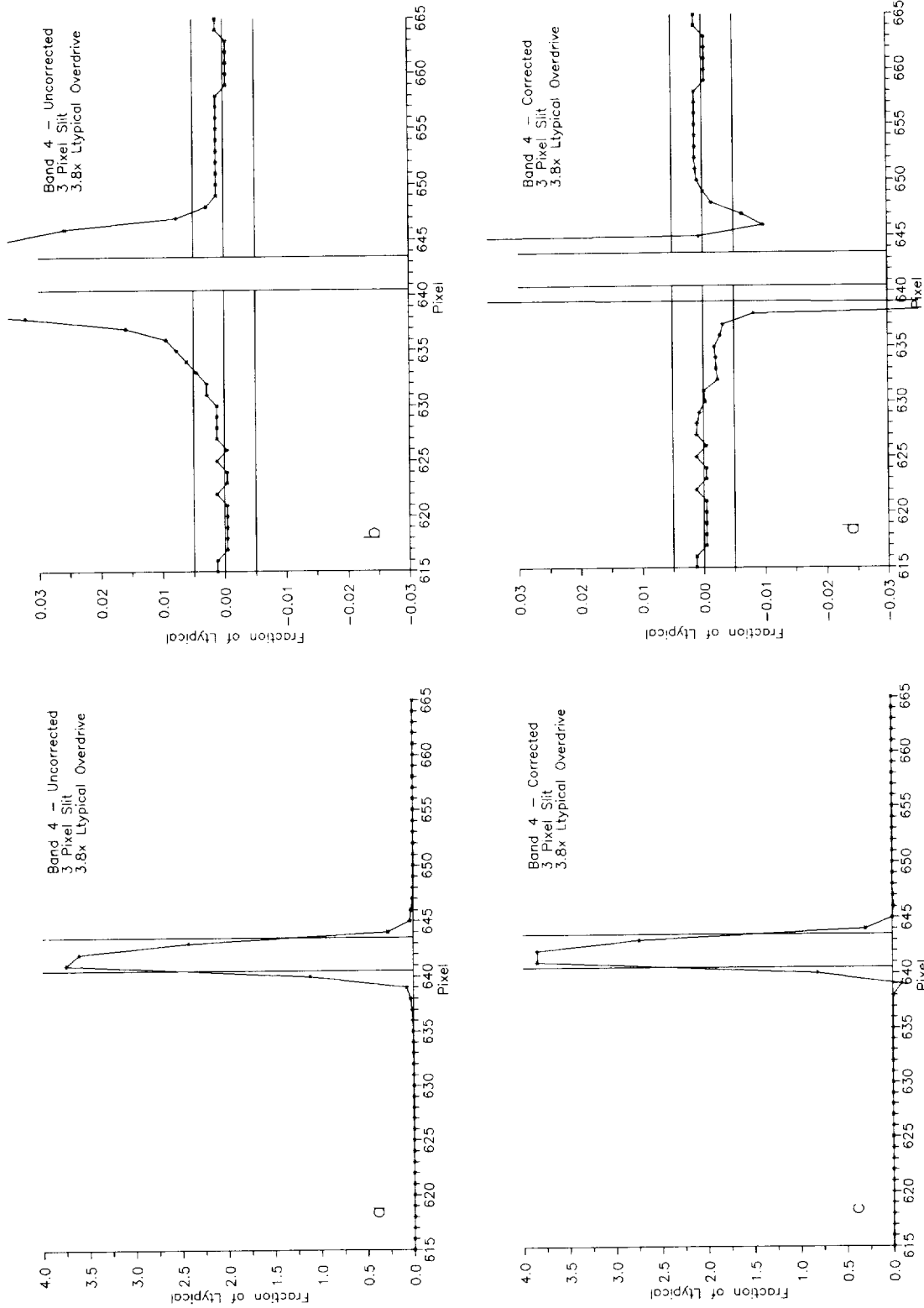


**Fig. 30.** The input and output responses from the stray light correction for band 4 are given, with experimental parameters of high input radiance and a 10 pixel slit. The radiance is  $1.15 L_{\text{typical}}$ . **a)** The input values are scaled to the peak radiances from the source. **b)** The input values are scaled to  $\pm 0.03 L_{\text{typical}}$ . (The one-time overshoot in the band's response past the bright source at pixel 645 is instrumentally based.) **c)** The output values from the stray light correction procedure are scaled to the peak radiances from the source. **d)** The output values are scaled to  $\pm 0.03 L_{\text{typical}}$ . (The correction creates a one-time overshoot before the bright source at pixel 632, and exaggerates the instrumental overshoot after the source at pixel 645.)

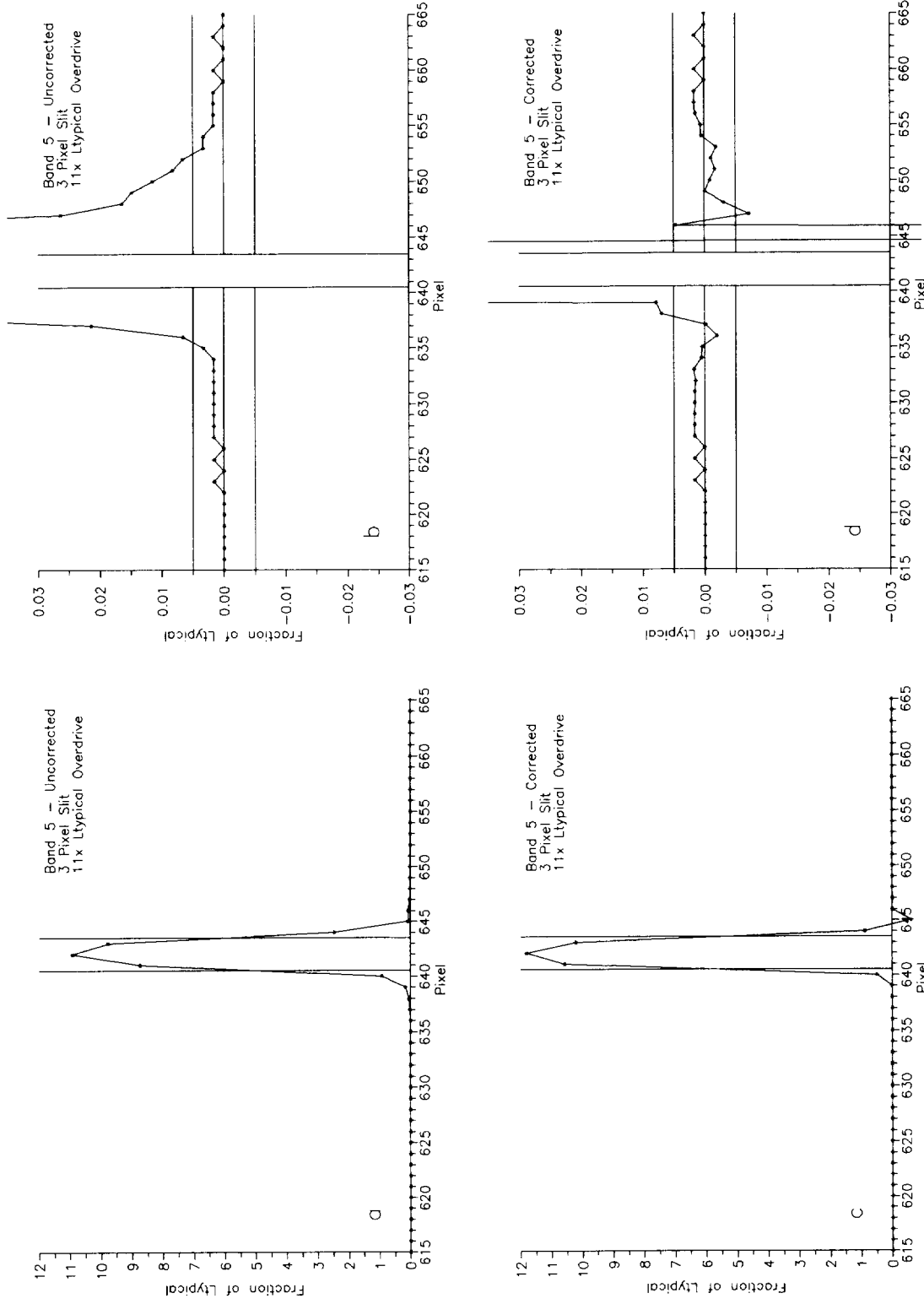


**Fig. 31.** The input and output responses from the stray light correction for band 5 are given, with experimental parameters of high input radiance and a 10 pixel slit. The radiance is  $1.15 L_{\text{typical}}$ . **a)** The input values are scaled to the peak radiances from the source. **b)** The input values are scaled to  $\pm 0.03 L_{\text{typical}}$ . (The one-time overshoot in the band's response past the bright source at pixel 645 is instrumentally based.) **c)** The output values from the stray light correction procedure are scaled to the peak radiances from the source. **d)** The output values are scaled to  $\pm 0.03 L_{\text{typical}}$ . (The correction creates a one-time overshoot before the bright source at pixel 632, and exaggerates the instrumental overshoot after the source at pixel 645.)

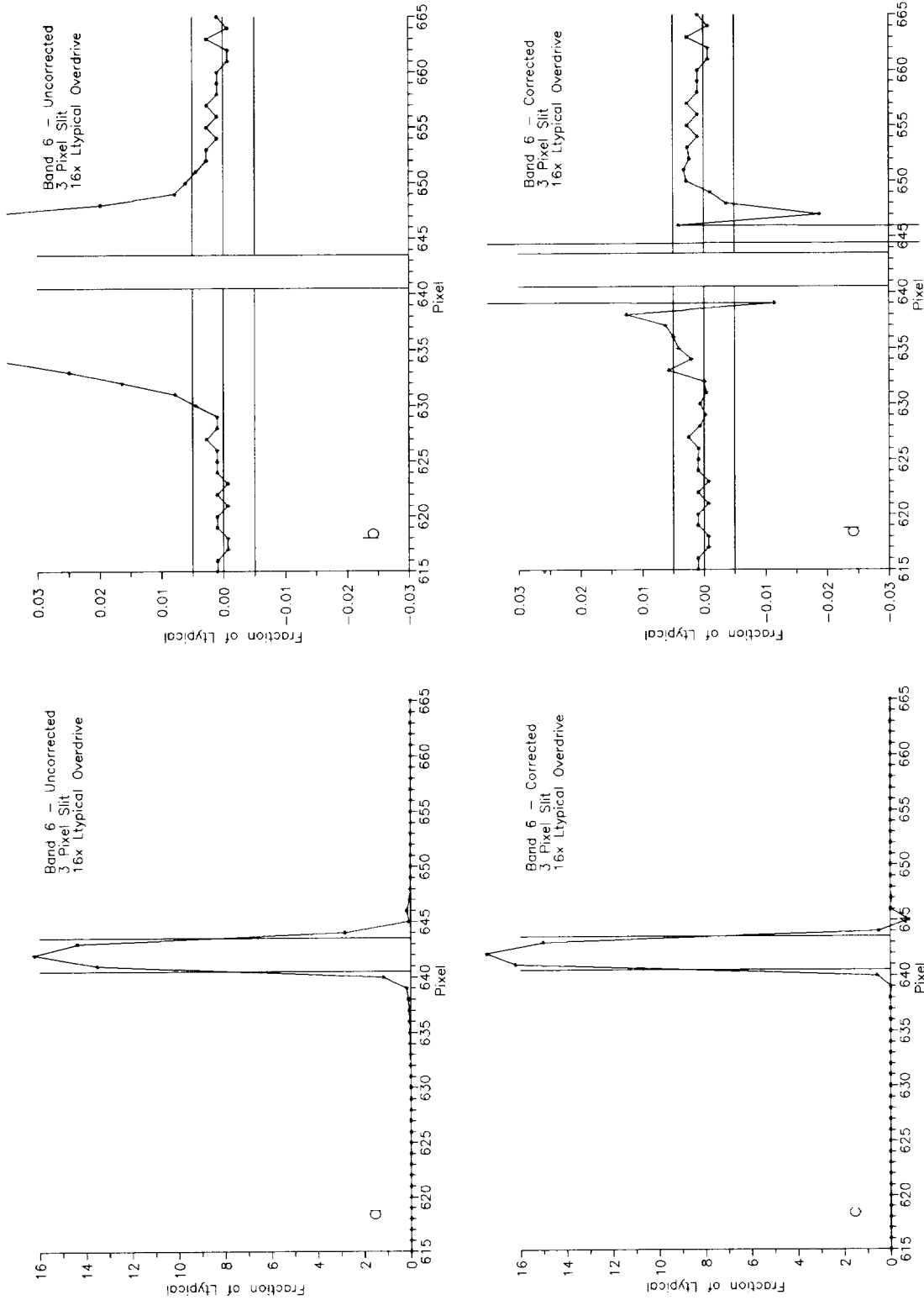


**Fig. 32.** The input and output responses from the stray light correction for band 6 are given, with experimental parameters of high input radiance and a 10 pixel slit. The radiance is  $1.15 L_{\text{typical}}$ . **a)** The input values are scaled to the peak radiances from the source. **b)** The input values are scaled to  $\pm 0.03 L_{\text{typical}}$ . (The one-time overshoot in the band's response past the bright source at pixel 645 is instrumentally based.) **c)** The output values from the stray light correction procedure are scaled to the peak radiances from the source. **d)** The output values are scaled to  $\pm 0.03 L_{\text{typical}}$ . (The correction creates a one-time overshoot before the bright source at pixel 632, and exaggerates the instrumental overshoot after the source at pixel 645.)

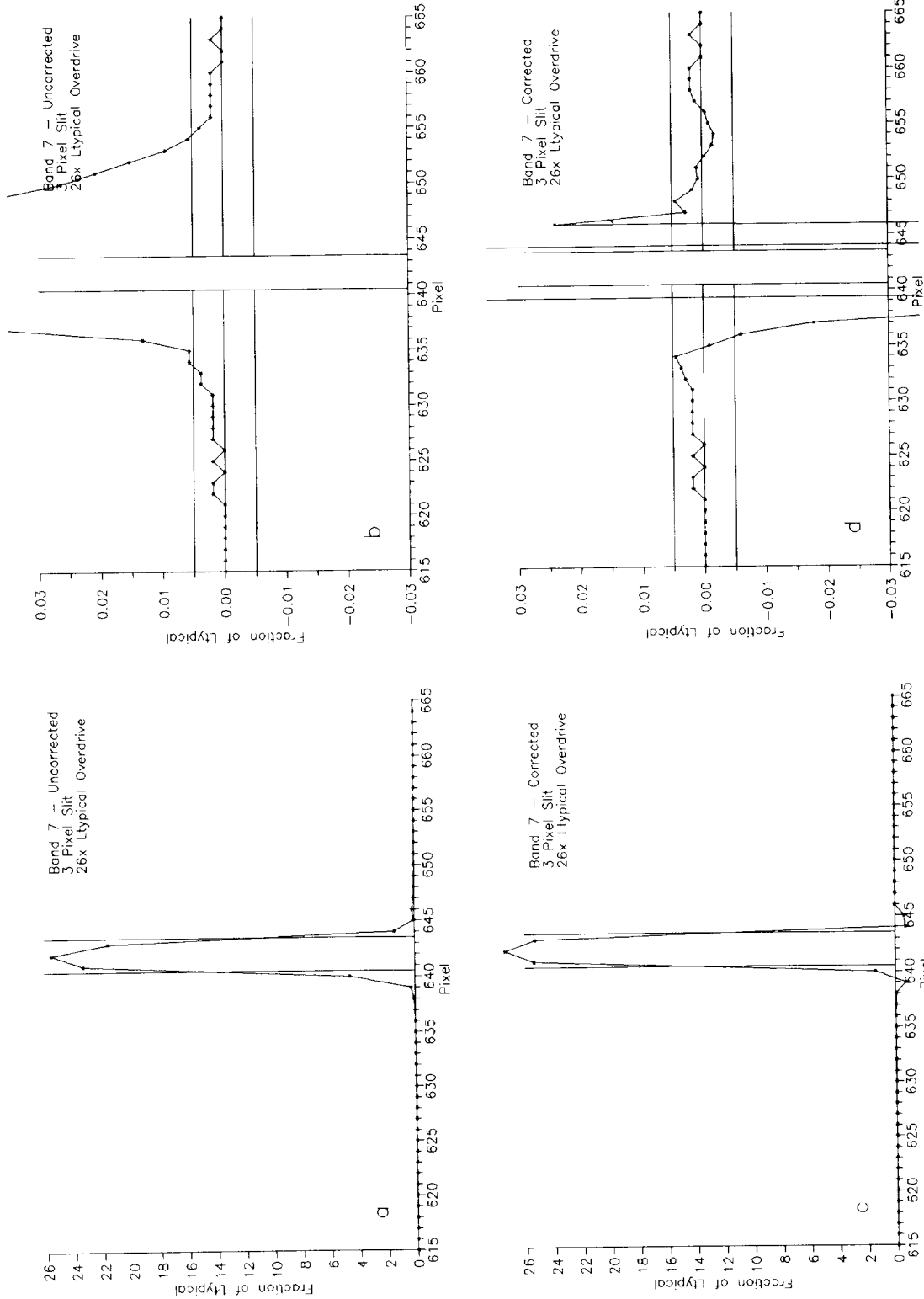


**Fig. 33.** The input and output responses from the stray light correction for band 7 are given, with experimental parameters of high input radiance and a 10 pixel slit. The radiance is  $1.15 L_{\text{typical}}$ . **a)** The input values are scaled to the peak radiances from the source. **b)** The input values are scaled to  $\pm 0.03 L_{\text{typical}}$ . (The one-time overshoot in the band's response past the bright source at pixel 645 is instrumentally based.) **c)** The output values from the stray light correction procedure are scaled to the peak radiances from the source. **d)** The output values are scaled to  $\pm 0.03 L_{\text{typical}}$ . (The correction creates a one-time overshoot before the bright source at pixel 632, and exaggerates the instrumental overshoot after the source at pixel 645.)

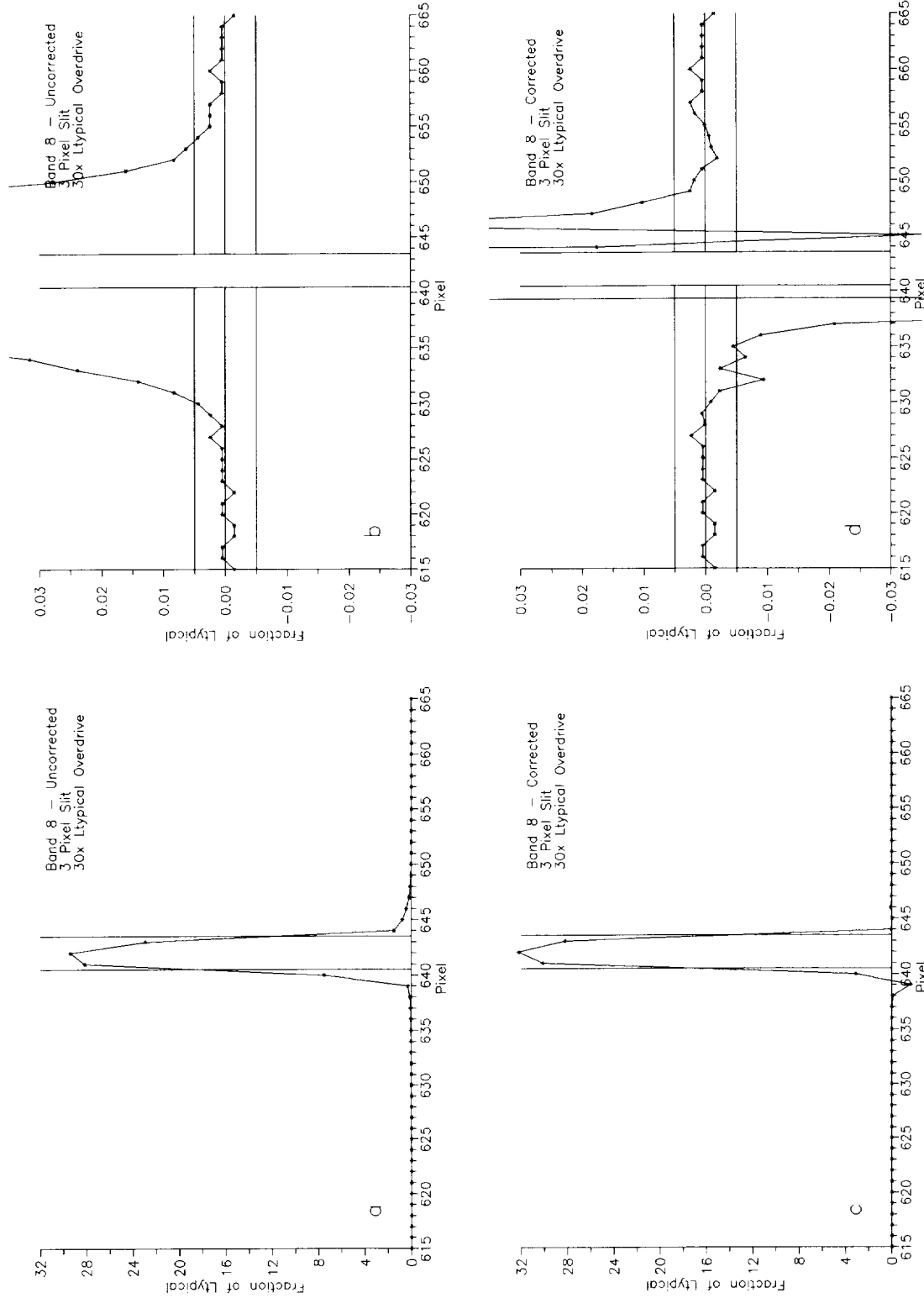


**Fig. 34.** The input and output responses from the stray light correction for band 8 are given, with experimental parameters of high input radiance and a 10 pixel slit. The radiance is  $1.15 L_{\text{typical}}$ . **a)** The input values are scaled to the peak radiances from the source. **b)** The input values are scaled to  $\pm 0.03 L_{\text{typical}}$ . (The one-time overshoot in the band's response past the bright source at pixel 645 is instrumentally based.) **c)** The output values from the stray light correction procedure are scaled to the peak radiances from the source. **d)** The output values are scaled to  $\pm 0.03 L_{\text{typical}}$ . (The correction creates a one-time overshoot before the bright source at pixel 632, and exaggerates the instrumental overshoot after the source at pixel 645.)

**Table 13.** Results from the stray light correction for band 7 with a 10 pixel slit, and high radiance output from the source. This table gives the input values to, and the output values from, the stray light correction. The radiance values have units of  $\text{mW cm}^{-2} \text{sr}^{-1} \mu\text{m}^{-1}$ .

Pixel Number	Radiance Units		$L_{\text{cloud}}$ Normalized		$L_{\text{typical}}$ Normalized	
	Input	Output	Input	Output	Input	Output
615	0.00101	0.00101	0.00002	0.00002	0.00063	0.00063
616	0.00101	0.00101	0.00002	0.00002	0.00063	0.00063
617	0.00404	0.00404	0.00009	0.00009	0.00251	0.00251
618	0.00404	0.00404	0.00009	0.00009	0.00251	0.00251
619	0.00404	0.00404	0.00009	0.00009	0.00251	0.00251
620	0.00404	0.00404	0.00009	0.00009	0.00251	0.00251
621	0.00707	0.00707	0.00016	0.00016	0.00439	0.00439
622	0.00404	0.00404	0.00009	0.00009	0.00251	0.00251
623	0.00707	0.00707	0.00016	0.00016	0.00439	0.00439
624	0.01009	0.01009	0.00023	0.00023	0.00627	0.00627
625	0.01009	0.01009	0.00023	0.00023	0.00627	0.00627
626	0.01312	0.01283	0.00031	0.00030	0.00815	0.00797
627	0.01615	0.01402	0.00038	0.00033	0.01003	0.00871
628	0.01615	0.00811	0.00038	0.00019	0.01003	0.00504
629	0.03129	0.00485	0.00073	0.00011	0.01943	0.00301
630	0.07671	-0.00081	0.00178	-0.00002	0.04765	-0.00050
631	0.19177	-0.02908	0.00446	-0.00068	0.11911	-0.01806
632	0.57633	-1.68687	0.01340	-0.03923	0.35797	-1.04775
633	9.69040	5.06424	0.22536	0.11777	6.01888	3.14549
634	38.88820	42.32283	0.90438	0.98425	24.15416	26.28747
635	41.13418	42.22813	0.95661	0.98205	25.54918	26.22865
636	41.47972	41.82420	0.96464	0.97266	25.76380	25.97776
637	41.65248	41.82302	0.96866	0.97263	25.87111	25.97703
638	41.82525	41.97839	0.97268	0.97624	25.97842	26.07353
639	41.82525	41.94110	0.97268	0.97537	25.97842	26.05037
640	41.82525	41.95810	0.97268	0.97577	25.97842	26.06093
641	41.82525	42.06381	0.97268	0.97823	25.97842	26.12659
642	41.82525	43.51957	0.97268	1.01208	25.97842	27.03079
643	35.26007	40.46626	0.82000	0.94108	21.90066	25.13432
644	5.37120	2.56723	0.12491	0.05970	3.33615	1.59455
645	0.25536	-1.28311	0.00594	-0.02984	0.15861	-0.79696
646	0.38254	-0.03002	0.00890	-0.00070	0.23760	-0.01865
647	0.17663	-0.01295	0.00411	-0.00030	0.10971	-0.00804
648	0.12213	-0.00370	0.00284	-0.00009	0.07586	-0.00230
649	0.08579	-0.00546	0.00200	-0.00013	0.05329	-0.00339
650	0.06157	-0.00432	0.00143	-0.00010	0.03824	-0.00268
651	0.04643	-0.00095	0.00108	-0.00002	0.02884	-0.00059
652	0.03129	-0.00279	0.00073	-0.00006	0.01943	-0.00173
653	0.01918	-0.00366	0.00045	-0.00009	0.01191	-0.00227
654	0.01009	-0.00417	0.00023	-0.00010	0.00627	-0.00259
655	0.01009	0.00172	0.00023	0.00004	0.00627	0.00107
656	0.00707	0.00285	0.00016	0.00007	0.00439	0.00177
657	0.00404	0.00261	0.00009	0.00006	0.00251	0.00162
658	0.00404	0.00388	0.00009	0.00009	0.00251	0.00241

**Table 13 (cont.)** Results from the stray light correction for band 7 with a 10 pixel slit, and high radiance output from the source. This table gives the input values to, and the output values from, the stray light correction. The radiance values have units of  $\text{mW cm}^{-2} \text{sr}^{-1} \mu\text{m}^{-1}$ .

Pixel Number	Radiance Units		$L_{\text{cloud}}$ Normalized		$L_{\text{typical}}$ Normalized	
	Input	Output	Input	Output	Input	Output
659	0.00404	0.00404	0.00009	0.00009	0.00251	0.00251
660	0.00404	0.00404	0.00009	0.00009	0.00251	0.00251
661	0.00404	0.00404	0.00009	0.00009	0.00251	0.00251
662	0.00404	0.00404	0.00009	0.00009	0.00251	0.00251
663	0.00101	0.00101	0.00002	0.00002	0.00063	0.00063
664	0.00101	0.00101	0.00002	0.00002	0.00063	0.00063
665	0.00101	0.00101	0.00002	0.00002	0.00063	0.00063

full illumination from the bright source, and 19b scaled to  $\pm 0.03$ , i.e.,  $\pm 3\%$  of  $L_{\text{typical}}$ . The horizontal scales for 19c and 19d are identical to those for 19a and 19b, respectively; however, 19c and 19d give the output (corrected) radiances from the stray light algorithm. For 19b and 19d, horizontal lines are added at  $\pm 0.005$  ( $\pm 0.5\%$ ) of  $L_{\text{typical}}$ . These limits are part of the stray light specification.

In all of the measurements, the down scan (rightmost) part of the bright slit was placed at pixel 643. The edges of the bright slits were set so that they divided the endmost pixels. Thus, for a 10 pixel slit, the slit was adjusted to give 9 full pixels in the center of the bright source, plus 0.5 pixel on each end. For a 3 pixel measurement, there were two central pixels plus 0.5 pixel on each end. The slit edge positions were repeatable to about  $\pm 0.5$  pixel from measurement to measurement. Both the measurement setup and the presentation of Figs. 19–50 were designed to provide results that are as uniform as possible. This is particularly true for the design of subpanels *b* and *d* of the figures, which show the details of the instrument's response to bright sources. This was done to allow quick visual comparisons of the results from each band, radiance level, and slit width.

Figure 25 shows the results for band 7, listed in Table 13. Both the tabulated results for this measurement and the figure (subpanel 25d) show the stray light correction to overshoot the zero level both before and after the bright source. Figure 25 also shows that the algorithm undercorrects for the stray light before the slit. The impulse provides essentially no correction for pixel 627 and below.

There is a small electronic overshoot in each band's response one pixel after a bright source. This characteristic lies ingrained within the instrument. As shown in Fig. 1 of Barnes et al. (1994a), each SeaWiFS band has a nearly identical one-time overshoot in its along-scan response. This effect derives from the design of the Goldberg noise reduction filter in each band's intermediate electronics. This design helps to ensure that the instrument meets the MTF portion of the Ocean Color Data Mission performance specifications in the along-scan direction (see Section 14 of Barnes et al. 1994a).

Since the instrument's radiometric calibration used an extended source with nearly uniform radiance, the electronic effect has been, in effect, *calibrated* into ocean scenes that have roughly constant radiances. For scenes with sharp transitions in radiance, particularly in the down-scan transitions from bright sources shown here, the electronic overshoot is present one pixel from the radiant source. There is no sign of the overshoot before bright targets. The effect of the Goldberg filter can be seen in Figs. 19–50: subpanels *a* and *b*. For bands 1–7 in these figures, the overshoot is present down scan of the bright source. For band 8 in these figures, the electronic overshoot cannot be seen to the right of the slit. For this band, the stray light down scan of the slit may be so great as to mask the electronic effect.

It is obvious from the results in Figs. 19–50 that the stray light algorithm overcompensates close to the bright source. In nearly all of the test cases, the corrected results run negative for the pixel before the bright source, returning to zero as distance from the bright source increases. For the down scan portion of the measurements, the correction algorithm also exaggerates the electronic overshoot one pixel from the bright source. This overcorrection by the stray light algorithm need not be considered a problem, as it may form the foundation for a method for determining the edges of clouds or other bright targets on orbit.

Clouds observed on orbit will not have the sharp edges characteristic of brightly lit slits in the laboratory. There is every possibility that the corrected instrument radiances from orbit will show the laboratory pattern of overcorrections, however, before and after cloud pixels. Such effects should have distinct fingerprints if the magnitude of the change in radiance of a pixel from its predecessor, along with the first- and second-derivatives of that change, is examined. Recognition of these patterns is not beyond the capacity of current computer programs. The location of the overshoot occurs one pixel from the edge of the source. Figs. 35–36 also show the over-ranging to be present for bright targets that are brighter, by 0.5–0.75 of  $L_{\text{typical}}$ , than the ocean radiances.

As noted above, the positions of the edges of the slits were repeatable to about  $\pm 0.5$  pixel. On orbit, the locations of the bright sources will not be known a priori. It will be interesting to see if this proposal for cloud edge location can be implemented in the on-orbit data reduction procedures. It is also important to note that these discussions of stray light corrections apply only to along-scan measurements.

### 10.3 Post-Correction Stray Light Effects

The results from Figs. 19–26, for high input radiances and 10 pixel slits, are summarized in Fig. 51a. This figure gives the average of the residual responses from the eight bands, plus their standard deviations ( $1\sigma$ ). The abscissa and ordinate of Fig. 51a duplicate those found in subpanel d in each of the figures for the individual bands. In the same manner, Fig. 51b summarizes the results from Figs. 27–34, with high input radiances and 3 pixel slits. Both subpanels of the figure show the residual stray light responses located 4–10 pixels from the slit edge; however, this statement is not entirely correct. The edges of the slits, as explained above, were set so that they divided the endmost pixels in the bright sources. The positions of the edges of the slits, also explained above, were repeatable to about  $\pm 0.5$  pixel. Thus, the responses in Fig. 51 are found from 3.5–9.5 pixels from the slit edges, give or take one-half pixel. With respect to the locations of the points where the correction algorithm overshoots, the responses are located 2–8 pixels away. This observation demonstrates an advantage of using the stray light algorithm results, which contain the overcorrection. The overshoot occurs at a pixel that can be determined with confidence, although the edges of clouds are less well defined.

For all of the results in Fig. 51, except those closest to the bright source, the  $1\sigma$  error bars lie at, or within, the requirements of the instrument specifications (0.5% of  $L_{\text{typical}}$ ). For on-orbit measurements, radiances more than four pixels from clouds (or more than three pixels from the overshoot in the correction algorithm) should be usable in the SeaWiFS data reduction.

Uniformity exists in the pattern to the residual stray light responses in Fig. 51, which can be seen in the tabulated values in Table 14. The mean values and standard deviations from this table were used to create Fig. 51. The similarity between the 3 and 10 pixel results reveal no significant dependence on the width of the bright source. Earlier examinations (unpublished) of the uncorrected stray light in SeaWiFS indicated a small but noticeable increase in stray light with slit width, for slits up to 6 pixels wide. Those preliminary results showed no such dependence for slit widths greater than 6 pixels. Since the masks over the detector arrays for the SeaWiFS bands are 6 pixels long, this effect appears to have a basis in the instrument design. This source-size dependence was the reason for incorporating the two different bright source widths in the

measurements presented here. The post-correction results in Fig. 51, however, show no significant differences between the stray light residuals of 3 and 10 pixels. Since the correction algorithm is based on the instrument's measured response to a 1 pixel laboratory slit, it was concluded that no significant dependence exists in the corrected results on the width of the bright source, i.e., there is no cloud size dependence.

The sizes of the standard deviations in Fig. 51 are also uniform. For all of the residuals, except for those closest to the bright source, the  $1\sigma$  error bars are 0.5% or less of  $L_{\text{typical}}$ . As explained above, the closest pixels will be masked in the reduction of the data from orbit. The brightness of the sources for the measurements ranged from 1–30 times the value of  $L_{\text{typical}}$ , but the scatter in the results has remained uniformly small. As a result, there is no dependence on source brightness in the stray light correction algorithm. It can be applied to very bright clouds, as well as the clouds producing less radiance.

The results from Figs. 35–50, i.e., with midrange input radiances, are summarized in Figs. 52a and 52b. These figures give the average of the residual responses from the eight bands, plus their standard deviations ( $1\sigma$ ). The format for these figures duplicates that for Figs. 51a and 51b. In fact, the results in Figs. 52a and 52b also duplicate the corresponding results in Figs. 51a and 51b. At the 0.1–0.2% level, there are differences between the high range and midrange residuals. For measurements whose light intensities vary by a factor of 2, however, the residuals are essentially identical.

The results shown in Figs. 51 and 52 provide the validation for these along-scan stray light corrections. There are no peculiarities in the results, so the band-to-band stray light response in the instrument is uniform. There are no differences in the results for radiances that vary by a factor of 2, so the stray light response of the instrument is linear with source brightness. These results, however, have been shown only for laboratory measurements. Flight results will provide the ultimate test of these corrections.

## 11. PROPOSED LAC CORRECTION

The following sections discuss the corrections for LAC (1 km resolution) data in both the along-scan and along-track directions.

### 11.1 Along-Scan LAC Correction

The calculation of the along-scan correction was described in Section 9. In that technique, a second 1,285 pixel array is created to hold the corrected radiances. For along-scan LAC data, the correction procedure in Section 9 will be applied to all scan lines.

There are significant stray light residuals, however, in the corrected radiances near bright sources (Section 10.3). Pixels with these large residuals lie within five pixels of

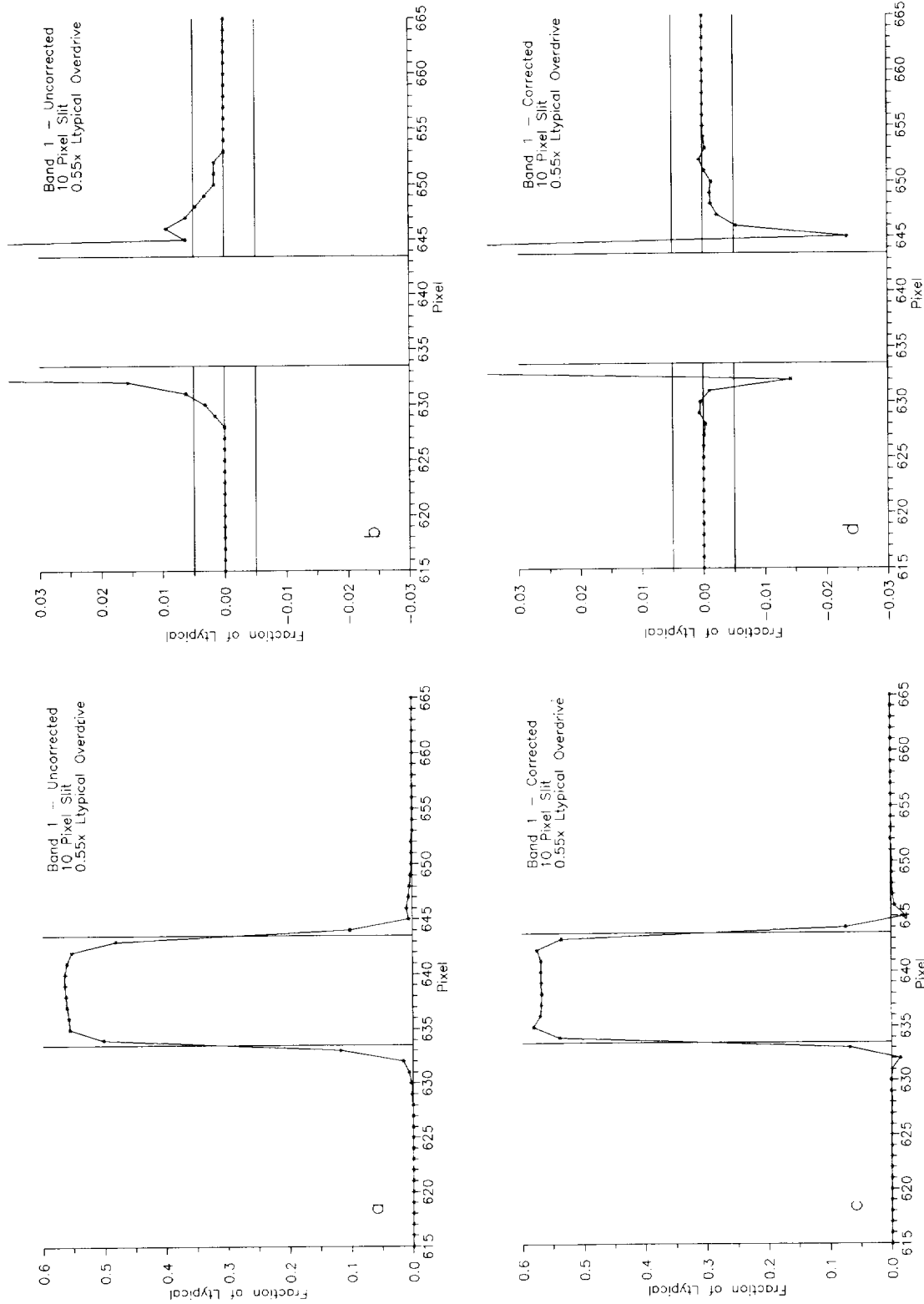


**Fig. 35.** The input and output responses from the stray light correction for band 1 are given, with experimental parameters of midrange input radiance and a 10 pixel slit. The radiance is  $0.55 L_{\text{typical}}$ . **a)** The input values are scaled to the peak radiances from the source. **b)** The input values are scaled to  $\pm 0.03 L_{\text{typical}}$ . (The one-time overshoot in the band's response past the bright source at pixel 645 is instrumentally based.) **c)** The output values from the stray light correction procedure are scaled to the peak radiances from the source. **d)** The output values are scaled to  $\pm 0.03 L_{\text{typical}}$ . (The correction creates a one-time overshoot before the bright source at pixel 632, and exaggerates the instrumental overshoot after the source at pixel 645.)

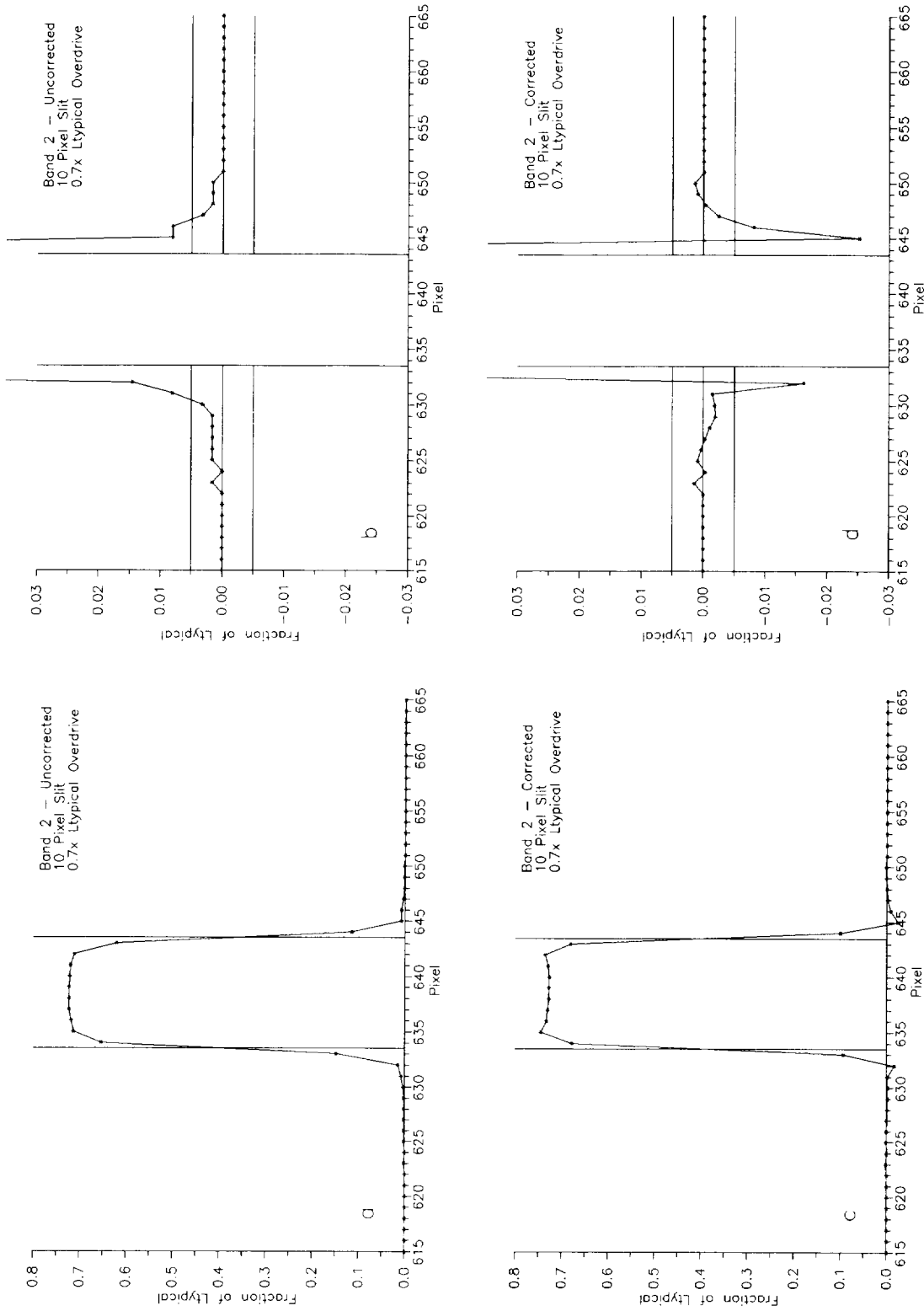


**Fig. 36.** The input and output responses from the stray light correction for band 2 are given, with experimental parameters of midrange input radiance and a 10 pixel slit. The radiance is  $0.7 L_{\text{typical}}$ . **a)** The input values are scaled to the peak radiances from the source. **b)** The input values are scaled to  $\pm 0.03 L_{\text{typical}}$ . (The one-time overshoot in the band's response past the bright source at pixel 645 is instrumentally based.) **c)** The output values from the stray light correction procedure are scaled to the peak radiances from the source. **d)** The output values are scaled to  $\pm 0.03 L_{\text{typical}}$ . (The correction creates a one-time overshoot before the bright source at pixel 632, and exaggerates the instrumental overshoot after the source at pixel 645.)

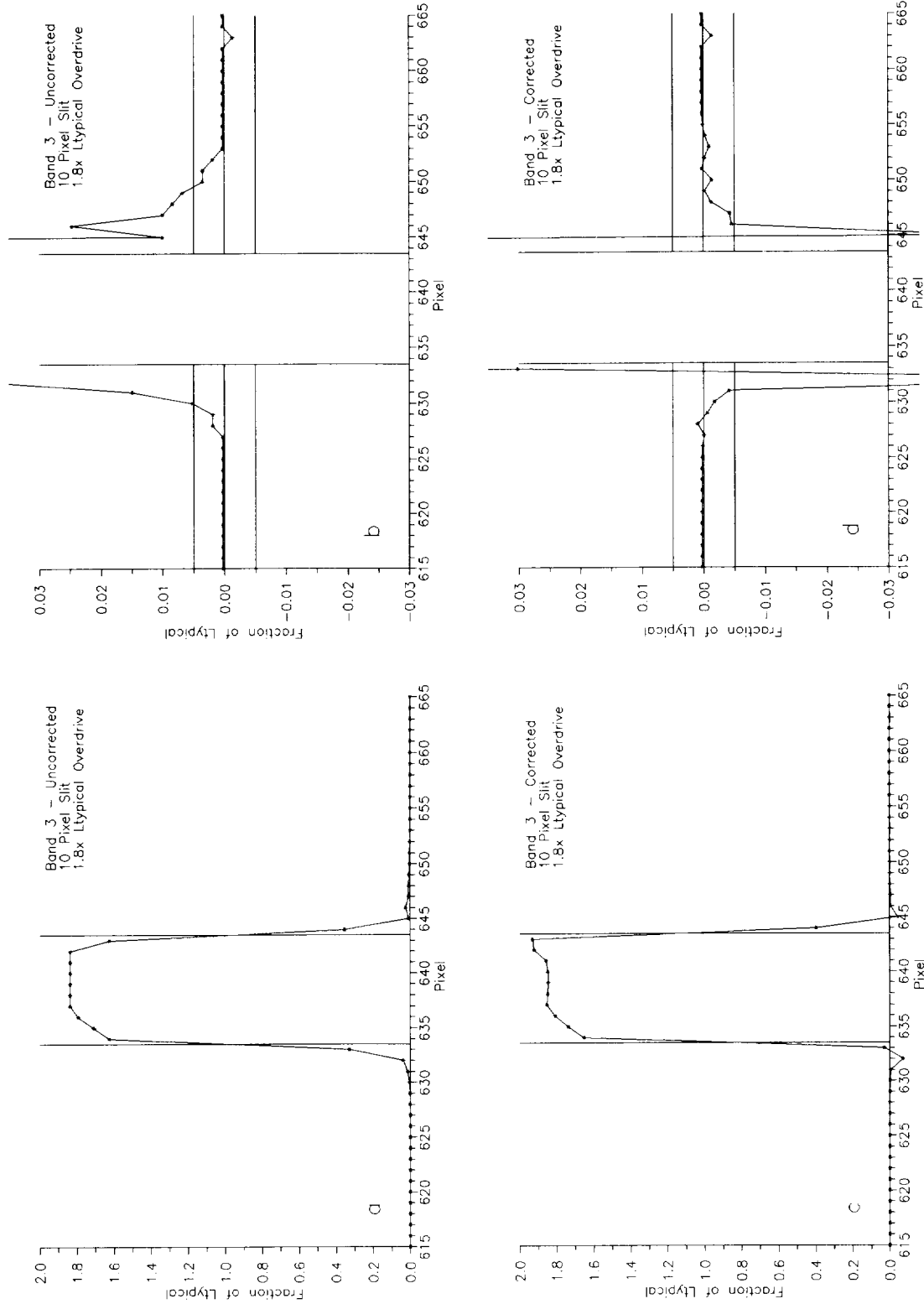


**Fig. 37.** The input and output responses from the stray light correction for band 3 are given, with experimental parameters of midrange input radiance and a 10 pixel slit. The radiance is  $1.8 L_{\text{typical}}$ . **a)** The input values are scaled to the peak radiances from the source. **b)** The input values are scaled to  $\pm 0.03 L_{\text{typical}}$ . (The one-time overshoot in the band's response past the bright source at pixel 645 is instrumentally based.) **c)** The output values from the stray light correction procedure are scaled to the peak radiances from the source. **d)** The output values are scaled to  $\pm 0.03 L_{\text{typical}}$ . (The correction creates a one-time overshoot before the bright source at pixel 632, and exaggerates the instrumental overshoot after the source at pixel 645.)

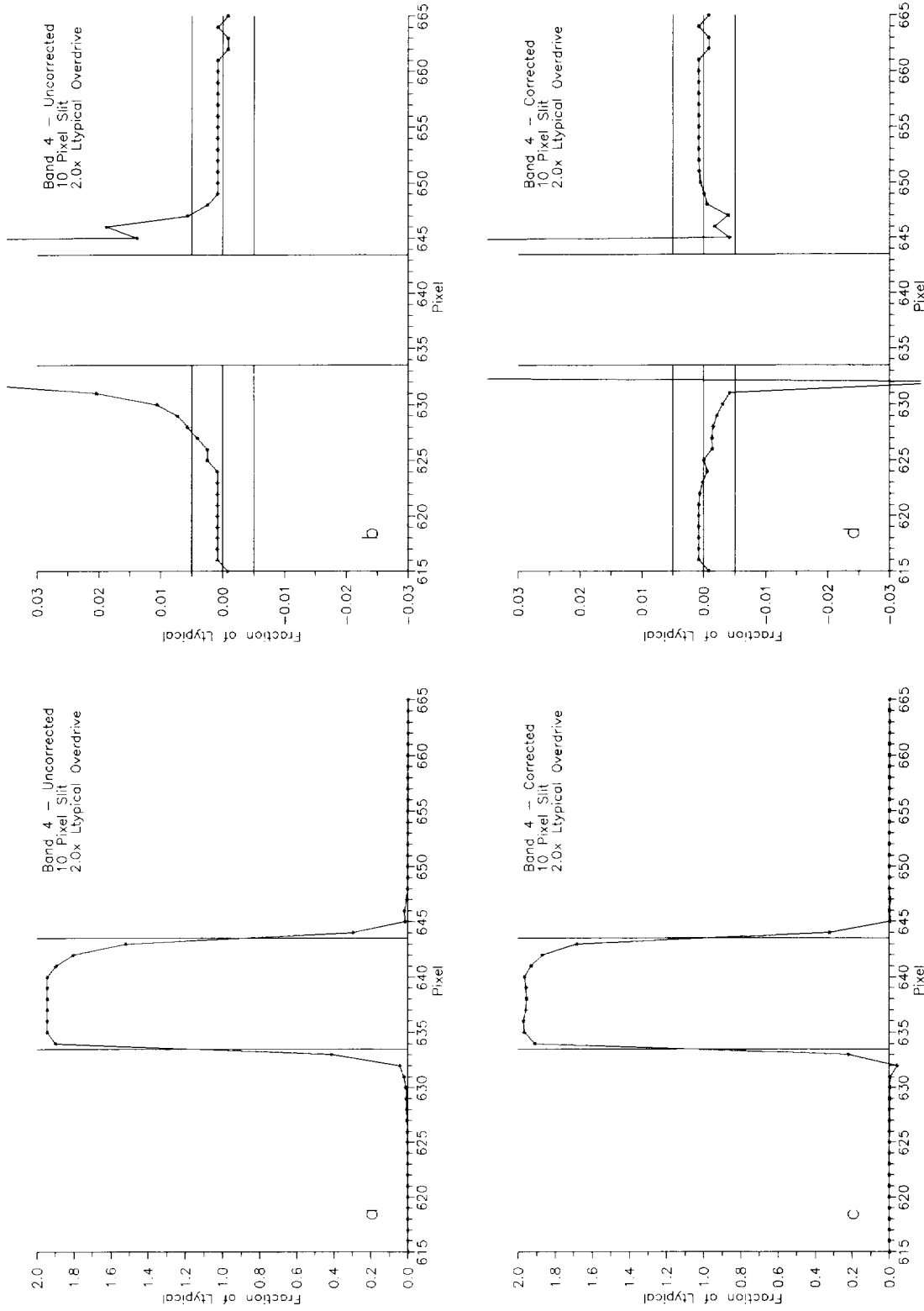


**Fig. 38.** The input and output responses from the stray light correction for band 4 are given, with experimental parameters of midrange input radiance and a 10 pixel slit. The radiance is  $2.0 L_{\text{typical}}$ . **a)** The input values are scaled to the peak radiances from the source. **b)** The input values are scaled to  $\pm 0.03 L_{\text{typical}}$ . (The one-time overshoot in the band's response past the bright source at pixel 645 is instrumentally based.) **c)** The output values from the stray light correction procedure are scaled to the peak radiances from the source. **d)** The output values are scaled to  $\pm 0.03 L_{\text{typical}}$ . (The correction creates a one-time overshoot before the bright source at pixel 632, and exaggerates the instrumental overshoot after the source at pixel 645.)

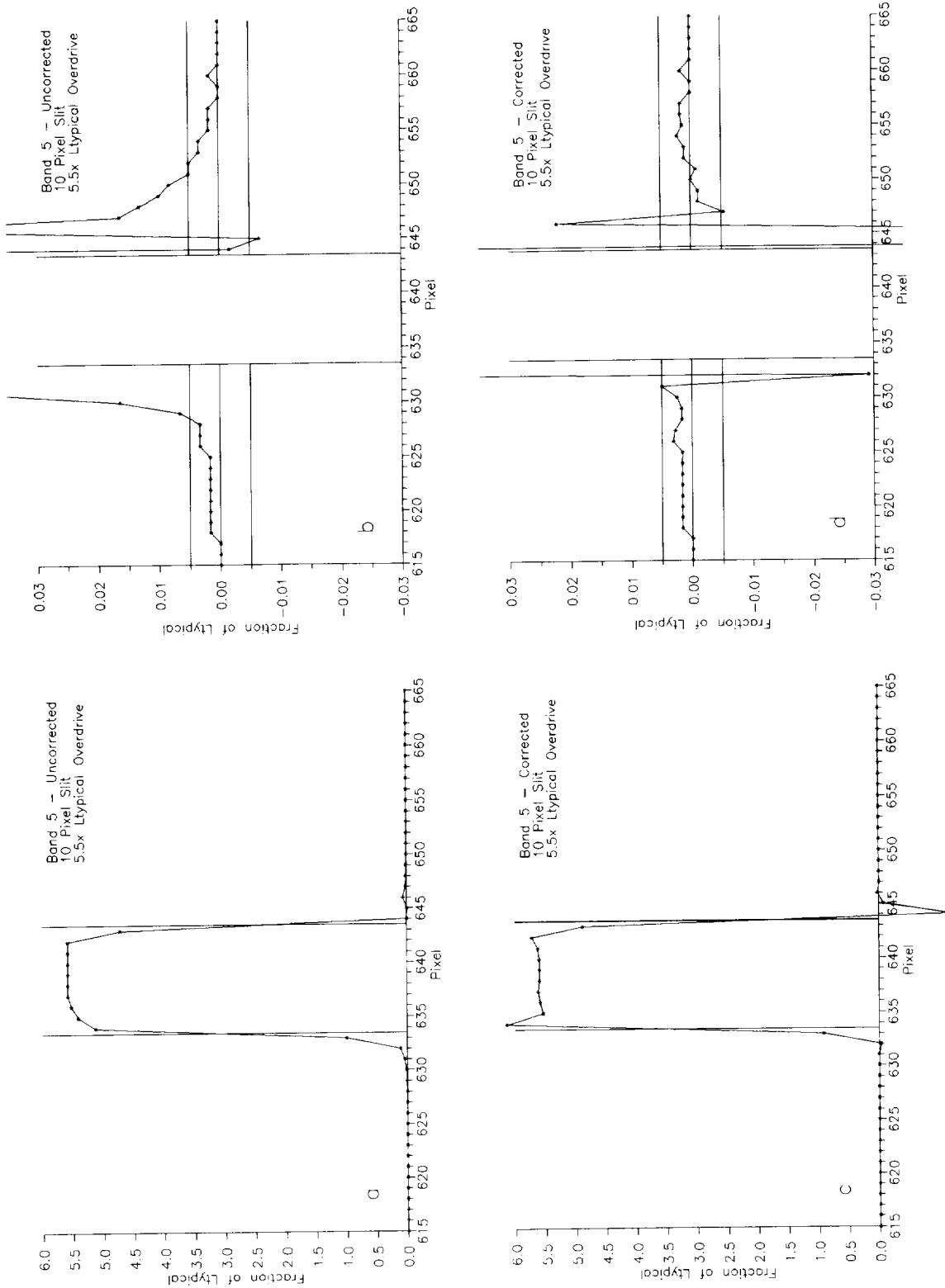


**Fig. 39.** The input and output responses from the stray light correction for band 5 are given, with experimental parameters of midrange input radiance and a 10 pixel slit. The radiance is  $5.5 L_{\text{typical}}$ . **a)** The input values are scaled to the peak radiances from the source. **b)** The input values are scaled to  $\pm 0.03 L_{\text{typical}}$ . (The one-time overshoot in the band's response past the bright source at pixel 645 is instrumentally based.) **c)** The output values from the stray light correction procedure are scaled to the peak radiances from the source. **d)** The output values are scaled to  $\pm 0.03 L_{\text{typical}}$ . (The correction creates a one-time overshoot before the bright source at pixel 632, and exaggerates the instrumental overshoot after the source at pixel 645.)

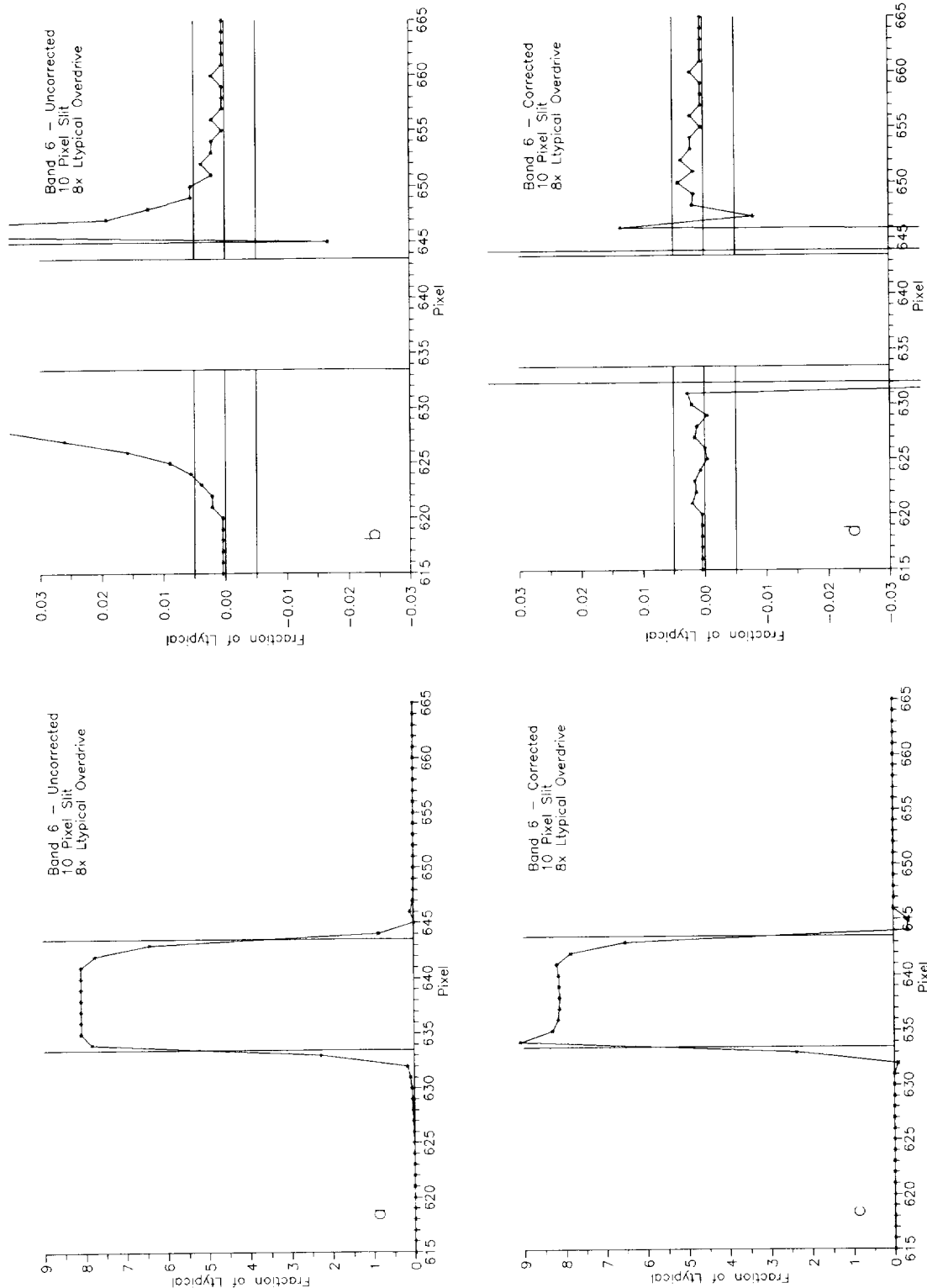


**Fig. 40.** The input and output responses from the stray light correction for band 6 are given, with experimental parameters of midrange input radiance and a 10 pixel slit. The radiance is  $8 L_{\text{typical}}$ . **a)** The input values are scaled to the peak radiances from the source. **b)** The input values are scaled to  $\pm 0.03 L_{\text{typical}}$ . (The one-time overshoot in the band's response past the bright source at pixel 645 is instrumentally based.) **c)** The output values from the stray light correction procedure are scaled to the peak radiances from the source. **d)** The output values are scaled to  $\pm 0.03 L_{\text{typical}}$ . (The correction creates a one-time overshoot before the bright source at pixel 632, and exaggerates the instrumental overshoot after the source at pixel 645.)

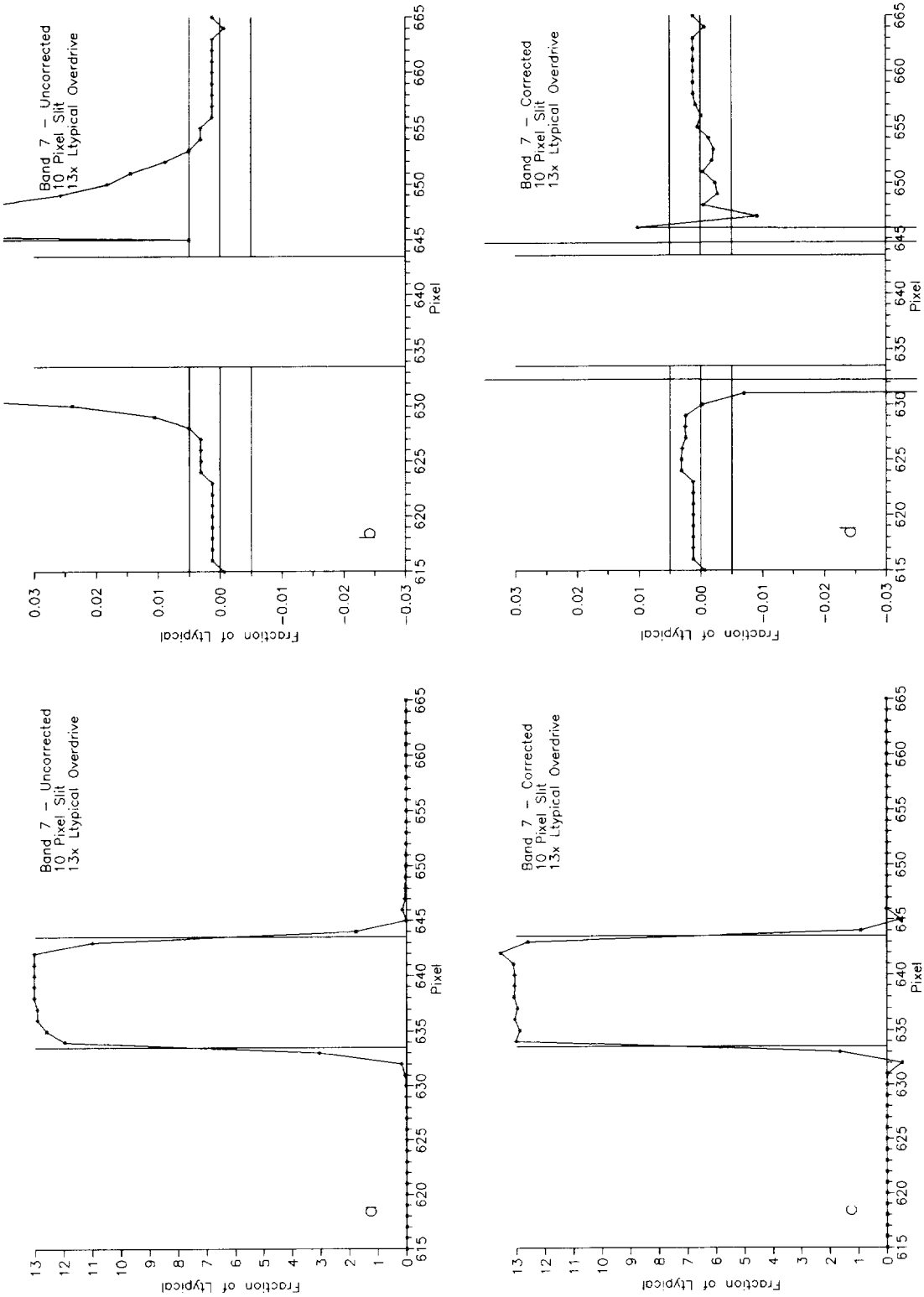


**Fig. 41.** The input and output responses from the stray light correction for band 7 are given, with experimental parameters of midrange input radiance and a 10 pixel slit. The radiance is  $13 L_{\text{typical}}$ . **a)** The input values are scaled to the peak radiances from the source. **b)** The input values are scaled to  $\pm 0.03 L_{\text{typical}}$ . (The one-time overshoot in the band's response past the bright source at pixel 645 is instrumentally based.) **c)** The output values from the stray light correction procedure are scaled to the peak radiances from the source. **d)** The output values are scaled to  $\pm 0.03 L_{\text{typical}}$ . (The correction creates a one-time overshoot before the bright source at pixel 632, and exaggerates the instrumental overshoot after the source at pixel 645.)

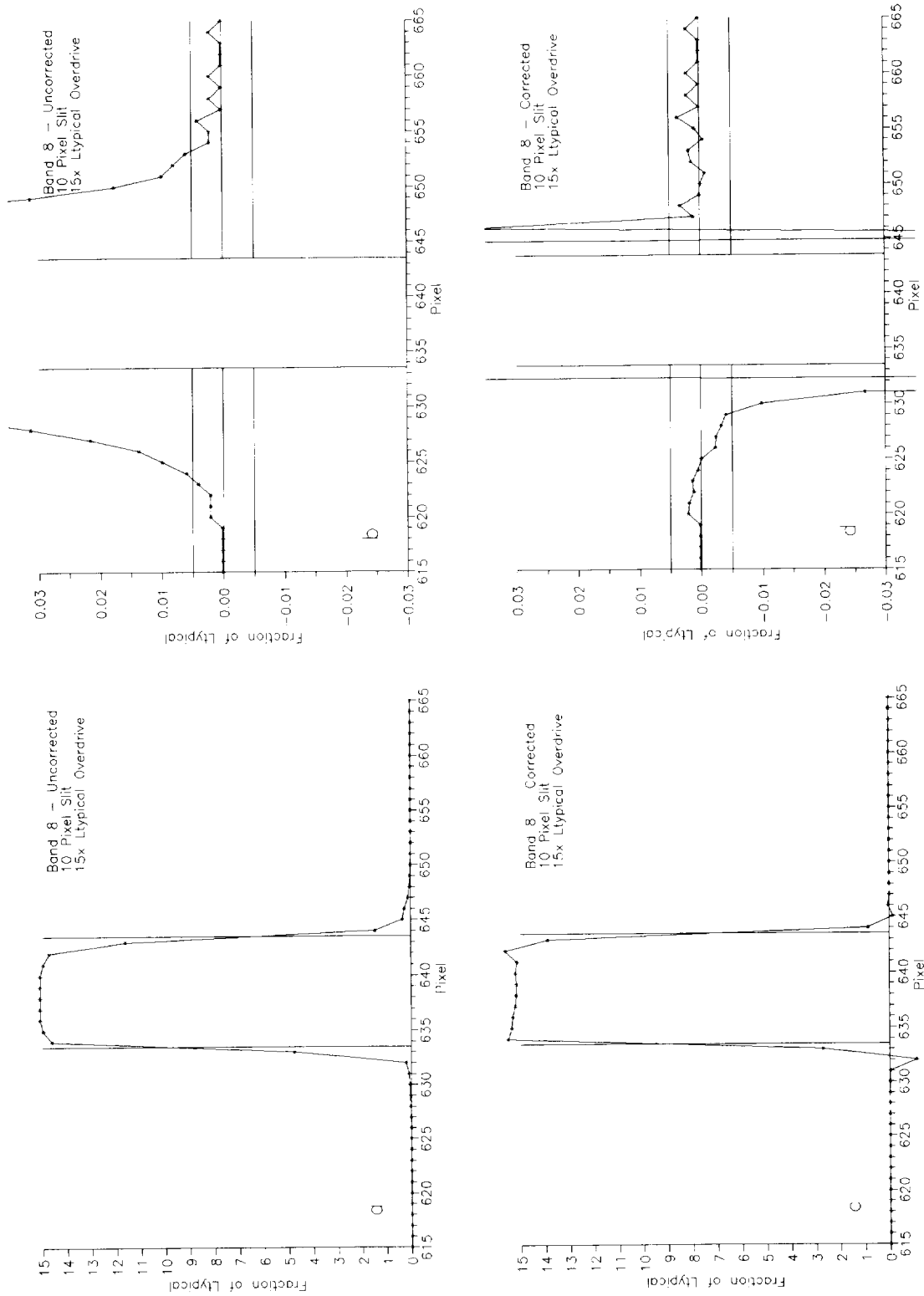


**Fig. 42.** The input and output responses from the stray light correction for band 8 are given, with experimental parameters of midrange input radiance and a 10 pixel slit. The radiance is  $15 L_{\text{typical}}$ . **a)** The input values are scaled to the peak radiance from the source. **b)** The input values are scaled to  $\pm 0.03 L_{\text{typical}}$ . (The one-time overshoot in the band's response past the bright source is masked by the response to the bright target. **c)** The output values from the stray light correction procedure are scaled to the peak radiance from the source. **d)** The output values are scaled to  $\pm 0.03 L_{\text{typical}}$ . (The correction creates a one-time overshoot before the bright source at pixel 632, and exaggerates the instrumental overshoot after the source at pixel 645.)

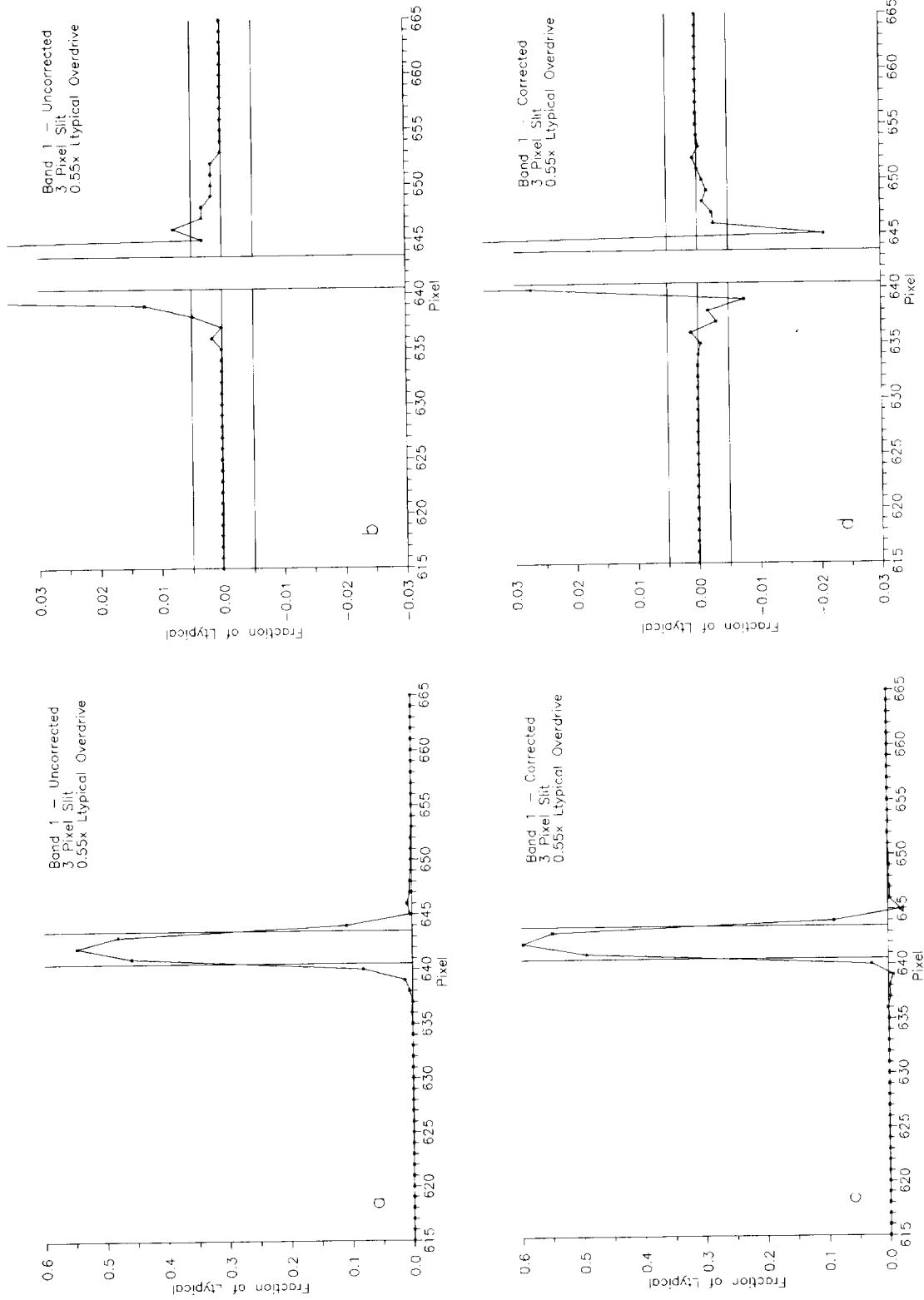


**Fig. 43.** The input and output responses from the stray light correction for band 1 are given, with experimental parameters of midrange input radiance and a 3 pixel slit. The radiance is  $0.55 L_{\text{typical}}$ . **a)** The input values are scaled to the peak radiances from the source. **b)** The input values are scaled to  $\pm 0.03 L_{\text{typical}}$ . (The one-time overshoot in the band's response past the bright source at pixel 645 is instrumentally based.) **c)** The output values from the stray light correction procedure are scaled to the peak radiances from the source. **d)** The output values are scaled to  $\pm 0.03 L_{\text{typical}}$ . (The correction creates a one-time overshoot before the bright source at pixel 639, and exaggerates the instrumental overshoot after the source and pixel 645.)

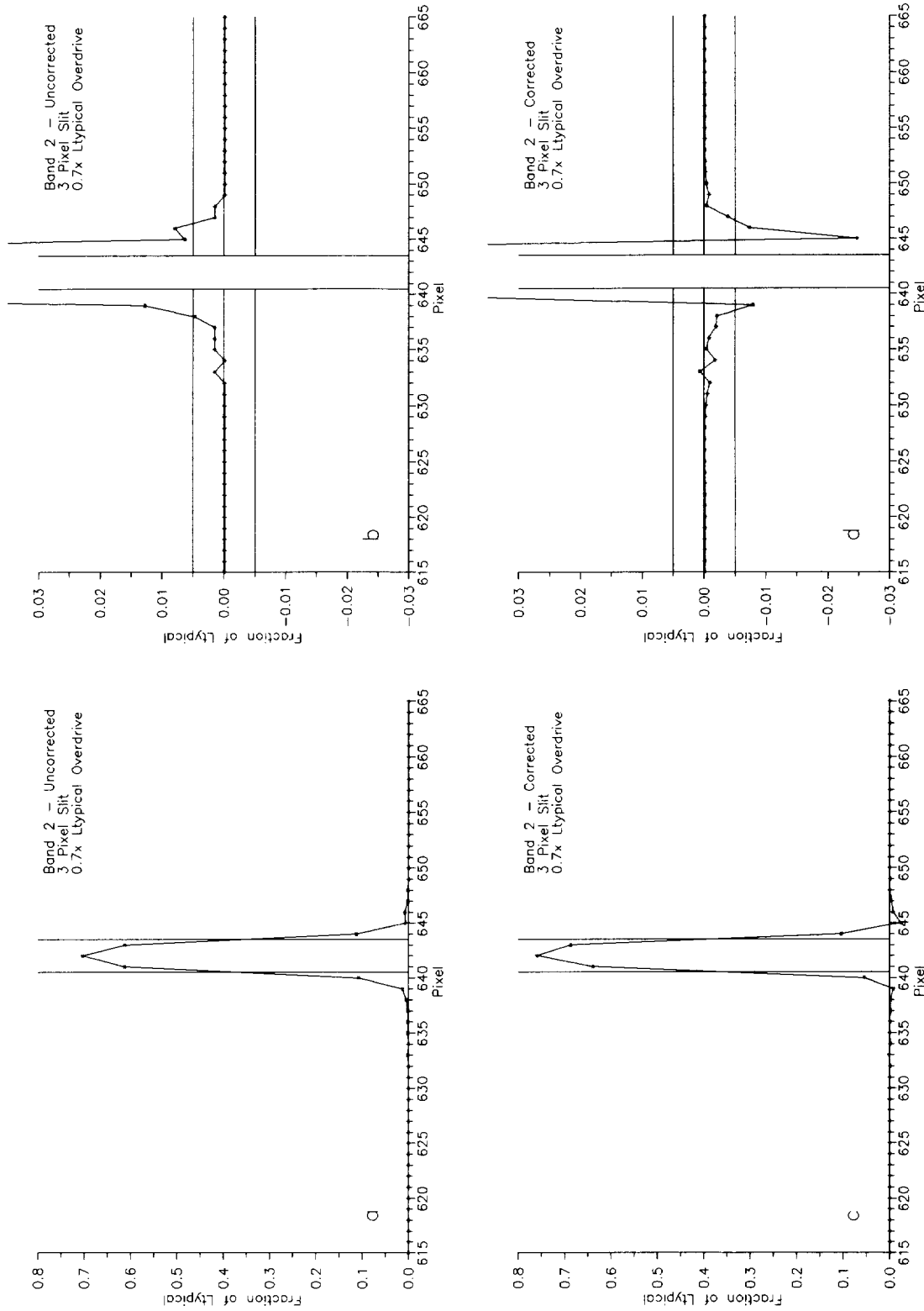


**Fig. 44.** The input and output responses from the stray light correction for band 2 are given, with experimental parameters of midrange input radiance and a 3 pixel slit. The radiance is  $0.7 L_{\text{typical}}$ . **a)** The input values are scaled to the peak radiances from the source. **b)** The input values are scaled to  $\pm 0.03 L_{\text{typical}}$ . (The one-time overshoot in the band's response past the bright source at pixel 645 is instrumentally based.) **c)** The output values from the stray light correction procedure are scaled to the peak radiances from the source. **d)** The output values are scaled to  $\pm 0.03 L_{\text{typical}}$ . (The correction creates a one-time overshoot before the bright source at pixel 639, and exaggerates the instrumental overshoot after the source pixel 645.)

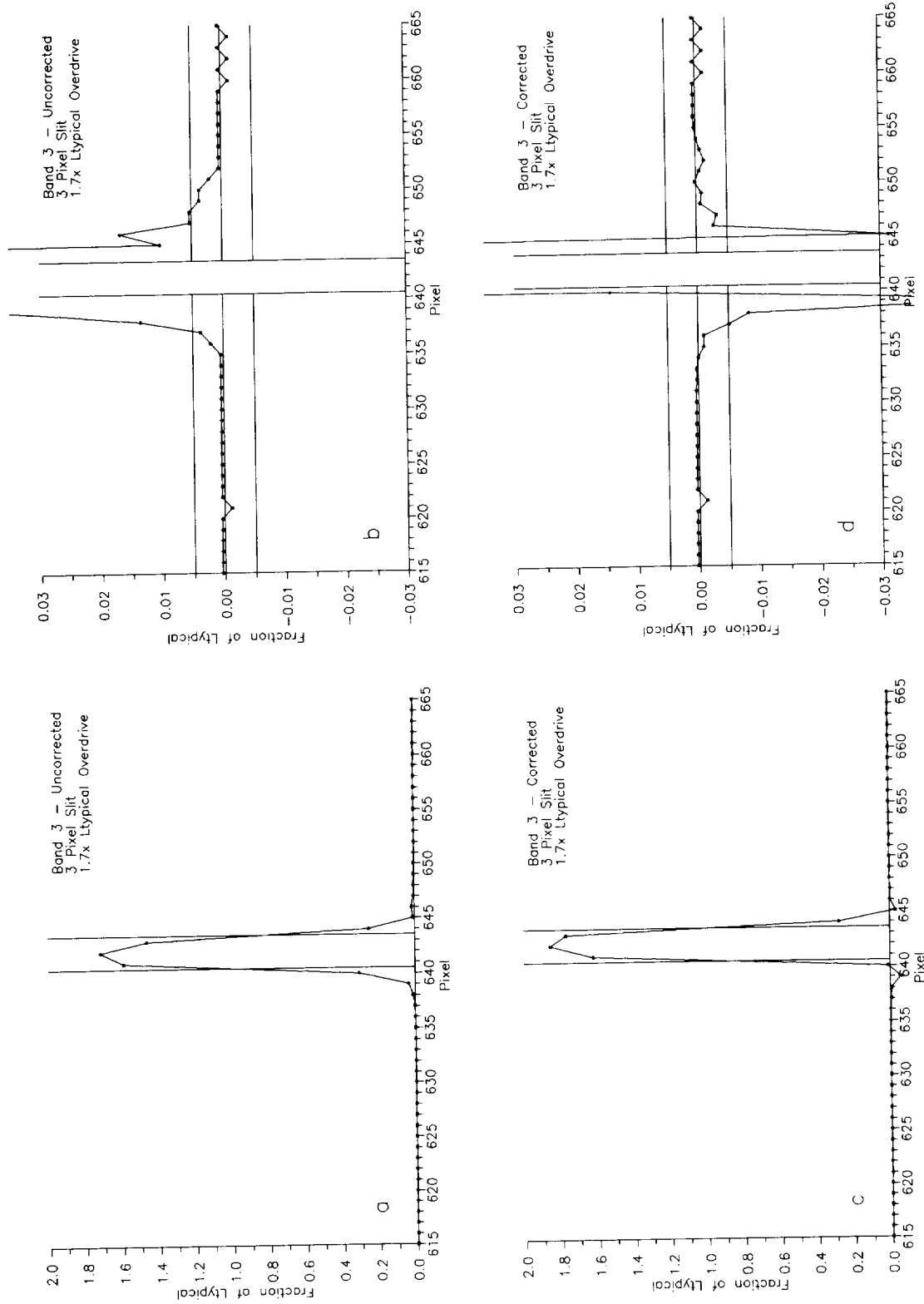


**Fig. 45.** The input and output responses from the stray light correction for band 3 are given, with experimental parameters of midrange input radiance and a 3 pixel slit. The radiance is  $1.7 L_{\text{typical}}$ . **a)** The input values are scaled to the peak radiances from the source. **b)** The input values are scaled to  $\pm 0.03 L_{\text{typical}}$ . (The one-time overshoot in the band's response past the bright source at pixel 645 is instrumentally based.) **c)** The output values from the stray light correction procedure are scaled to the peak radiances from the source. **d)** The output values are scaled to  $\pm 0.03 L_{\text{typical}}$ . (The correction creates a one-time overshoot before the bright source at pixel 639, and exaggerates the instrumental overshoot after the source at pixel 645.)

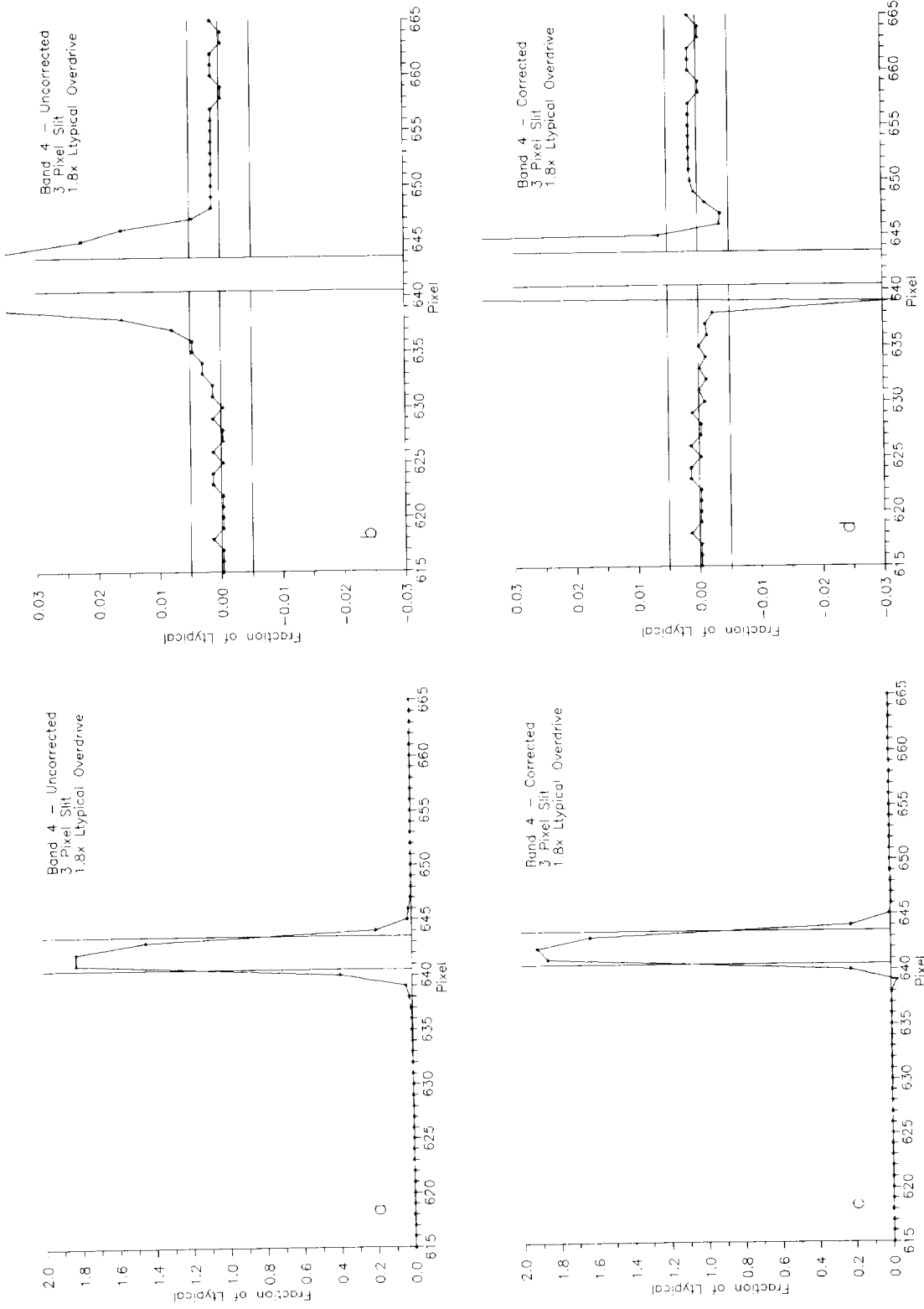


**Fig. 46.** The input and output responses from the stray light correction for band 4 are given, with experimental parameters of midrange input radiance and a 3 pixel slit. The radiance is  $1.8 L_{\text{typical}}$ . **a)** The input values are scaled to the peak radiances from the source. **b)** The input values are scaled to  $\pm 0.03 L_{\text{typical}}$ . (The one-time overshoot in the band's response past the bright source is masked by the response to the bright target. **c)** The output values from the stray light correction procedure are scaled to the peak radiances from the source. **d)** The output values are scaled to  $\pm 0.03 L_{\text{typical}}$ . (The correction creates a one-time overshoot before the bright source at pixel 639, and exaggerates the instrumental overshoot after the source at pixel 645.)

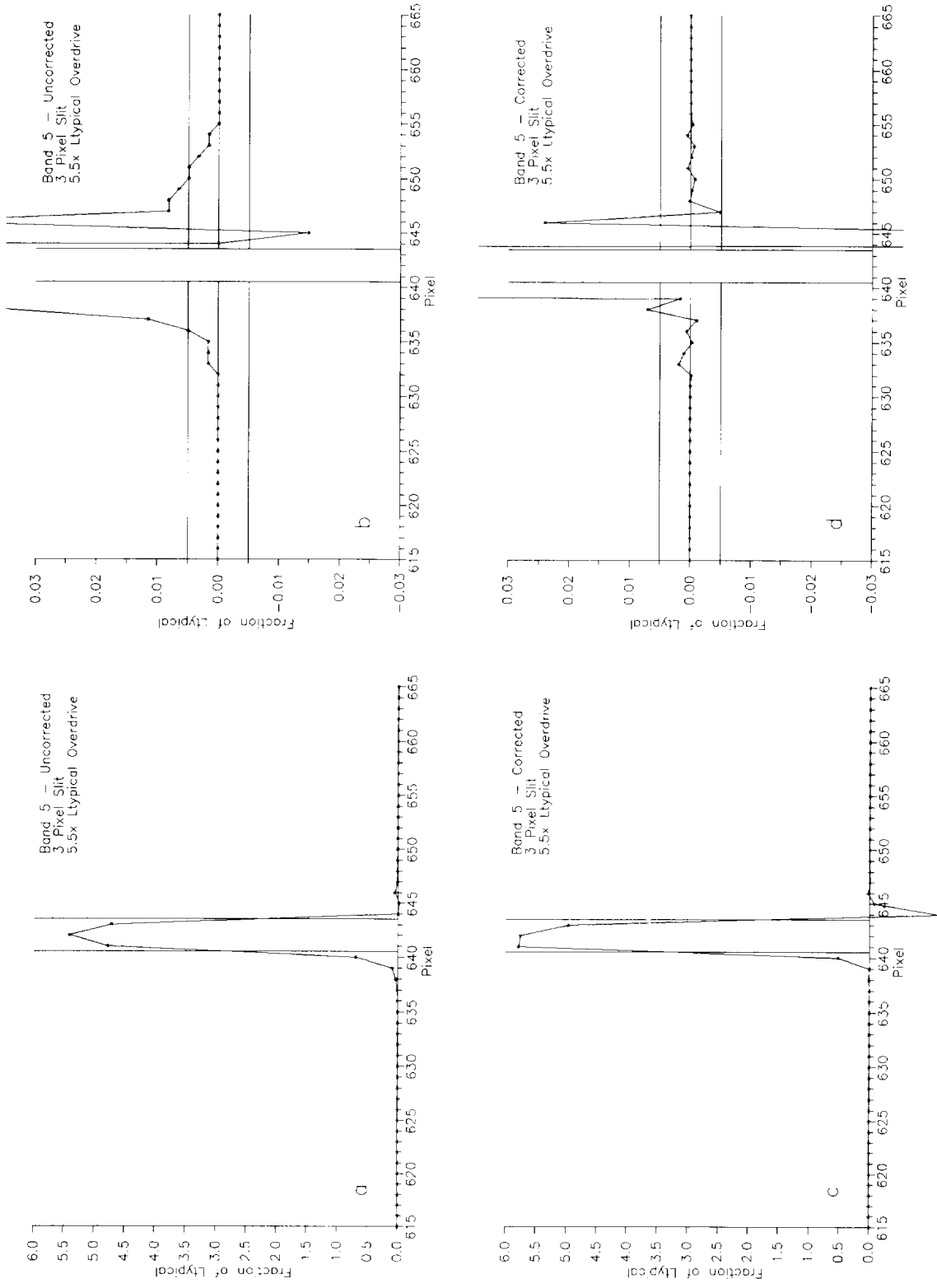


**Fig. 47.** The input and output responses from the stray light correction for band 5 are given, with experimental parameters of midrange input radiance and a 3 pixel slit. The radiance is  $5.5 L_{\text{typical}}$ . **a)** The input values are scaled to the peak radiances from the source. **b)** The input values are scaled to  $\pm 0.03 L_{\text{typical}}$ . (The one-time overshoot in the band's response past the bright source at pixel 645 is instrumentally based.) **c)** The output values from the stray light correction procedure are scaled to the peak radiances from the source. **d)** The output values are scaled to  $\pm 0.03 L_{\text{typical}}$ . (The correction does not show a one-time overshoot before the bright source at pixel 639. It exaggerates the instrumental overshoot after the source at pixel 645.)

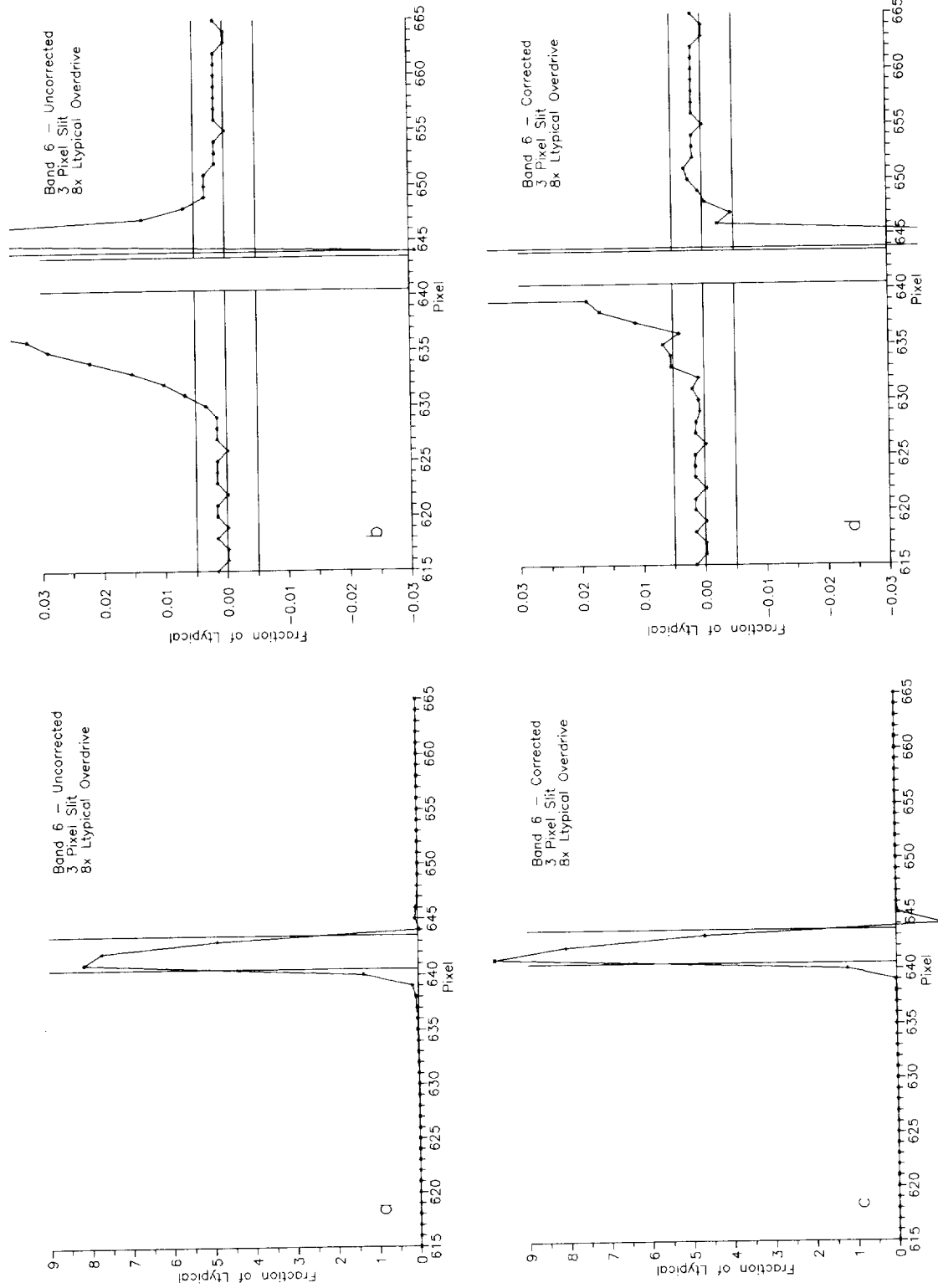


**Fig. 48.** The input and output responses from the stray light correction for band 6 are given, with experimental parameters of midrange input radiance and a 3 pixel slit. The radiance is  $8 L_{\text{typical}}$ . **a)** The input values are scaled to the peak radiances from the source. **b)** The input values are scaled to  $\pm 0.03 L_{\text{typical}}$ . (The one-time overshoot in the band's response past the bright source at pixel 644 is instrumentally based.) **c)** The output values from the stray light correction procedure are scaled to the peak radiances from the source. **d)** The output values are scaled to  $\pm 0.03 L_{\text{typical}}$ . (The correction does not show a one-time overshoot before the bright source at pixel 639. It exaggerates the instrumental overshoot after the source at pixel 645.)

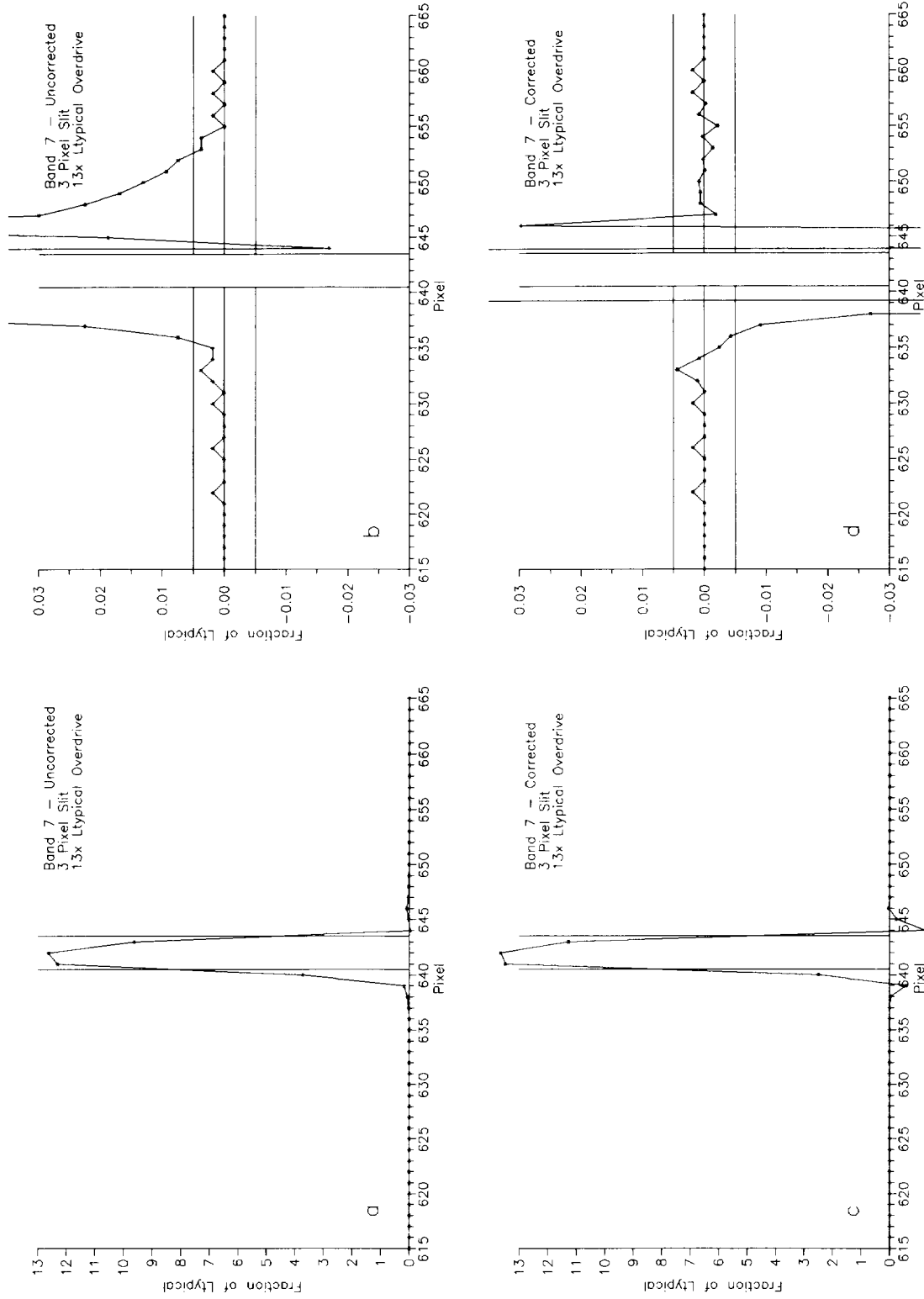


**Fig. 49.** The input and output responses from the stray light correction for band 7 are given, with experimental parameters of midrange input radiance and a 3 pixel slit. The radiance is  $13 L_{\text{typical}}$ . **a)** The input values are scaled to the peak radiances from the source. **b)** The input values are scaled to  $\pm 0.03 L_{\text{typical}}$ . (The one-time overshoot in the band's response past the bright source at pixel 644 is instrumentally based.) **c)** The output values from the stray light correction procedure are scaled to the peak radiances from the source. **d)** The output values are scaled to  $\pm 0.03 L_{\text{typical}}$ . (The correction creates a one-time overshoot before the bright source at pixel 639, and exaggerates the instrumental overshoot after the source at pixel 645.)

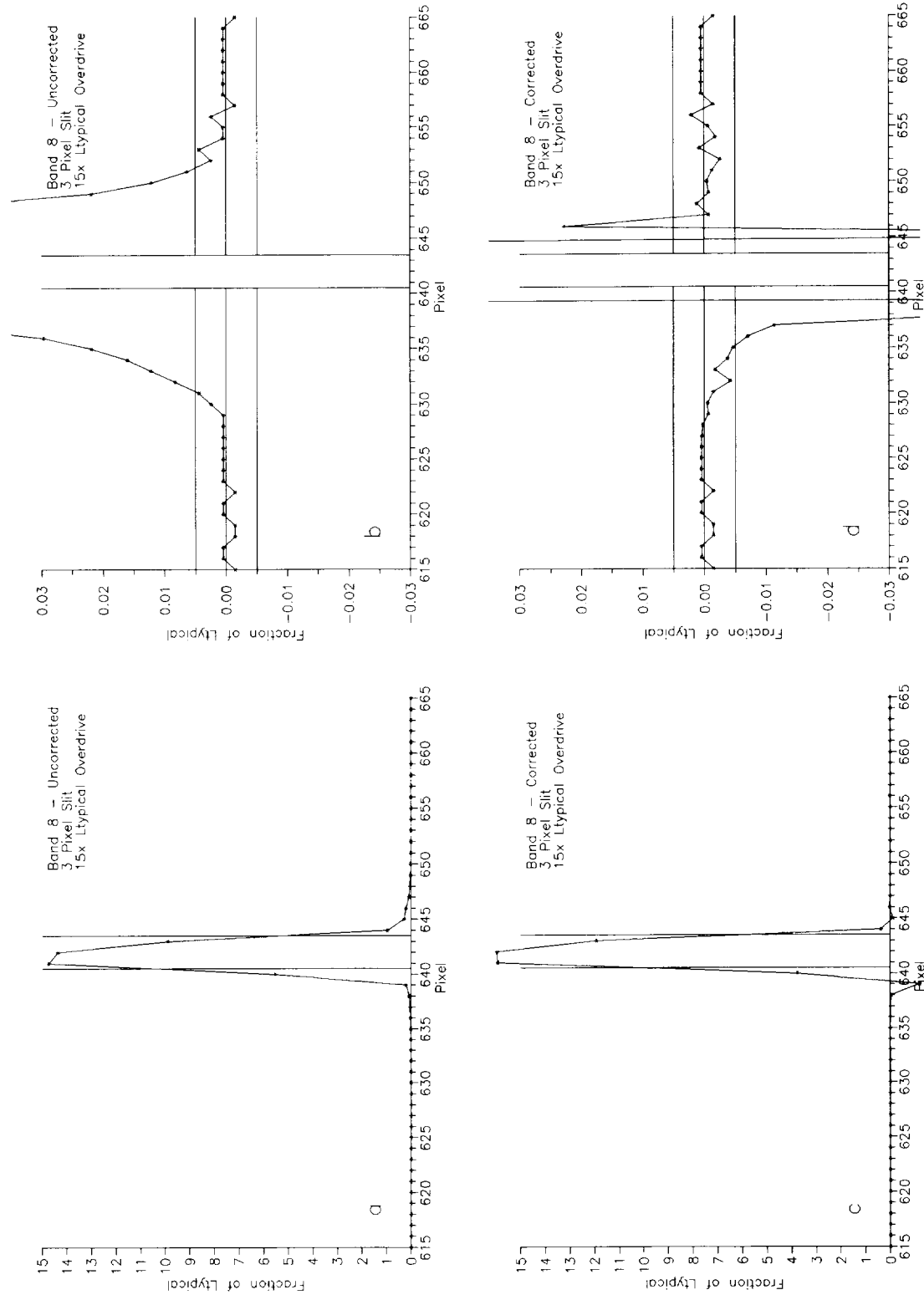


**Fig. 50.** The input and output responses from the stray light correction for band 8 are given, with experimental parameters of midrange input radiance and a 3 pixel slit. The radiance is  $15 L_{\text{typical}}$ . **a)** The input values are scaled to the peak radiances from the source. **b)** The input values are scaled to  $\pm 0.03 L_{\text{typical}}$ . (The one-time overshoot in the band's response past the bright source is masked by the response to the bright target. **c)** The output values from the stray light correction procedure are scaled to the peak radiances from the source. **d)** The output values are scaled to  $\pm 0.03 L_{\text{typical}}$ . (The correction creates a one-time overshoot before the bright source at pixel 639, and exaggerates the instrumental overshoot after the source at pixel 645.)

**Table 14.** Residual along-scan stray light responses. These values are also shown in Figs. 51 and 52. The mean values and the standard deviations are presented here as a percentage of  $L_{\text{typical}}$ .

Radiance Range	Distance from Slit [pixels]	10 Pixel Slit		3 Pixel Slit	
		Mean	$\sigma$	Mean	$\sigma$
High	-10	0.177	0.214	-0.013	0.085
	-9	0.160	0.247	-0.070	0.180
	-8	0.165	0.315	0.092	0.266
	-7	0.126	0.389	-0.061	0.172
	-6	0.075	0.376	-0.105	0.243
	-5	-0.039	0.412	-0.198	0.325
	-4	-0.295	0.573	-0.410	0.548
	4	-0.519	0.717	-0.633	0.527
	5	-0.011	0.358	-0.154	0.193
	6	-0.014	0.230	-0.043	0.075
Middle	7	0.090	0.189	0.028	0.136
	8	0.115	0.214	0.052	0.146
	9	0.142	0.232	-0.006	0.138
	10	0.105	0.166	0.027	0.143
	-10	0.067	0.113	0.005	0.088
	-9	0.069	0.109	-0.052	0.160
	-8	0.036	0.179	0.113	0.221
	-7	0.034	0.170	0.008	0.263
	-6	0.002	0.185	-0.031	0.300
	-5	-0.054	0.201	-0.108	0.316
-4	-0.145	0.366	-0.272	0.631	
4	-0.429	0.307	-0.316	0.133	
5	0.004	0.155	-0.018	0.074	
6	-0.034	0.129	-0.029	0.079	
7	0.011	0.145	0.027	0.101	
8	0.003	0.078	0.032	0.121	
9	0.068	0.148	-0.007	0.129	
10	0.029	0.134	0.008	0.099	

the edges of those bright targets. Thus, pixels located four pixels, or closer, to the edge of a cloud or another bright source must be masked. Such masking procedures exist for clouds, sun glint, and land surfaces (McClain et al. 1995 and Arrigo and McClain 1995). Those masks will be extended in size to account for stray light in the instrument. In addition, those masks will be applied to the LAC data after the stray light correction. The corrections and the masking procedures developed here will also supersede those masks for bright sources.

The masking procedure for bright targets presented here is far from an accomplished fact. Indeed, there is no guarantee that the actual computer code for flight data will resemble this procedure at all, as a *final* (i.e., based on observational data) masking procedure will be developed post-launch. A proposed procedure for mask creation is discussed here in terms of a single SeaWiFS band. The masks for the flight data must be uniform for all bands, so a mask for a pixel in any band requires a mask for that pixel in all eight bands. Also, the correction and masking procedures are presented here in terms of  $L_{\text{typical}}$  radian-

ces. This presentation puts the radiances and the radiance changes, for the eight SeaWiFS bands, on equal footings. Two methods of bright target detection (BTD) are presented here—detection based on differences from Rayleigh scattering radiances, and detection based on changes in radiance along the scan line.

### 11.1.1 Rayleigh Scattering Radiance BTD

It is possible to consider SeaWiFS as a sensor of atmospheric radiances having small perturbations due to color changes in the ocean. This result is shown in Fig. 3 of McClain et al. (1992). It is also possible to calculate the radiances viewed by the sensor from the scattering of solar flux by air molecules, i.e., from Rayleigh scattering. Radiances from the ocean surface increase those from molecular scattering by only 5–10%, while radiances from clouds give increases of an order of magnitude or more. In theory, the use of Rayleigh scattering for BTD is reasonably simple. A bright target contains a pixel (or pixels) with radiances greater than, for example, 1.3 times the Rayleigh radiance. This fractional difference, or bright target threshold,

## Stray Light in the SeaWiFS Radiometer

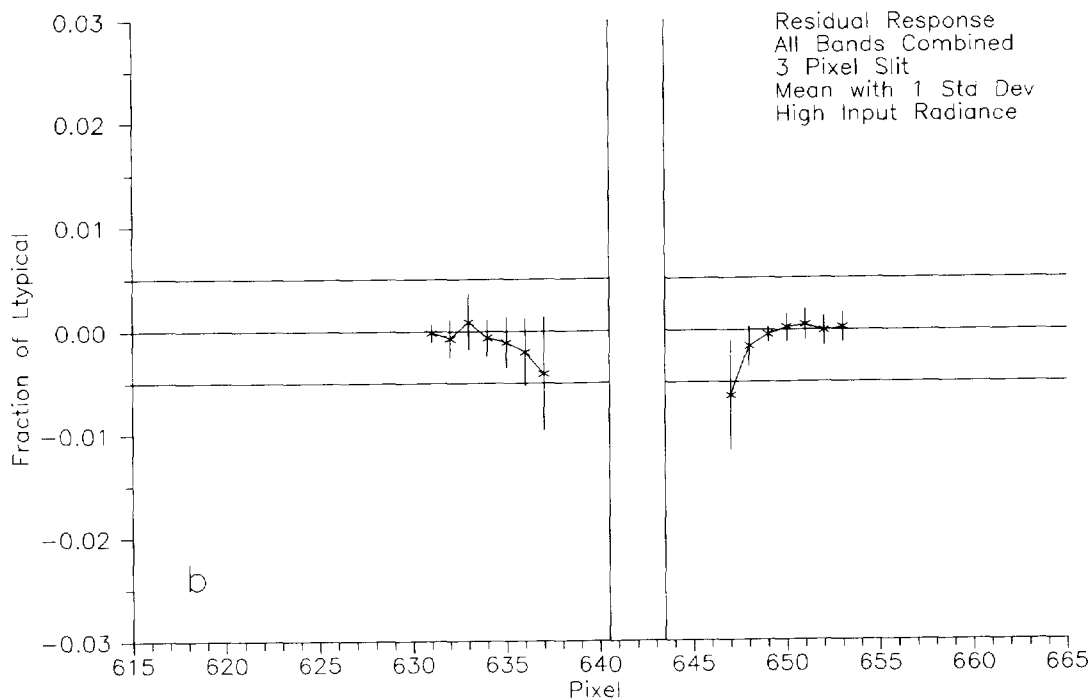
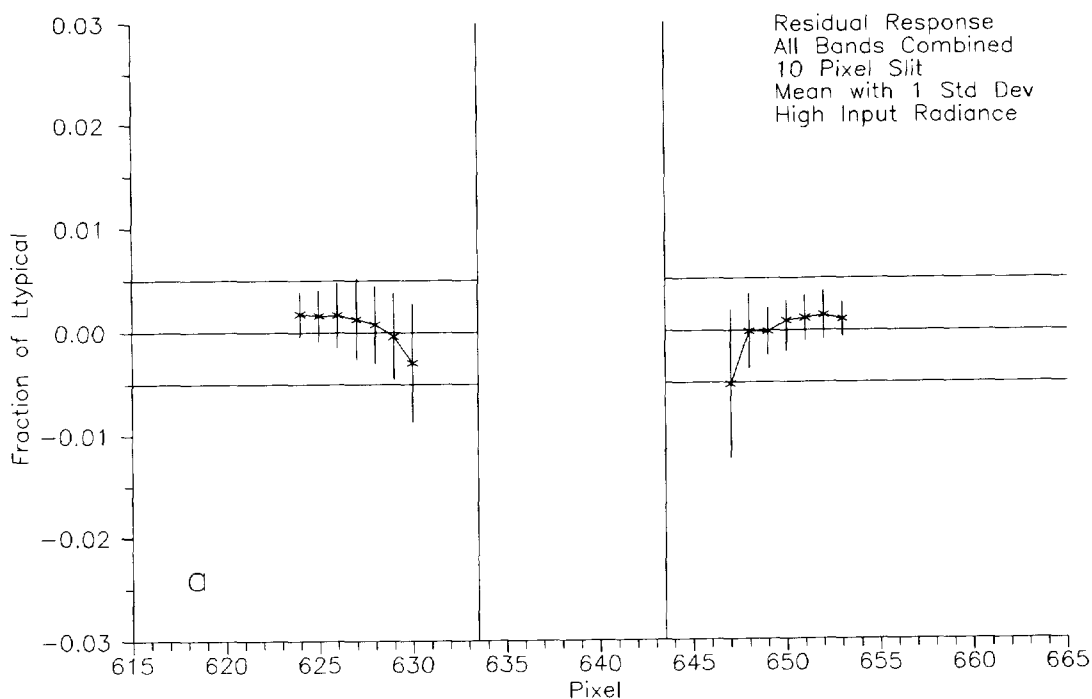


**Fig. 51.** The residual SeaWiFS along-scan stray light responses after correction. These results give the means and standard deviations ( $1\sigma$ ) for the post-correction residuals. Shown here in this figure are the: **a)** results from the 10 pixel high radiance measurements—the averages for all eight bands, i.e., for the results from subpanel d of Figs. 19–26; and **b)** results from the 3 pixel high radiance measurements—the averages for all eight bands, i.e., for the results from subpanel d of Figs. 27–34.

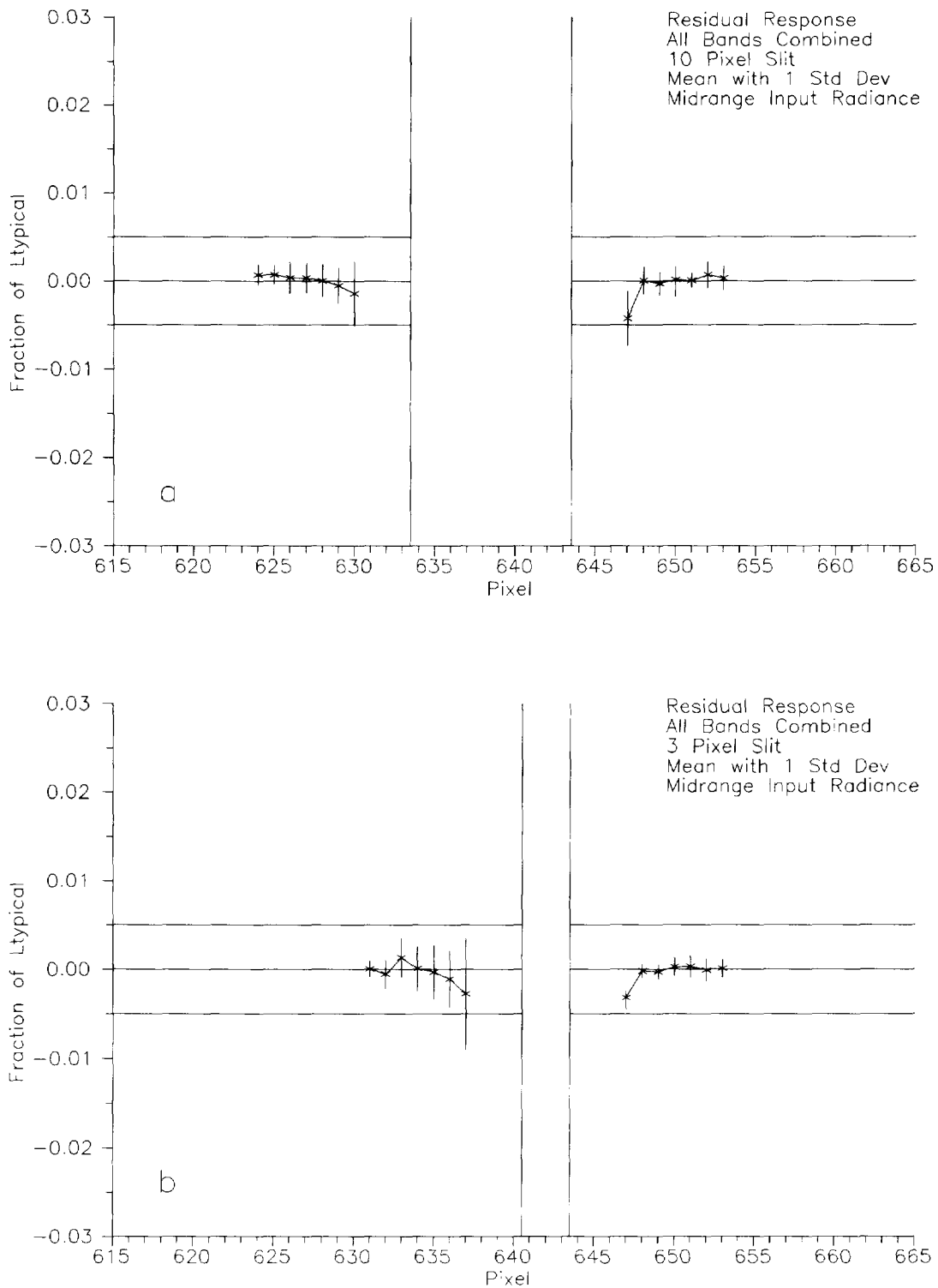


**Fig. 52.** The residual SeaWiFS along-scan stray light responses after correction. These results give the means and standard deviations ( $1\sigma$ ) for the post-correction residuals. Shown here in this figure are the: a) results from the 10 pixel high radiance measurements—the averages for all eight bands, i.e., for the results from subpanel d of Figs. 35–42; and b) results from the 3 pixel high radiance measurements—the averages for all eight bands, i.e., for the results from subpanel d of Figs. 43–50.

is arbitrary and based on judgement and experience. The threshold, in effect, defines what is or what is not a bright target. The value for this threshold can also be changed. The bright targets in the laboratory measurements with the smallest optical overdrives (Figs. 35 and 43) had radiances that correspond to 1.6–1.7 of those from Rayleigh scattering on orbit. In the laboratory, the bright targets were displayed relative to a black background. On orbit, the bright targets are located in the midst of *typical* radiances. An initial estimate for the bright target threshold is 1.3 times the Rayleigh radiance. This is the fractional multiplier for a bright source with a radiance of approximately half of the radiance found in Fig. 35.

Each pixel's radiance from Rayleigh scattering can be calculated, based on values transmitted in the data stream from the satellite. The actual data products, calculated in the initial step of SeaWiFS data reduction, are:

- The view angle of the instrument relative to nadir (also called the scan angle);
- The zenith angle of the sun; and
- The azimuth angle between the view angle and the solar zenith angle of the instrument.

Rayleigh scattering accounts for two effects in the radiances measured by SeaWiFS on orbit. First, the radiances become brighter as the instrument scans away from nadir, since the pathlength through the atmosphere (and the number of molecular scatterers in that pathlength) increases. Second, the radiances become dimmer with increasing solar zenith angle, since the solar flux becomes attenuated by passing through more atmosphere before it reaches the molecular scatterers in the path between the instrument and the Earth. As a result, Rayleigh scattering gives a relatively flat background radiance over a scan line for BTM, i.e., it gives a background that changes smoothly with view angle and with solar zenith angle. The exact calculation of the Rayleigh radiance is somewhat lengthy and computationally cumbersome. Calculation of the Rayleigh radiances for each pixel in each scan line would take a significant amount of computer time. The direct calculation of individual Rayleigh radiances is not recommended here. It seems more reasonable to determine the radiances from a set of simplified equations based on approximations or, more simply, from a set of look-up tables. These tables could be somewhat complex, since the azimuth angle changes as the satellite moves from north to south in an orbit, and also changes with the seasons.

For the Rayleigh radiance procedure, a bright target exists where there are radiances above the threshold value, and the edge of the target exists at the transition through the threshold. The stray light mask in this procedure includes the pixel next to the transition and the three pixels beyond it. For the benefit of the along-track correction procedure presented in Section 11.2, it is important to distinguish between the pixels masked for the bright source and those pixels in the mask's extension for stray light.

### 11.1.2 Scan Line Radiance Change BTM

This technique examines the first and second derivatives of radiance changes across a scan line. The transitions between ocean and bright target radiances are expected to be relatively sharp, i.e., occurring over intervals from one to a few pixels. The transitions are expected to be relatively large, since bright sources are, by definition, bright compared to ocean measurements.

This technique also examines slopes and slope changes, without a fixed reference, such as the Rayleigh radiance. It uses these values to determine the edges of bright sources with greater precision than the Rayleigh radiance technique. In portions of the scan line where radiances are relatively constant, the radiance change technique cannot discriminate between a bright source and a background ocean measurement.

The first derivative is examined in terms of the difference of a given pixel's radiance from that of its predecessor in the scan line. As the scan reaches a bright source, it is expected that the change will be 0.25 times the value of  $L_{\text{typical}}$  ( $0.25 L_{\text{typical}}$ ), or greater, i.e., a positive slope with a relatively large change in radiance. As the scan leaves a bright source, another relatively large change is expected, but with a negative slope. As with the Rayleigh radiance procedure, the size of the changes required to determine a bright target is arbitrary. The value of  $0.25 L_{\text{typical}}$  used here represents a smaller transition than in the Rayleigh technique, since transitions between the ocean and bright targets are not necessarily completed over the span of one pixel.

The second derivative is also examined in terms of changes in radiance. It is used to find the overshoot in the correction algorithm discussed in Section 10.3. The pixel at the point of this overshoot shows less radiance than either its predecessor or its successor. The slope before the overshoot pixel is negative; the slope after is positive. In this procedure, the magnitude of the changes both before and after the overshoot pixel must be 1% of  $L_{\text{typical}}$  or greater. Insofar as is currently known, when the correction algorithm has been applied, in all cases, the overshoot occurs *after* the bright source, and in the large majority of cases, it also occurs *before* the bright source.

Similar methods are used to determine the left and right sides of bright sources. Approaching the bright source from the left side, i.e., from the start of the scan line, a search is made for a positive change of  $0.25 L_{\text{typical}}$  or greater. The pixel after this change is considered to be the leftmost pixel in the bright target. A search is then made backwards (towards the beginning of the scan line) for the pixel at the overshoot. When this pixel has been located, the range of pixels starting three pixels before the overshoot and ending immediately before the leftmost pixel of the bright target is then masked for stray light effects. Note that the overshoot from the correction algorithm may not be present in all bands; however, its presence in at least

four bands should be sufficient to define the location of the overshoot for all eight bands.

Leaving the bright source, a search is made for a negative change of  $0.25 L_{\text{typical}}$  or greater. The pixel before this change is considered to be the rightmost pixel in the bright target. A search is then made forward (toward the end of the scan line) for the pixel at the overshoot. When this pixel has been located, the range of pixels starting immediately after the rightmost pixel of the bright target and ending three pixels after the overshoot is then masked for stray light effects.

In this procedure, the left and rightmost pixels in the bright targets are determined, and the signatures of the overshoots from the correction algorithm are found. From the locations of these overshoot pixels, the stray light masks are added to the bright target masks. By itself, however, this procedure is flawed. There is no certainty that the transitions in the procedure, that is, the first derivatives, will always be between ocean measurements and bright targets. Transitions from land to (or from) clouds, or transitions from ocean glint to (or from) clouds, can be confused with transitions to and from the oceans. A combination of the procedure presented here and the Rayleigh radiance procedure from Section 11.1.1 is recommended. The Rayleigh radiances should be used first to determine the location of the bright sources and mask those bright targets. Then, there should be a search for the overshoots in the correction algorithm, in order to determine the locations of the pixels for the stray light additions to the bright target masks.

### 11.1.3 Arbitrary Radiance Threshold BTD

Bright target corrections will be applied early in the set of computer programs that reduce SeaWiFS data. The SeaWiFS data volume is large, and as a result, the detection schemes presented in Sections 11.1.1 and 11.1.2 may be too cumbersome and time consuming to incorporate into these programs. An alternative detection scheme may be to declare all radiances above an arbitrary value, such as the knee radiance in the bilinear gain, to come from a bright source. A second alternative may be to apply the existing cloud mask, which is provided in McClain et al. (1995). Both alternatives can give the edges of bright targets and the reference pixels for the start of the stray light masks.

The BTB schemes in Sections 11.1.1 and 11.1.2 may prove to be too computationally complex for the routine reduction of flight data, and therefore, a less complicated scheme may be needed. Sections 11.1.1 and 11.1.2, however, provide insights into the characteristics of bright targets that can be used to test and improve the algorithms for the on-orbit data. Since the stray light analysis in this document is prelaunch and zeroeth order, in the same manner, so are the masking algorithms that will be used at launch.

## 11.2 Along-Track LAC Correction

There is no correction algorithm in the along-track direction, and thus, there are no calculations to be made. The along-track LAC correction only includes expansion of the bright target masks. The stray light correction procedure masks two additional pixels on each along-track side of bright targets. In principle, this masking procedure is very simple. Using the along-scan procedures in Section 11.1, the locations of the bright targets have already been determined for each scan line in the LAC scene. Thus, the scene need only be searched in the along-track direction for bright target masks, and stray light masks can be added before and after the bright targets. In this along-track search, it is important to discriminate between bright target masks and the stray light masks that were added to them in the along-scan direction.

The addition of along-track masks requires a new appreciation of the relationship between scan lines in LAC (and GAC) scenes. Before the study of stray light in SeaWiFS, individual Earth scans by the instrument were considered independent of each other. As a result, the analysis of on-orbit measurements was scheduled to be performed on a line-by-line basis only. The two-dimensional ocean scenes were considered to be composites of independent one-dimensional scan lines. The inclusion of along-track stray light requires an additional, albeit simple, analysis in a second dimension. The LAC (and GAC) data arrays must be manipulated in a different fashion. This requirement adds possible complications to the SeaWiFS on-orbit data analyses.

## 12. PROPOSED GAC CORRECTION

As discussed in Section 1.1, there is a 3 pixel spacing between GAC pixels, both in the along-scan and along-track directions. Knowledge of the edges of bright targets, in the manner of LAC measurements, is much coarser.

It is possible, however, to determine which of the GAC pixels are bright targets, and which are ocean measurements. This can be done through the Rayleigh scattering technique from Section 11.1.1. In that technique, the background Rayleigh radiance is determined from geometric factors in the SeaWiFS measurements. Using the procedure in Section 11.1.1, it is possible to mask the bright targets in each scan line.

A prelaunch method for determining the edges of bright targets must be developed if GAC stray light corrections are to be applied at the start of on-orbit sampling. As the set of LAC and GAC measurements from SeaWiFS accumulates, an improved method for determining bright target edges will be designed and implemented (Section 1.2). From those on-orbit samples, a statistically derived data set should improve the two assumptions presented here.

First, in GAC scenes, it is assumed that the edge of each bright target, i.e., each cloud, is located midway between the endmost GAC pixel that is masked as a bright

source and the next GAC pixel. This places the bright target edge 2 LAC pixels ( $\pm 1$  LAC pixel) from the nearest unmasked GAC pixel. Thus, it is assumed that the unmasked GAC pixels (i.e., unmasked as bright targets) lie in the progression of 2, 6, 10 LAC pixels, and so forth, from the bright source.

Second, it is assumed that the edge pixels for all of the bright sources have the same radiance as the closest pixel masked as a bright target. In other words, it is assumed that the endmost few pixels of bright sources have the same radiances. This particular assumption can be improved using on-orbit measurements. It is known that clouds and cloud banks can taper off at their edges, and many clouds do not end abruptly. A cloud radiance located one or two pixels from the edge of a cloud may be significantly different from those closer to the edge. Thus, the use of the nearest bright pixel for stray light corrections may cause a miscorrection in the nearby GAC pixels. In this case, a statistically derived data set based on on-orbit measurements should determine the magnitude of any such miscorrections.

With these assumptions, and with knowledge of the locations of the bright sources in the GAC scene, it is possible to apply stray light corrections and masks to the adjoining pixels. The procedure is simple in the along-track direction—mask the GAC pixels that neighbor the bright targets for stray light. These GAC pixels are a distance of 1–3 LAC pixels from the bright source, and the along-track LAC mask is applied at distances up to 2 LAC pixels from bright targets. The GAC pixels that are one place further removed from the bright sources should not be masked, as they are from 5–7 LAC pixels distant from the bright source. As with the along-track LAC masking procedure in Section 11.2, masking for along-track GAC stray light will require the manipulation of the GAC scene in a second dimension. This can also add significant complications to the analysis of on-orbit GAC measurements from SeaWiFS.

In the along-scan direction, the GAC stray light masks are determined using the same procedure as that for the GAC along-scan masks. The GAC pixel closest to the bright source is masked for stray light. For along-scan GAC pixels that are two and three GAC positions away from the bright target, however, a stray light correction must be applied. In terms of LAC distances, these GAC positions are  $6 \pm 1$  and  $10 \pm 1$  LAC pixels removed from the bright source. The stray light corrections for these GAC positions are based on the along-scan impulses discussed in Section 7.5. However, the application of the corrections must reflect the uncertainties in position and brightness of the full set of pixels in the bright target.

As shown in Table 12, the stray light correction algorithm is cumulative. It includes contributions from all of the adjacent pixels along the scan line. When the adjacent pixels on both sides are counted, the total for the contributing pixels reaches about twenty. As a result, the LAC along-scan algorithm, with its impulses, cannot be

used in GAC, since there are gaps in the GAC scenes. Instead, the GAC along-scan correction presented here uses the test results shown in Figs. 27–34. The radiances in those results include the stray light from the full set of adjacent pixels.

The calculation of the GAC along-scan correction factors can be demonstrated using the test results in Table 13. These results are for band 7, with high radiance output, and a 10 pixel slit. For the purpose of GAC correction factor calculation, the bright source in Table 13 extends from pixel 634 to pixel 643. The data point that is 6 LAC (or 2 GAC) pixels before the bright source is located at pixel 628. The correction factor is the corrected residual, minus the uncorrected residual, divided by the radiance at the source. For pixel 628, the relative correction from the stray light algorithm (using data from Table 13) is

$$F_{\text{GAC}} = 2 \left[ \frac{0.00504 - 0.01003}{24.15416 + 26.28747} \right], \quad (8)$$

where  $F_{\text{GAC}}$  is the GAC correction factor (dimensionless), 0.01003 and 0.00504 are the input and output radiances from the stray light correction at pixel 628, and 24.15416 and 26.28747 are the radiances at the edge of the bright source that correspond with those input and output radiances. The average of the two edge radiances (corresponding to the corrected and uncorrected residuals) is used in the correction factor to minimize the bias that might arise from selecting either one. These radiances are given in terms of  $L_{\text{typical}}$ , but the actual radiances or the radiances normalized to  $L_{\text{cloud}}$  can also be used, since the results are given as a relative correction.

The calculated correction factor,  $-0.00020$ , compares favorably with the correction factor of  $-0.00027$  in Table 15 for band 7 (2 GAC pixels before the bright source). The correction factor is applied to the measured radiances as follows:

$$R(P_{\text{edge} \pm P_{\Delta}}) = R(P_{\text{edge} \pm P_{\Delta}}) + F_{\text{GAC}}(P_{\text{edge} \pm P_{\Delta}})R(P_{\text{edge}}), \quad (9)$$

where  $P_{\text{edge}}$  represents a pixel located exactly on the edge of the bright source in the GAC scene;  $\pm P_{\Delta}$  is the location of the pixel to be corrected in GAC pixels relative to the (bright target) edge pixel; and  $F_{\text{GAC}}$  is the correction factor from Table 15. For a pixel from band 1 that is 2 pixels before a bright source, the correction factor,  $F_{\text{GAC}}(P_{\text{edge}} - 2)$ , is  $-0.0079$  (Table 15). This value is multiplied by the radiance of the edge pixel in the bright source. The product is then added to the on-orbit radiance for the pixel from band 1 that is 2 pixels before the bright source.

Since these correction factors are ultimately based upon the along-scan impulses, they should show the odd-band even-band asymmetry from Figs. 15 and 16. Band 8 shows a special case. For this band, there is a correction after the

**Table 15.** Along-scan GAC correction factors ( $F_{GAC}$ ). These factors are multiplied by the radiance from the endmost pixel of the bright target, and that product is subtracted from the radiance in the given GAC pixel. The correction factors are dimensionless, and the correction calculations are performed, using the standard SeaWiFS radiance units. There are no corrections for the GAC pixels immediately before and after bright sources.

Band Number	GAC Pixels Before Bright Source			GAC Pixels After Bright Source		
	3	2	1	1	2	3
1	-0.00000	-0.00079	Mask	Mask	-0.00733	-0.00090
2	-0.00060	-0.00363	Mask	Mask	-0.00110	-0.00001
3	-0.00000	-0.00069	Mask	Mask	-0.00303	-0.00055
4	-0.00074	-0.00322	Mask	Mask	-0.00043	-0.00000
5	-0.00000	-0.00028	Mask	Mask	-0.00194	-0.00053
6	-0.00055	-0.00359	Mask	Mask	-0.00061	-0.00000
7	-0.00000	-0.00027	Mask	Mask	-0.00199	-0.00055
8	-0.00037	-0.00201	Mask	Mask	-0.00233	-0.00033

bright source that is the same magnitude as that for band 7. At the wavelength range for band 8, the silicon in the detectors starts to become transparent to long wavelength photons. This effect causes some photons to penetrate within the silicon substrate before the photon is absorbed by the detector. This increased distance causes the photon-created electrons to travel further before leaving the detector. These delays cause the small additional tail in band 8 after the bright source. The transparency of the silicon increases with longer wavelength until the response deteriorates badly at about 1,000 nm. The correction factors for radiances located 2 GAC pixels from bright sources seem very small. For example, the factor for band 8 for 2 GAC pixels before a cloud is -0.00201. Clouds in band 8 can be over 30 times brighter than the typical ocean radiance, however. If the correction factor is incorrect by 0.00020, i.e., by 10% of its value, then the error in the corrected radiance is 0.006  $L_{typical}$ . The limit for residual stray light in the SeaWiFS performance specifications is 0.005  $L_{typical}$ .

According to this error analysis, the correction factors for radiances located two GAC pixels from bright sources may be inadequate to provide the required proper stray light removal. This is also true of the knowledge of the brightness of clouds near their edges in GAC scenes. It is suggested that the along-scan mask for stray light be extended to 2 GAC pixels from bright targets. This is a determination made before launch. It may be possible that the statistical analysis of on-orbit LAC measurements, as described in Section 1.2, will show this suggestion to be overly cautious.

APPENDIX A

SUMMARY OF SeaWiFS STRAY LIGHT REDUCTION SCENARIOS

(Note: This appendix is a reprint of an internal SeaWiFS document written by Wayne Esaias. It is presented here to describe some of the items taken under consideration by the SeaWiFS Project to find alternative modifications to reduce stray light. Some minor modifications of the original text has been made in order to conform to the format of the *SeaWiFS Technical Report Series*.)

From: Wayne E. Esaias

Date: May 11, 1993

This is a partial compilation of possible alterations being studied to alleviate stray light/bright target recovery. Studies are under way, and this document is expected to change considerably. Short of scrapping the whole thing or launching as is, changes in the following areas may make some difference. There is no priority indicated, and some of the scenarios are mutually exclusive. Magnitudes of improvements are not well quantified, and usually are not additive. Additional approaches might arise from the studies, or impacts refined. Risks, cost, and schedule impacts are crude estimates at the present time, but are expected to be refined considerably as studies are completed.

1. Re-coat optics.
2. Tilt interference filters.
3. Change TDI.
4. Completely mask one or two detectors.
5. Implement bilinear gain for band 1.
6. Implement bilinear response for more bands, intermediate focus mask.
7. Reverse the band positions on focal planes.
8. Software corrections.
9. Collect one full LAC band in GAC data.
10. Assemble the HRPT LAC data.
11. Redesign the focal planes.

CHANGE 1

*Re-coat optics with better anti-reflection coatings.*

**Intent:** Decrease reflections from lenses. Improve response near all bright targets. Decrease distance affected.

**Magnitude of improvement:** Awaiting results. Could decrease stray light by 20-200%. Lenses already show very good anti-reflection properties.

**Negative impact:** None to science data. Affected data will still show asymmetry (from interband cross talk).

**Risk:** Medium.

**Cost/Schedule impact:** Major. Requires new lenses, reassembly, recalibration.

**CHANGE 2**

*Tilt interference filters.*

*Intent:* Redirect reflections from primary source and to eliminate them by tilting the interference filters or the focal planes along the axis of the detectors.

*Magnitude of improvement:* This is uncertain pending modeling. Could virtually eliminate the stray light problem. Possible 120% increase in uncontaminated data (2.2 times as much) if 75% effective. This could mean 3 pixel cloud masks versus 12 pixel masks. Could reduce degree of asymmetry (from interband cross talk).

*Negative impact:* Broadening of bandpass or some loss of transmission if new filters are required.

*Risk:* High

*Cost/Schedule:* Major. May require buying new filters unless specifications are relaxed. May require making new focal plane filter mount.

**CHANGE 3**

*Change TDI to two detectors (Operational change).*

*Intent:* Select only the central two detectors for TDI. Change the distance affected by two IFOVS.

*Magnitude of improvement:* Increase ocean data by 8% relative to 12 pixel mask. No change in amount of stray light present or asymmetry (correction still difficult).

*Negative impact:* Decrease SNR by 30% (still within spec). Decrease redundancy.

*Risk:* None.

*Cost/Schedule:* None. TDI under command control already.

**CHANGE 4**

*Mask one or more detectors on focal plane (paint filters partially black).*

*Intent:* Permanently blacken or mask a portion of the filter to both decrease the amount of stray light and decrease the distance affected.

*Magnitude of improvement:* Uncertain until model and test are done, but could cause significant improvement in intensity at edges. Increases ocean data by 8% relative to 12 pixel mask (potentially more depending on stray light reduction), plus aids correction near land.

*Difficulties:* Masking the f/2 system in front of the filter will lead to vignetting.

*Negative impact:* Decrease SNR (by 30% if two channels are blackened). Permanent change compared to #3 above. Possible MTF change. Loss in redundancy.

*Risk:* Medium. Focal plane 1 is hard to access.

*Cost/Schedule:* Significant.

**CHANGE 5**

*Bilinear response for band 1.*

*Intent:* Increase dynamic range of band 1 (412nm) so it can quantify bright target radiances. Reduces gain of one of four detectors in band 1 to 20% of present value, so that the sum of 4 detectors shows a bilinear response with a knee at about 800 counts and overall saturation at cloud radiance.

*Magnitude of improvement:* Necessary for any correction that requires knowledge of intensity of bright targets. Solves no problem by itself. May provide sufficient information to infer cloud radiances for all bands. Not sufficient for overall land radiance.

*Negative impact:* Decreases resolution of ocean level radiance by 20% , decreases the range of quantization 20%. Both may be acceptable, but will impact DOM corrections to chlorophyll derivations. Range limit would primarily affect scan edges and low latitude bright waters.

*Risk:* Low.

*Cost/Schedule:* Significant, but changes only the electronics module, not the instrument.

**CHANGE 6**

*Bilinear response for bands other than band 1. Partially mask one detector per band at intermediate focus.*

*Intent:* Increase dynamic range of all bands to quantify bright target radiance. Reduce stray light by partially masking the outer detectors on each band at the intermediate focus mask (pinhole).

*Magnitude of improvement:* Awaits model results. Provides full Earth albedo dynamic range on all channels. Aids corrections at all wavelengths (land). Solves no problem by itself. Occlusion decreases distance of effect by about a pixel, and reduces stray light by 20%. Provides redundant bright target sensors. Increases ocean data by less than 5% relative to 12 pixel mask, without correction.

*Negative impact:* Decreases radiometric resolution by 20–30% in the ocean range. Limits range of high resolution data (primarily affects scan edges and low latitudes, but probably acceptable). Requires both instrument and electronics module work. Pinhole would have to reduce light. level by about 1:16 (all bands) to accommodate bands 7 and 8. Potential impacts on diffuser and lunar accuracy.

*Risk:* Medium-high.

*Cost/Schedule:* Major. Requires instrument work, calibration, tests, and electronics work.

*Added benefit:* Mission would collect good (250 levels) global land and cloud data as well (making an 8-bit MODIS simulator).

**CHANGE 7**

*Reverse odd and even channel positions on one or more focal planes.*

*Intent:* To provide a useful quartet of spectral bands which do not anticipate bright targets, by switching positions on various focal planes. Ratios of the counts in odd bands show very similar responses to the anticipation stray light and have minimal bright target anticipation. Present odd channels are 412, 490, 555, and 765 nm.

*Magnitude of improvement:* Partial. Potentially enables CZCS-like results up to 5 pixels from the up-scan edge of land and clouds (by reversing the 412 and 443 bands), or reliable atmospheric correction for the same region (by reversing three focal planes). Provides 22% increase with CZCS-like data relative to 12 pixel masks.

*Negative impact:* None. Contributes little to solution of trailing edge or electronic recovery.

*Risk:* Medium-high. Filters have been replaced on one focal plane before. Focal plane 1 is hard to access.

*Cost/Schedule:* Major. Requires disassembly and removal of filters, with risk of damage. Only one spare filter exists for band 5. Would require recalibration, realignment.

## CHANGE 8

*Software Corrections.*

*Intent:* Solve the problem in software. Need the focal plane response function and methodology.

*Magnitude of improvement:* Uncertain. Asymmetry of odd and even band effects places a major constraint on the errors allowed. If effects are corrected to 50% (of 12 pixels total), this would provide a 44% increase in ocean data, or 75% increase if 75% correction is possible (relative to 12 pixels).

*Negative impact:* Major software and coding task. Requires knowledge of bright target spectral radiance and focal plane response. Amounts to passing a variable response, 25 element filter through the data. Any change in focal plane response over time will be difficult to resolve. May necessitate production and archive of a level-1b data set. Corrections to GAC data are more difficult.

*Risk:* None to flight segment, high risk of guaranteed success.

*Cost/Schedule:* Requires some combination of changes 1 or 2, 5 or 6, and 7, plus a full focal plane BRDF, significant computer upgrades, intensive validation measurements, and 6 months to a year post-launch for a significant improvement.

## CHANGE 9

*Collect full scan of one band in GAC data.*

*Intent:* Provide high resolution data along-scan for one band on GAC scan lines, to enable position of bright targets to be determined in GAC data. Provides unambiguous flag for corrupt data when small clouds are missed in GAC subsamples.

*Magnitude of improvement:* Impact being assessed.

*Negative impact:* Major impact on spacecraft data system, requires data compression.

*Risk:* High.

*Cost/Schedule:* Increased data storage by 11/8, and changing 2 Gbits unpacked data per day to 2.75 Gbits to keep the same potential coverage frequency. Major rework of spacecraft data system, data formats.

## CHANGE 10

*Collate global LAC HRPT data.*

*Intent:* Since the location of bright targets is not known in GAC data to better than 3 pixels, correction of the stray light effect is only possible with LAC data.

*Magnitude of improvement:* Dependent on change 8. Most of North Atlantic and coastal waters are covered.

*Negative impact:* None, benefit regional science by having all data available.

*Cost/Schedule:* Major, since it implies doing a correction, plus processing 16 times the GAC volume to arrive at a global data set.

## CHANGE 11

*Rearrange bands on focal planes (parallel bands).*

*Intent:* Put bands in parallel instead of in line, to reduce-along scan distance effect, and odd-even responses.

*Magnitude of improvement:* Could be significant from about 12 to about 5 pixels anticipation. Total area of effect remains about the same.

*Negative impact:* Increases distance along-track in which a bright target would affect a given pixel. Total area affected would remain the same.

*Risk:* High.

*Cost/Schedule:* Major, major impact.

## GLOSSARY

A/D	Analog-to-Digital
BRDF	Bidirectional Reflectance Distribution Function
BTR	Bright Target Recovery
BTD	Bright Target Detection
CZCS	Coastal Zone Color Scanner
FOV	Field of View
GAC	Global Area Coverage
GSFC	Goddard Space Flight Center
IFOV	Instantaneous Field-of-View
LAC	Local Area Coverage
MTF	Modulation Transfer Function
NASA	National Aeronautics and Space Administration
NIMBUS	Not an acronym, but a series of NASA experimental satellites containing a wide variety of atmosphere, ice, and ocean sensors.
OSC	Orbital Sciences Corporation
RC	Resistor-Capacitor (circuit)
SBRC	Santa Barbara Research Center
SCADP	SeaWiFS Calibration and Acceptance Data Package
SCDR	SeaWiFS Critical Design Review
SeaWiFS	Sea-viewing Wide Field-of-view Sensor
SNR	Signal-to-Noise Ratio
SPR	SeaWiFS Preship Review
SPMPR	SeaWiFS Post-Modification Preship Review
SSLSP	SeaWiFS Stray Light Signal Paths
TDI	Time Delay and Integration

## SYMBOLS

$F_{GAC}$	GAC correction factor.
$F_{SL}$	Correction factor for stray light.
$K_i$	Correction constant at the $i$ th pixel.
$L_{cloud}$	Maximum radiance from reflected light off of clouds.
$L_{typical}$	Expected radiance from the ocean measured on orbit.
$P_{edge}$	A pixel located on the exact edge of a bright source in a GAC scene.
$P_i$	The $i$ th pixel under correction.
$P_{slit}$	Designates the number of pixels after the slit for the instrument to return to the residual counts allowed in the specification.
$P_{zero}$	Designates the number of pixels required for the instrument to settle to a level of zero residual counts.
$P_{\Delta}$	The location of the pixel to be corrected in GAC pixels relative to the (bright target) edge pixel.
$R_i$	Radiance of the $i$ th pixel.
$R_B$	Bidirectional reflectance distribution function.
$\alpha$	Off-axis angle.
$\sigma$	Standard deviation of a set of data values.

## REFERENCES

- Arrigo, K.R., and C.R. McClain, 1995: "Cloud and ice detection at high latitudes for processing of CZCS imagery." In: McClain, C.R., W.E. Esaias, M. Darzi, F.S. Patt, R.H. Evans, J.W. Brown, K.R. Arrigo, C.W. Brown, R.A. Barnes, and L. Kumar, 1995: SeaWiFS Algorithms, Part 1. *NASA Tech. Memo. 104566, Vol. 28*, S.B. Hooker, E.R. Firestone, and J.G. Acker, Eds., NASA Goddard Space Flight Center, 8-12.
- Barnes, R.A., W.L. Barnes, W.E. Esaias, and C.L. McClain, 1994a: Prelaunch Acceptance Report for the SeaWiFS Radiometer. *NASA Tech. Memo. 104566, Vol. 22*, S.B. Hooker, E.R. Firestone, and J.G. Acker, Eds., NASA Goddard Space Flight Center, Greenbelt, Maryland, 32 pp.
- , A.W. Holmes, W.L. Barnes, W.E. Esaias, and C.R. McClain, 1994b: SeaWiFS Prelaunch Radiometric Calibration and Spectral Characterization. *NASA Tech. Memo. 104566, Vol. 23*, S.B. Hooker, E.R. Firestone, and J.G. Acker, Eds., NASA Goddard Space Flight Center, Greenbelt, Maryland, 55 pp.
- Diefenderfer, A.J., 1972: *Principles of Electronic Instrumentation*. W.B. Saunders, Philadelphia, 675 pp.
- Hooker, S.B., W.E. Esaias, G.C. Feldman, W.W. Gregg, and C.R. McClain, 1992: An Overview of SeaWiFS and Ocean Color. *NASA Tech. Memo. 104566, Vol. 1*, S.B. Hooker and E.R. Firestone, Eds., NASA Goddard Space Flight Center, Greenbelt, Maryland, 25 pp., plus color plates.
- Justice, J.O., B.L. Markham, J.R.C. Townshend, and R.L. Kennard, 1989: Spatial degradation of satellite data. *Int. J. Remote Sens.*, **10**, 1,539-1,561.
- McClain, C.R., E. Yeh, and G. Fu, 1992: An Analysis of GAC Sampling Algorithms: A Case Study. *NASA Tech. Memo. 104566, Vol. 4*, S.B. Hooker and E.R. Firestone, Eds., NASA Goddard Space Flight Center, Greenbelt, Maryland, 22 pp., plus color plates.
- , R. Evans, J. Brown, and M. Darzi, 1995: "SeaWiFS Quality Control Masks, and Flags: Initial Algorithms and Implementation Strategy," In: McClain, C.R., W.E. Esaias, M. Darzi, F.S. Patt, R.H. Evans, J.W. Brown, K.R. Arrigo, C.W. Brown, R.A. Barnes, and L. Kumar, 1995: SeaWiFS Algorithms, Part 1. *NASA Tech. Memo. 104566, Vol. 28*, S.B. Hooker, E.R. Firestone, and J.G. Acker, Eds., NASA Goddard Space Flight Center, 3-7.
- Mueller, J.L., 1988: NIMBUS-7 CZCS: Electronic overshoot due to cloud reflectance. *Appl. Opt.*, **27**, 438-440.
- Westphal, T.L., Y. Ge, and S.B. Hooker, 1994: "The SBRC Database." In: Hooker, S.B., C.R. McClain, J.K. Firestone, T.L. Westphal, E-n. Yeh, and Y. Ge, 1994: The SeaWiFS Bio-Optical Archive and Storage System (SeaBASS), Part 1. *NASA Tech. Memo. 104566, Vol. 20*, S.B. Hooker and E.R. Firestone, Eds., NASA Goddard Space Flight Center, Greenbelt, Maryland, 31-34.
- Woodward, R.H., R.A. Barnes, C.R. McClain, W.E. Esaias, W.L. Barnes, and A.T. Mecherikunnel, 1993: Modeling of the SeaWiFS Solar and Lunar Observations. *NASA Tech. Memo. 104566, Vol. 10*, S.B. Hooker and E.R. Firestone, Eds., NASA Goddard Space Flight Center, Greenbelt, Maryland, 26 pp.

## THE SEAWIFS TECHNICAL REPORT SERIES

Vol. 1

- Hooker, S.B., W.E. Esaias, G.C. Feldman, W.W. Gregg, and C.R. McClain, 1992: An Overview of SeaWiFS and Ocean Color. *NASA Tech. Memo. 104566, Vol. 1*, S.B. Hooker and E.R. Firestone, Eds., NASA Goddard Space Flight Center, Greenbelt, Maryland, 24 pp., plus color plates.

Vol. 2

- Gregg, W.W., 1992: Analysis of Orbit Selection for SeaWiFS: Ascending vs. Descending Node. *NASA Tech. Memo. 104566, Vol. 2*, S.B. Hooker and E.R. Firestone, Eds., NASA Goddard Space Flight Center, Greenbelt, Maryland, 16 pp.

Vol. 3

- McClain, C.R., W.E. Esaias, W. Barnes, B. Guenther, D. Endres, S.B. Hooker, G. Mitchell, and R. Barnes, 1992: Calibration and Validation Plan for SeaWiFS. *NASA Tech. Memo. 104566, Vol. 3*, S.B. Hooker and E.R. Firestone, Eds., NASA Goddard Space Flight Center, Greenbelt, Maryland, 41 pp.

Vol. 4

- McClain, C.R., E. Yeh, and G. Fu, 1992: An Analysis of GAC Sampling Algorithms: A Case Study. *NASA Tech. Memo. 104566, Vol. 4*, S.B. Hooker and E.R. Firestone, Eds., NASA Goddard Space Flight Center, Greenbelt, Maryland, 22 pp., plus color plates.

Vol. 5

- Mueller, J.L., and R.W. Austin, 1992: Ocean Optics Protocols for SeaWiFS Validation. *NASA Tech. Memo. 104566, Vol. 5*, S.B. Hooker and E.R. Firestone, Eds., NASA Goddard Space Flight Center, Greenbelt, Maryland, 43 pp.

Vol. 6

- Firestone, E.R., and S.B. Hooker, 1992: SeaWiFS Technical Report Series Summary Index: Volumes 1-5. *NASA Tech. Memo. 104566, Vol. 6*, S.B. Hooker and E.R. Firestone, Eds., NASA Goddard Space Flight Center, Greenbelt, Maryland, 9 pp.

Vol. 7

- Darzi, M., 1992: Cloud Screening for Polar Orbiting Visible and IR Satellite Sensors. *NASA Tech. Memo. 104566, Vol. 7*, S.B. Hooker and E.R. Firestone, Eds., NASA Goddard Space Flight Center, Greenbelt, Maryland, 7 pp.

Vol. 8

- Hooker, S.B., W.E. Esaias, and L.A. Rexrode, 1993: Proceedings of the First SeaWiFS Science Team Meeting. *NASA Tech. Memo. 104566, Vol. 8*, S.B. Hooker and E.R. Firestone, Eds., NASA Goddard Space Flight Center, Greenbelt, Maryland, 61 pp.

Vol. 9

- Gregg, W.W., F.C. Chen, A.L. Mezaache, J.D. Chen, J.A. Whiting, 1993: The Simulated SeaWiFS Data Set, Version 1. *NASA Tech. Memo. 104566, Vol. 9*, S.B. Hooker, E.R. Firestone, and A.W. Indest, Eds., NASA Goddard Space Flight Center, Greenbelt, Maryland, 17 pp.

Vol. 10

Woodward, R.H., R.A. Barnes, C.R. McClain, W.E. Esaias, W.L. Barnes, and A.T. Mecherikunnel, 1993: Modeling of the SeaWiFS Solar and Lunar Observations. *NASA Tech. Memo. 104566, Vol. 10*, S.B. Hooker and E.R. Firestone, Eds., NASA Goddard Space Flight Center, Greenbelt, Maryland, 26 pp.

Vol. 11

Patt, F.S., C.M. Hoisington, W.W. Gregg, and P.L. Coronado, 1993: Analysis of Selected Orbit Propagation Models for the SeaWiFS Mission. *NASA Tech. Memo. 104566, Vol. 11*, S.B. Hooker, E.R. Firestone, and A.W. Indest, Eds., NASA Goddard Space Flight Center, Greenbelt, Maryland, 16 pp.

Vol. 12

Firestone, E.R., and S.B. Hooker, 1993: SeaWiFS Technical Report Series Summary Index: Volumes 1–11. *NASA Tech. Memo. 104566, Vol. 12*, S.B. Hooker and E.R. Firestone, Eds., NASA Goddard Space Flight Center, Greenbelt, Maryland, 28 pp.

Vol. 13

McClain, C.R., K.R. Arrigo, J. Comiso, R. Fraser, M. Darzi, J.K. Firestone, B. Schieber, E-n. Yeh, and C.W. Sullivan, 1994: Case Studies for SeaWiFS Calibration and Validation, Part 1. *NASA Tech. Memo. 104566, Vol. 13*, S.B. Hooker and E.R. Firestone, Eds., NASA Goddard Space Flight Center, Greenbelt, Maryland, 52 pp., plus color plates.

Vol. 14

Mueller, J.L., 1993: The First SeaWiFS Intercalibration Round-Robin Experiment, SIRREX-1, July 1992. *NASA Tech. Memo. 104566, Vol. 14*, S.B. Hooker and E.R. Firestone, Eds., NASA Goddard Space Flight Center, Greenbelt, Maryland, 60 pp.

Vol. 15

Gregg, W.W., F.S. Patt, and R.H. Woodward, 1994: The Simulated SeaWiFS Data Set, Version 2. *NASA Tech. Memo. 104566, Vol. 15*, S.B. Hooker and E.R. Firestone, Eds., NASA Goddard Space Flight Center, Greenbelt, Maryland, 42 pp., plus color plates.

Vol. 16

Mueller, J.L., B.C. Johnson, C.L. Cromer, J.W. Cooper, J.T. McLean, S.B. Hooker, and T.L. Westphal, 1994: The Second SeaWiFS Intercalibration Round-Robin Experiment, SIRREX-2, June 1993. *NASA Tech. Memo. 104566, Vol. 16*, S.B. Hooker and E.R. Firestone, Eds., NASA Goddard Space Flight Center, Greenbelt, Maryland, 121 pp.

Vol. 17

Abbott, M.R., O.B. Brown, H.R. Gordon, K.L. Carder, R.E. Evans, F.E. Muller-Karger, and W.E. Esaias, 1994: Ocean Color in the 21st Century: A Strategy for a 20-Year Time Series. *NASA Tech. Memo. 104566, Vol. 17*, S.B. Hooker and E.R. Firestone, Eds., NASA Goddard Space Flight Center, Greenbelt, Maryland, 20 pp.

Vol. 18

Firestone, E.R., and S.B. Hooker, 1995: SeaWiFS Technical Report Series Summary Index: Volumes 1–17. *NASA Tech. Memo. 104566, Vol. 18*, S.B. Hooker and E.R. Firestone, Eds., NASA Goddard Space Flight Center, Greenbelt, Maryland, 47 pp.

Vol. 19

McClain, C.R., R.S. Fraser, J.T. McLean, M. Darzi, J.K. Firestone, F.S. Patt, B.D. Schieber, R.H. Woodward, E-n. Yeh, S. Mattoo, S.F. Biggar, P.N. Slater, K.J. Thome, A.W. Holmes, R.A. Barnes, and K.J. Voss, 1994: Case Studies for SeaWiFS Calibration and Validation, Part 2. *NASA Tech. Memo. 104566, Vol. 19*, S.B. Hooker, E.R. Firestone, and J.G. Acker, Eds., NASA Goddard Space Flight Center, Greenbelt, Maryland, 73 pp.

Vol. 20

Hooker, S.B., C.R. McClain, J.K. Firestone, T.L. Westphal, E-n. Yeh, and Y. Ge, 1994: The SeaWiFS Bio-Optical Archive and Storage System (SeaBASS), Part 1. *NASA Tech. Memo. 104566, Vol. 20*, S.B. Hooker and E.R. Firestone, Eds., NASA Goddard Space Flight Center, Greenbelt, Maryland, 40 pp.

Vol. 21

Acker, J.G., 1994: The Heritage of SeaWiFS: A Retrospective on the CZCS NIMBUS Experiment Team (NET) Program. *NASA Tech. Memo. 104566, Vol. 21*, S.B. Hooker and E.R. Firestone, Eds., NASA Goddard Space Flight Center, Greenbelt, Maryland, 43 pp.

Vol. 22

Barnes, R.A., W.L. Barnes, W.E. Esaias, and C.R. McClain, 1994: Prelaunch Acceptance Report for the SeaWiFS Radiometer. *NASA Tech. Memo. 104566, Vol. 22*, S.B. Hooker, E.R. Firestone, and J.G. Acker, Eds., NASA Goddard Space Flight Center, Greenbelt, Maryland, 32 pp.

Vol. 23

Barnes, R.A., A.W. Holmes, W.L. Barnes, W.E. Esaias, C.R. McClain, and T. Svitek, 1994: SeaWiFS Prelaunch Radiometric Calibration and Spectral Characterization. *NASA Tech. Memo. 104566, Vol. 23*, S.B. Hooker, E.R. Firestone, and J.G. Acker, Eds., NASA Goddard Space Flight Center, Greenbelt, Maryland, 55 pp.

Vol. 24

Firestone, E.R., and S.B. Hooker, 1995: SeaWiFS Technical Report Series Summary Index: Volumes 1–23. *NASA Tech. Memo. 104566, Vol. 24*, S.B. Hooker and E.R. Firestone, Eds., NASA Goddard Space Flight Center, Greenbelt, Maryland, 36 pp.

Vol. 25

Mueller, J.L., and R.W. Austin, 1995: Ocean Optics Protocols for SeaWiFS Validation, Revision 1. *NASA Tech. Memo. 104566, Vol. 25*, S.B. Hooker and E.R. Firestone, Eds., NASA Goddard Space Flight Center, Greenbelt, Maryland, 66 pp.

Vol. 26

Siegel, D.A., M.C. O'Brien, J.C. Sorensen, D.A. Konhoff, E.A. Brody, J.L. Mueller, C.O. Davis, W.J. Rhea, and S.B. Hooker, 1995: Results of the SeaWiFS Data Analysis Round-Robin (DARR), July 1994. *NASA Tech. Memo. 104566, Vol. 26*, S.B. Hooker and E.R. Firestone, Eds., NASA Goddard Space Flight Center, Greenbelt, Maryland, 58 pp.

Vol. 27

Mueller, J.L., R.S. Fraser, S.F. Biggar, K.J. Thome, P.N. Slater, A.W. Holmes, R.A. Barnes, C.T. Weir, D.A. Siegel, D.W. Menzies, A.F. Michaels, and G. Podesta, 1995: Case Studies for SeaWiFS Calibration and Validation, Part 3. *NASA Tech. Memo. 104566, Vol. 27*, S.B. Hooker, E.R. Firestone, and J.G. Acker, Eds., NASA Goddard Space Flight Center, Greenbelt, Maryland, 46 pp.

## Stray Light in the SeaWiFS Radiometer

### Vol. 28

McClain, C.R., K.R. Arrigo, W.E. Esaias, M. Darzi, F.S. Patt, R.H. Evans, J.W. Brown, C.W. Brown, R.A. Barnes, and L. Kumar, 1995: SeaWiFS Algorithms, Part 1. *NASA Tech. Memo. 104566, Vol. 28*, S.B. Hooker, E.R. Firestone, and J.G. Acker, Eds., NASA Goddard Space Flight Center, Greenbelt, Maryland, 38 pp., plus color plates.

### Vol. 29

Aiken, J., G.F. Moore, C.C. Trees, S.B. Hooker, and D.K. Clark, 1995: The SeaWiFS CZCS-Type Pigment Algorithm. *NASA Tech. Memo. 104566, Vol. 29*, S.B. Hooker and E.R. Firestone, Eds., NASA Goddard Space Flight Center, Greenbelt, Maryland, 34 pp.

### Vol. 30

Firestone, E.R., and S.B. Hooker, 1995: SeaWiFS Technical Report Series Summary Index: Volumes 1-29. *NASA Tech. Memo. 104566, Vol. 30*, S.B. Hooker and E.R. Firestone, Eds., NASA Goddard Space Flight Center, Greenbelt, Maryland, (in production).

### Vol. 31

Barnes, R.A., A.W. Holmes, and W.E. Esaias, 1995: Stray Light in the SeaWiFS Radiometer. *NASA Tech. Memo. 104566, Vol. 31*, S.B. Hooker, E.R. Firestone, and J.G. Acker, Eds., NASA Goddard Space Flight Center, Greenbelt, Maryland, 76 pp.



# REPORT DOCUMENTATION PAGE

*Form Approved*  
OMB No. 0704-0188

Public reporting burden for this collection of information is estimated to average 1 hour per response, including the time for reviewing instructions, searching existing data sources, gathering and maintaining the data needed, and completing and reviewing the collection of information. Send comments regarding this burden estimate or any other aspect of this collection of information, including suggestions for reducing this burden, to Washington Headquarters Services, Directorate for Information Operations and Reports, 1215 Jefferson Davis Highway, Suite 1204, Arlington, VA 22202-4302, and to the Office of Management and Budget, Paperwork Reduction Project (0704-0188), Washington, DC 20503.

<b>1. AGENCY USE ONLY (Leave blank)</b>	<b>2. REPORT DATE</b> July 1995	<b>3. REPORT TYPE AND DATES COVERED</b> Technical Memorandum	
<b>4. TITLE AND SUBTITLE</b> SeaWiFS Technical Report Series Volume 31—Stray Light in the SeaWiFS Radiometer		<b>5. FUNDING NUMBERS</b>  Code 970.2	
<b>6. AUTHOR(S)</b> Robert A. Barnes, Alan W. Holmes, and Wayne E. Esaias  Series Editors: Stanford B. Hooker and Elaine R. Firestone Technical Editor: James G. Acker			
<b>7. PERFORMING ORGANIZATION NAME(S) AND ADDRESS(ES)</b> Laboratory for Hydrospheric Processes Goddard Space Flight Center Greenbelt, Maryland 20771		<b>8. PERFORMING ORGANIZATION REPORT NUMBER</b>  95B00108	
<b>9. SPONSORING/MONITORING AGENCY NAME(S) AND ADDRESS(ES)</b> National Aeronautics and Space Administration Washington, D.C. 20546-0001		<b>10. SPONSORING/MONITORING AGENCY REPORT NUMBER</b>  TM-104566, Vol. 31	
<b>11. SUPPLEMENTARY NOTES</b> Elaine R. Firestone: General Sciences Corporation, Laurel, MD; James G. Acker: Hughes STX, Lanham, MD; Robert A. Barnes: ManTech, Inc., Wallops Island, VA; and Alan W. Holmes: Santa Barbara Research Center, Goleta, CA			
<b>12a. DISTRIBUTION/AVAILABILITY STATEMENT</b> Unclassified—Unlimited Subject Category 48 Report is available from the Center for AeroSpace Information (CASI), 800 Elkridge Landing Road, Linthicum Heights, MD 21090; (301)621-0390		<b>12b. DISTRIBUTION CODE</b>	
<b>13. ABSTRACT (Maximum 200 words)</b> Some of the measurements from the Sea-viewing Wide Field-of-view Sensor (SeaWiFS) will not be useful as ocean measurements. For the ocean data set, there are procedures in place to mask the SeaWiFS measurements of clouds and ice. Land measurements will also be masked using a geographic technique based on each measurement's latitude and longitude. Each of these masks involves a source of light much brighter than the ocean. Because of stray light in the SeaWiFS radiometer, light from these bright sources can contaminate ocean measurements located a variable number of pixels away from a bright source. In this document, the sources of stray light in the sensor are examined, and a method is developed for masking measurements near bright targets for stray light effects. In addition, a procedure is proposed for reducing the effects of stray light in the flight data from SeaWiFS. This correction can also reduce the number of pixels masked for stray light. Without these corrections, local area scenes must be masked 10 pixels before and after bright targets in the along-scan direction. The addition of these corrections reduces the along-scan masks to four pixels before and after bright sources. In the along-track direction, the flight data are not corrected, and are masked two pixels before and after. Laboratory measurements have shown that stray light within the instrument changes in a direct ratio to the intensity of the bright source. The measurements have also shown that none of the bands show peculiarities in their stray light response. In other words, the instrument's response is uniform from band to band. The along-scan correction is based on each band's response to a bright source that is 1 pixel wide. Since these results are based solely on preflight laboratory measurements, their successful implementation requires compliance with two additional criteria. First, since SeaWiFS has a large data volume, the correction and masking procedures must be such that they can be converted into computationally fast algorithms. Second, they must be shown to operate properly on flight data. The laboratory results, and the corrections and masking procedures that derive from them, should be considered as zeroeth order estimates of the effects that will be found on orbit.			
<b>14. SUBJECT TERMS</b> SeaWiFS, Oceanography, Stray Light, Bright Target Recovery, GAC Correction, LAC Correction		<b>15. NUMBER OF PAGES</b> 76	
		<b>16. PRICE CODE</b>	
<b>17. SECURITY CLASSIFICATION OF REPORT</b> Unclassified	<b>18. SECURITY CLASSIFICATION OF THIS PAGE</b> Unclassified	<b>19. SECURITY CLASSIFICATION OF ABSTRACT</b> Unclassified	<b>20. LIMITATION OF ABSTRACT</b> Unlimited

National Aeronautics and  
Space Administration

**Goddard Space Flight Center**  
Greenbelt, Maryland 20771

Official Business  
Penalty for Private Use, \$300

SPECIAL FOURTH-CLASS RATE  
POSTAGE & FEES PAID  
NASA  
PERMIT No. G27



POSTMASTER: If Undeliverable (Section 158,  
Postal Manual) Do Not Return

---